Aalborg Universitet

AALBORG UNIVERSITY
DENMARK

Analysis and Modeling of Transformerless Photovoltaic Inverter Systems

Kerekes, Tamas

Publication date:
2009

Document Version
Publisher's PDF, also known as Version of record

[Link to publication from Aalborg University](#)

Analysis and Modeling of Transformerless Photovoltaic Inverter Systems

by

Tamás Kerekes

Dissertation submitted to the Faculty of Engineering, Science & Medicine at Aalborg University in partial fulfillment of the requirements for the degree of Doctor of Philosophy in Electrical Engineering

Aalborg University
Institute of Energy Technology
Denmark, August 2009

Preface

This thesis is written in the frame of two research projects: the first, entitled "Transformerlose solcelle invertere", was financially supported by the Eltra PSO-F&U contract nr. 5780 signed between Aalborg University and Energinet in cooperation with Powerlynx A/S, now Danfoss Solar A/S. The second part of the research, entitled "Electrical energy conversion and condition-ECON2", was supported by the EU framework entitled "Marie Curie Host Fellowships for Early Stage Researcher Training", financially supported by the EC Contract MEST-CT-2004-504243. Acknowledgements are given to Aalborg University and the above mentioned institutions for their financial support.

The research was carried out under the supervision of Professor Remus Teodorescu from Institute of Energy Technology (IET) at Aalborg University. My deepest gratitude goes to my supervisor for his guidance and professional support during the elaboration of the work done in this thesis.

I would like to express my sincere thanks to Dr. Christian Klumpner and Dr. Mark Sumner for their guidance and support during my one-year stay at Nottingham University. I'm also grateful to Dr. Marco Liserre from Politecnico di Bari for his kindness and professional guidance during my six month stay at the Dipartimento di Elettrotecnica ed Elettronica. I would also like to thank Uffe Borup, from Danfoss Solar A/S, for participating in the steering meetings and for his active support.

I want to thank to all my colleagues from Institute of Energy Technology for their friendly companionship which guided me through life at Aalborg University. Special thanks go to Dr. Pedro Rodriguez and Professor Vassilios Agelidis for their unselfish help and moral support, during their stay at IET. Also many thanks to all my fellow PhD students, who assisted me many times and gave me support in different ways. In particular, I thank to Dezső Séra, Mihai Ciobotaru and Máthé László for their friendly help and encouragement. I would also like to thank Gerardo Vazquez from Universitat Politecnica de Catalonya for sharing his experience and time with me during his visit at IET.

And, last but not least, I want to express my deepest gratitude to my wife Erzsébet Kerekes and to my entire family in Romania for the substantial and continuous support which I have received during the elaboration and finalization of this work.

Tamás Kerekes
August 2009; Aalborg

Abstract

The need for a cleaner environment and the continuous increase in power demands makes decentralized renewable energy production, like solar and wind, more and more interesting. Decentralized energy production using solar energy could be a solution for balancing the continuously-increasing power demands. This continuously increasing consumption overloads the distribution grids as well as the power stations, therefore having a negative impact on power availability, security and quality. One of the solutions for overcoming this is the grid-connected photovoltaic (PV) system.

PV inverter systems can be improved in terms of efficiency using transformerless topologies, but new problems related to leakage current need to be dealt with.

The work presented in this thesis deals with analyzing and modeling of transformerless PV inverter systems regarding the leakage current phenomenon that can damage solar panels and pose safety problems.

The major task of this research was the investigation and verification of transformerless topologies and control strategies to minimize the leakage current of PV inverter topologies in order to comply with the standard requirements and make them safe for human interaction.

The thesis is divided into two parts: Part I – Report and Part II – Publications. Part I is a summary report of the work done throughout the research and contains 6 chapters.

Chapter 1: Introduction, focuses on the background and motivation regarding the research done in this thesis. Furthermore, the objectives and limitations of the project are enumerated. The chapter finishes with the outline of the thesis.

Chapter 2: Overview of grid connected PV systems, gives an overview about grid connected PV inverters, focusing on transformerless inverters and related safety issues. The parasitic capacitance of several commercial mono- and multi-crystalline PV panels has been measured, and an appropriate value has been defined for use in the simulations. Also, two commercial current sensors that can be used for leakage current measurement, have been tested and the results are presented in Appendix A.

A detailed investigation of different inverter topologies regarding the ground leakage current is described in Chapter 3: Investigation of transformerless topologies, showing the ground voltage and leakage current for the analyzed topologies, concluding with whether the topology is suited for transformerless PV systems.

Chapter 4: Common mode voltage in PV inverter topologies, explains the common-mode behavior of single and three-phase PV inverter topologies by presenting a comprehensive analysis of the single and three-phase transformerless converter with

respect to the problem of the leakage current that flows through the parasitic capacitance of the PV array.

In Chapter 5: H-Bridge Zero Voltage Rectifier topology, a new inverter called H-Bridge Zero Voltage Rectifier (HB-ZVR) is proposed, where the mid-point of the DC link is clamped to the grid only during the Zero Voltage period by means of a diode rectifier bridge and one switch. A comparison of known transformerless topologies and the HB-ZVR is performed using simulations, focusing on the voltage to earth harmonics and ground leakage current. Furthermore, experimental results are shown, confirming the simulations, and finally, the efficiency curve of the compared topologies is detailed.

In Chapter 6: Conclusion, the final conclusion is presented, based on the theoretical and experimental results performed. Also a list is given, detailing the contributions presented in this thesis. Additionally, guidelines for future work are given.

The second part of the thesis: Part II – Publications contains the papers that have been published during the period of the research. The articles describe in detail the methods, simulations and the experimental results that make up the backbone of the work described in this thesis.

Dansk resumé

Behovet for et renere miljø og den fortsatte stigning i ydelse krav gør decentral produktion af vedvarende energi, såsom solcelle og vindenergi, mere og mere interessant. Decentral energiproduktion ved hjælp af solenergi kan være en løsning for at afbalancere det stadigt stigende strøm behov. Det stadigt stigende forbrug belaster distributionsnettet, samt kraftværker, derfor har forbruget en negativ indvirkning på magten af pålidelighed, sikkerhed og kvalitet. En af de løsninger for at overvinde dette er nettilsluttet solcelle system.

Solcelle inverter systemer kan forbedres ved hjælp af transformerløse topologier, men nye problemer i forbindelse med lækstrøm har behov for at blive behandlet.

I denne forbindelse præsenteres denne afhandling der beskæftiger sig med analyse og modellering af transformerløse solcelle inverter systemer med fokus på lækstrøms fænomener, der kan skade solpaneler og udgøre en sikkerheds-risiko.

Den største opgave i denne afhandling blev undersøgelsen og verifikation af transformerløse topologier og kontrolstrategier, der vil minimere lækstrøm af solcelle inverter topologier for at overholde standardkrav og gøre dem sikre for menneskelig interaktion.

Afhandlingen er opdelt i to dele: Del I - Rapport og Del II - Publikationer. Del I er en sammenfattende rapport over det udførte arbejde i hele forskningsperioden og indeholder 6 kapitler.

Kapitel 1 fokuserer på baggrunden og motivationen i forbindelse med forskningen beskrevet i denne afhandling. Desuden er mål og begrænsninger for projektet er fremsat, afsluttende med et overblik over afhandlingen.

Kapitel 2 giver en oversigt over nettilsluttede solcelle invertere, der fokuserer på transformerløse frekvensomformere og de relaterede sikkerhedsspørgsmål. Den parasitiske kapacitans af flere kommercielle mono-og multi-krystallinske solcelle paneler er blevet målt, og en repræsentativ værdi er fastsat til anvendelse i simuleringerne. Også to nuværende sensorer, som vil kunne bruges til lækstrøm måling, er blevet testet, og resultaterne præsenteres i tillæg A.

En detaljeret undersøgelse af forskellige inverter topologier med hensyn til jord-lækstrom er beskrevet i kapitel 3, der viser DC til jord potentialet og lækstrømmen for de analyserede topologier, indgåelse hvis topologi er velegnet til transformerløse solcelle anlæg.

Kapitel 4 forklarer common-mode opførsel af en og tre-fase solcelle inverter topologier ved at fremlægge en omfattende analyse af enkelt og tre-fase transformerløse konvertere med hensyn til problemet med lækstrøm, der løber gennem den parasitiske kapacitans i solcelle anlæg.

I kapitel 5 er en ny inverter kaldet H-Bridge Zero Voltage Rectifier (HB-ZVR) foreslået, hvor DC-link midtpunktet af er fastholdt på frekvensomformeren kun under nul spænding perioden ved hjælp af en diode ensretter og en transistor. En sammenligning af kendte transformerløse topologier og HB-ZVR udføres ved hjælp af simulering, der fokuserer på spændingen til jord, og jordlækstrøm. Desuden er den givet eksperimentelle resultater, der bekræfter simuleringerne, og sluttelig præsenteres virkningsgraden for de forskellige topologier.

I kapitel 6 præsenteres den endelige konklusion baseret på de teoretiske og eksperimentelle resultater. Derudover findes også en angivelse at de bidrag der præsenteres i denne afhandling. Derudover er der også givet retningslinjer for fremtidige arbejde.

Den anden del af afhandlingen: Part II - Publikationer indeholder de artikler, der er publiceret løbet af denne forskningsperiode. Artiklerne beskriver i detaljer, de metoder, de simuleringer, eller de eksperimentelle resultater, der udgør grundlaget i det arbejde, der er beskrevet i denne afhandling.

Table of contents

Glossary of terms

3FB	Three-phase Full Bridge
3FBSC	Three-phase Full Bridge with Split Capacitor
3xNPC	Three-phase Neutral Point Clamped
DSP	Digital Signal Processor
DUT	Device Under Test
EMI	Electro Magnetic Interference
FET	Field Effect Transistor
FFT	Fast Fourier Transform
HB-Bip	H-Bridge with Bipolar PWM
HB-Unip	H-Bridge with Unipolar PWM
HB-ZVR	H-Bridge Zero Voltage Rectifier
HERIC	Highly Efficient and Reliable Inverter Concept
HF	High Frequency
IEA PVPS	International Energy Agency Photovoltaic Power Systems Program
IGBT	Insulated Gate Bipolar Transistor
LF	Low Frequency
MPP	Maximum Power Point
MPPT	Maximum Power Point Tracker
NPC	Neutral Point Clamped
PCC	Point of Common Coupling
PF	Power Factor
PV	Photovoltaic
PWM	Pulse Width Modulation

RCMU	Residual Current Monitoring Unit
RMS	Root Mean Square
SMA	SMA Solar Technology AG
THD	Total Harmonic Distortion
UPS	Uninterruptible Power Supply
VAT	Value Added Tax

Nomenclature list

η - conversion efficiency

η_{EU} - European efficiency, weighted

C_{AG}, C_{BG} and C_{CG} - stray capacitances between the converter output points and the ground

C_{dc} - DC-link capacitor

C_f - capacitor of output filter

C_{G_PV} - parasitic capacitance of PV array

C_t - stray capacitance between the transformer primary and secondary windings

f_g - grid frequency

f_{sw} - switching frequency of inverter

$f_{sw\text{-}LCR}$ - switching frequency of LCR meter

I_g - grid current

$I_{G\text{-}PV}$ - ground current through parasitic capacitance of PV panel

L_A, L_B, L_C and L_N - output filter inductor

L_{cA}, L_{cB} and L_{cC} - series inductance of each phase

L_{cG} - inductance between the ground connection of the inverter and the grid neutral

L_{cN} - series inductance of the neutral

L_f - output filter inductor

L_g - inductance of the grid

R - load resistor

T_s - simulation step time

V_{ab1}, V_{bc1} and V_{ca1} - common-mode voltage due to inductor imbalance

V_{XY} - voltage between X and Y, where $X,Y=\{A,B,C,N\}$ and $X \neq Y$

V_{cm} - single-phase common-mode voltage

$V_{cmm3\sim}$ - three-phase common-mode voltage

$V_{cmm\text{-}tot}$ - total common-mode voltage

V_{dc} - DC-link voltage for converter

$Vdc1$ - DC-link voltage for single-phase converter

$Vdc3$ - DC-link voltage for three-phase converter

V_g - grid peak voltage

V_{MPP} - voltage at maximum power point of PV array

V_{OC} - open circuit voltage of PV array

$V_{out\text{-}LCR}$ - output voltage for LCR meter

Chapter 1

Introduction

This chapter presents the background and the motivation of the thesis, continuing with a short overview of grid-connected PV systems. Furthermore, it details the aims of the project, continuing with a list of the main contributions and finishing with the outline of the thesis.

1.1 Background and motivation

The need for a cleaner environment and the continuous increase in energy needs makes decentralized renewable energy production more and more important. This continuously-increasing energy consumption overloads the distribution grids as well as the power stations, therefore having a negative impact on power availability, security and quality [1]. One of the solutions for overcoming this is the Distributed Generation (DG) system. DG systems using renewable energy sources like solar, wind or hydro, have the advantage that the power is produced in close proximity to where it is consumed. This way the losses due to transmission lines are not present.

In the last decade solar energy technologies have become less expensive and more efficient, which have made it to an attractive solution, being cleaner and more environmentally friendly energy resource than traditional ones like fossil fuels, coal or nuclear. Nevertheless, a PV system is still much more expensive than traditional ones, due to the high manufacturing costs of PV panels, but the energy that drives them -the light from the sun- is free, available almost everywhere and will still be present for millions of years, long after all non-renewable energy sources have been depleted.

One of the major advantages of PV technology is that it has no moving parts. Therefore, the hardware is very robust; it has a long lifetime and low maintenance requirements. And, most importantly, it is one solution that offers environmentally friendly power generation [2].

Nowadays, PV panels are not only used in space applications, but they are present in everyday life: powering wrist watches, small calculators, supplying loads in

remote sites and, last but not least, they are connected to the public grid, generating the green power of the future. [3]

1.2 Grid connected PV systems

As mentioned before, decentralized energy production using solar energy could be a solution for balancing continuously-increasing energy needs. Grid connected PV systems have had an enormous increase in their market share over the last decade. With a reasonable set of incentives, the solar photovoltaic market in the U.S. could grow more than *30%* per year over the next 20 years, from *340MW* of installed capacity to *9600 MW* [4]. This market growth is also present in other countries worldwide.

According to the latest report of IEA PVPS on installed PV power, during 2007 there was a total of *2.25 GW* of installed PV systems, of which the majority (*90%*) are installed in Germany, Spain, USA and Japan. At the end of 2007 the total installed PV capacity reached *7.9 GW* of which around *92%* is grid connected [5] [6].

The growth of installed capacity since 1992 and the split of this capacity between the two primary applications for PV, representing grid connected and stand-alone applications, can be seen in Fig. 1.1.
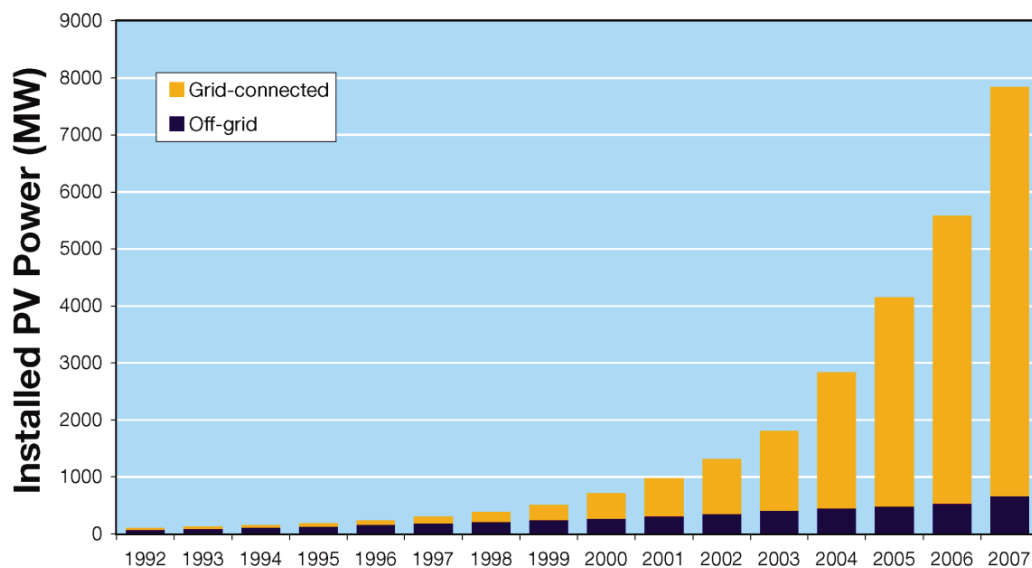
Fig. 1.1 Cumulative installed capacity between 1992 and 2007 in the IEA-PVPS reporting countries [6].

The European solar PV market has increased a lot during these last years. As shown in Fig. 1.2, at the end of 2008 the Global cumulative capacity was just below *15 GW* of installed PV, out of which *9 GW*, representing *65%*, is installed in Europe, followed by Japan with *2.1 GW* and USA with *1.2 GW*. This European market boom in 2008 is a result of the *2.5 GW* of installation in Spain and the *1.5 GW* in Germany. Regarding the total PV installations Germany is still leading with *5.3 GW*, with Spain

nearing second place with a total of *3.2 GW*, followed by Japan with *2.1 GW* and the USA with only *1.2 GW*, while the rest of the countries are lagging far behind [7].
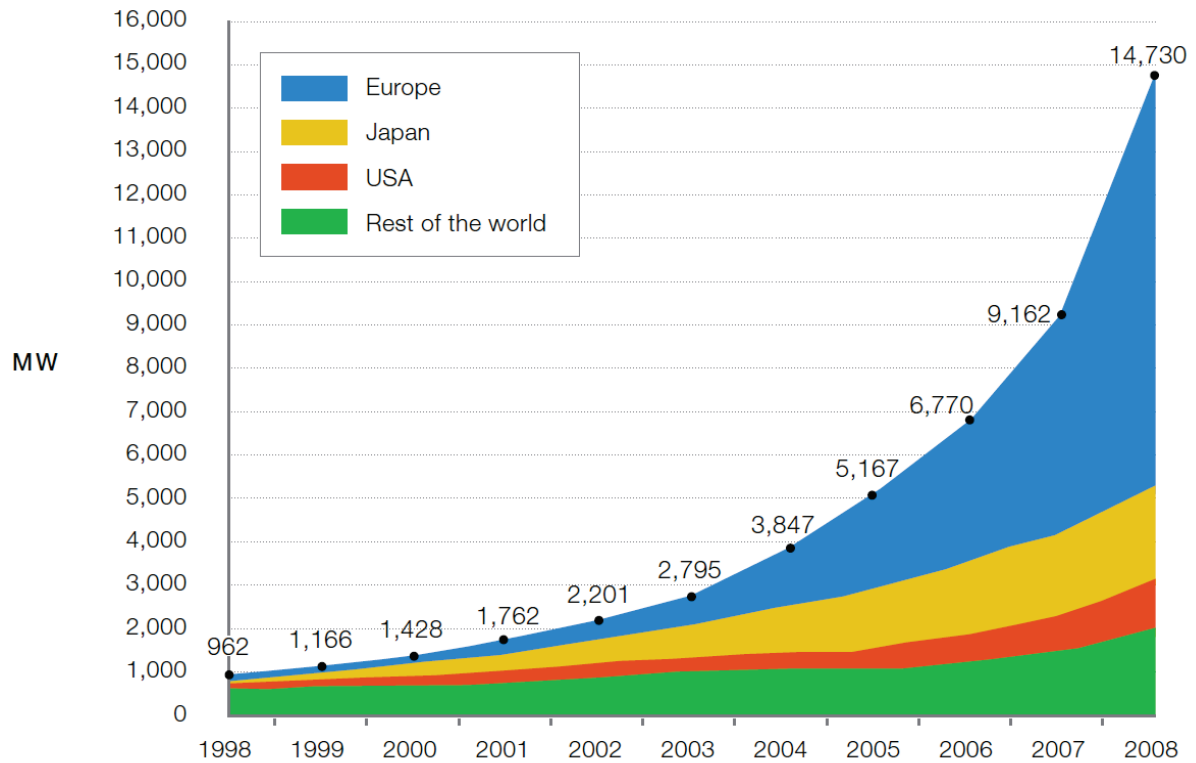
Fig. 1.2: Historical development of the Global cumulative PV power installed per Region [7].

1.3 Aims of the project

1.3.1 Problem formulation

The efficiency of commercial PV panels is around 15-20%. Therefore, it is very important that the power produced by these panels is not wasted, by using inefficient power electronics systems. The efficiency and reliability of both single-phase and three phase PV inverter systems can be improved using transformerless topologies, but new problems related to leakage current and safety need to be dealt with.

1.3.2 Objectives

The main goal of this project is to analyze and model transformerless PV inverter systems with respect to the leakage current phenomenon that can damage the solar panels and pose safety problems. New topologies and control strategies that will minimize the leakage current and exhibit a high efficiency will be proposed, investigated and verified.

1.3.3 Limitations

The majority of PV inverters on the market include a boost stage in order to raise the low voltage of the PV array to the needed DC-link voltage of around *400V* (single-phase system in Europe) or *700V* (three-phase system in Europe). During this research only single stage DC to AC topologies for single- and three-phase grid connection have been studied with a power rating of up to *5-6kW*/phase for the low power utility grid. The PV array has been simplified by using a DC power source to rule out the need for a Maximum Power Point Tracker (MPPT), both in simulation and experimental tests. Therefore only a current control strategy has been implemented in the case of grid connection, as presented in Chapter 3. In case the load was a resistive one, to simplify the implementation, only voltage control was used, as detailed in Chapters 4 and 5. The grid has been modeled as an inductance and resistance in series with an ideal sinusoidal voltage source. For simulation the MATLAB/Simulink environment has been used together with the PLECS toolbox, to simulate power electronic circuits. All the active and passive components within the modeled electrical circuit were taken to be ideal.

1.4 Main contributions

A short list of contributions is included in the order they appear in the thesis.

- Review and simulation of PV topologies

A comprehensive review is presented modeling several single- and three-phase transformerless topologies, focusing on the leakage ground current. It has been shown that the H-Bridge topology with unipolar PWM, as well as the three-phase full bridge topology, generate very high leakage current and are therefore not suitable as transformerless PV inverters. It is also emphasized that connecting the midpoint of the DC-link to the neutral of the grid will substantially reduce the generated leakage current in the case of the half-bridge or neutral-point clamped topologies, although the chosen grid side filter configuration might negatively influence the common-mode behavior of the topology.

- Interleaved PWM

The capacitor in the inverters' DC-link tends to get reduced, due to cost reduction from the manufacturers side. This means that the ripple in the DC-link will be increased, leading to higher leakage ground currents through the parasitic capacitance of the PV array. This thesis includes a new application of the interleaved PWM for three-phase inverters that has been modeled in simulation. The ripple of the DC-link voltage is reduced, thereby further reducing the leakage current in case of the three-phase full bridge split capacitor topology.

- Modeling of common-mode voltage

The leakage current of a certain topology is greatly influenced by the generated common-mode voltage that will be imposed on the parasitic capacitance of the PV array. To show the influence on the common-mode behavior of the topology in the case of inductor unbalance or inductance in the neutral wire, a model-based method for calculating the total common-mode voltage of transformerless topologies has been developed in this thesis.

- New topology

Nowadays, PV inverters feed only active power to the grid, having a power factor of 1. When there are many inverters injecting active power at the same time, the voltage at Point of Common Coupling might rise over the limits stated in the standards and trigger the safety of the inverters leading to disconnection or limit the power production below the available power. To overcome the before-mentioned disadvantage, a new high efficiency transformerless PV inverter topology called HB-ZVR (with very low leakage ground current) is proposed. The topology uses a bidirectional switch for short-circuiting the output of the converter during the zero voltage period using a switch and a diode bridge, capable of active and reactive power injection.

1.5 Outline of the thesis

The need for a cleaner environment and the continuous increase in power demands makes decentralized renewable energy production, like solar and wind, more and more interesting. Decentralized energy production using solar energy could be a solution for balancing the continuously-increasing power demands. This continuously increasing consumption overloads the distribution grids as well as the power stations, therefore having a negative impact on power availability, security and quality. One of the solutions for overcoming this is the grid-connected photovoltaic (PV) system.

PV inverter systems can be improved in terms of efficiency using transformerless topologies, but new problems related to leakage current need to be dealt with.

The work presented in this thesis deals with analyzing and modeling of transformerless PV inverter systems regarding the leakage current phenomenon that can damage solar panels and pose safety problems.

The major task of this research was the investigation and verification of transformerless topologies and control strategies to minimize the leakage current of PV inverter topologies in order to comply with the standard requirements and make them safe for human interaction.

The thesis is divided into two parts: Part I – Report and Part II – Publications. Part I is a summary report of the work done throughout the research and contains 6 chapters.

Chapter 1: Introduction, focuses on the background and motivation regarding the research done in this thesis. Furthermore, the objectives and limitations of the project are enumerated. The chapter finishes with the outline of the thesis.

Chapter 2: Overview of grid connected PV systems, gives an overview about grid connected PV inverters, focusing on transformerless inverters and related safety issues. The parasitic capacitance of several commercial mono- and multi-crystalline PV panels has been measured, and an appropriate value has been defined for use in the simulations. Also, two commercial current sensors that can be used for leakage current measurement, have been tested and the results are presented in Appendix A.

A detailed investigation of different inverter topologies regarding the ground leakage current is described in Chapter 3: Investigation of transformerless topologies, showing the ground voltage and leakage current for the analyzed topologies, concluding with whether the topology is suited for transformerless PV systems.

Chapter 4: Common mode voltage in PV inverter topologies, explains the common-mode behavior of single and three-phase PV inverter topologies by presenting a comprehensive analysis of the single and three-phase transformerless converter with respect to the problem of the leakage current that flows through the parasitic capacitance of the PV array.

In Chapter 5: H-Bridge Zero Voltage Rectifier topology, a new inverter called H-Bridge Zero Voltage Rectifier (HB-ZVR) is proposed, where the mid-point of the DC link is clamped to the grid only during the Zero Voltage period by means of a diode rectifier bridge and one switch. A comparison of known transformerless topologies and the HB-ZVR is performed using simulations, focusing on the voltage to earth harmonics and ground leakage current. Furthermore, experimental results are shown, confirming the simulations, and finally, the efficiency curve of the compared topologies is detailed.

In Chapter 6: Conclusion, the final conclusion is presented, based on the theoretical and experimental results performed. Also a list is given, detailing the contributions presented in this thesis. Additionally, guidelines for future work are given.

The second part of the thesis: Part II – Publications contains the papers that have been published during the period of the research. The articles describe in detail the methods, simulations and the experimental results that make up the backbone of the work described in this thesis.

1.6 List of publications

I.   D. Sera, T. Kerekes, R. Teodorescu, PV inverter control using a TMS320F2812 DSP; Proceedings of EDERS 2006; Page(s) 51 - 57.

II.   M. Ciobotaru, T. Kerekes, R. Teodorescu and A. Bouscayrol, PV inverter simulation using MATLAB/Simulink graphical environment and PLECS blockset IEEE Industrial Electronics, IECON 2006 - 32nd Annual Conference on: 6-10 Nov. 2006; Page(s):5313 - 5318

III.   T. Kerekes, R. Teodorescu and U. Borup, Transformerless Photovoltaic Inverters Connected to the Grid; Twenty Second Annual IEEE Applied Power Electronics Conference, APEC 2007 -; Feb. 25 2007-March 1 2007; Page(s):1733 – 1737

IV.   T. Kerekes, R. Teodorescu, C. Klumpner, M. Sumner, D. Floricau, P. Rodriguez, Evaluation of three-phase transformerless photovoltaic inverter topologies; European Conference on Power Electronics and Applications, 2007; 2-5 Sept. 2007 Page(s):1 – 10

V.   T. Kerekes, R. Teodorescu, M. Liserre, R. Mastromauro, A. Dell'Aquila, MPPT algorithm for voltage controlled PV inverters; 11th International Conference on Optimization of Electrical and Electronic Equipment, 2008. OPTIM 2008; 22-24 May 2008 Page(s):427 - 432

VI.   T. Kerekes, R. Teodorescu, M. Liserre, Common mode voltage in case of transformerless PV inverters connected to the grid; IEEE International Symposium on Industrial Electronics, 2008. ISIE 2008. June 30 2008-July 2 2008; Page(s):2390 – 2395

VII.   A. Dell'Aquila, M. Liserre, R. Mastromauro and T. Kerekes, A Single-Phase Voltage Controlled Grid Connected Photovoltaic System With Power Quality Conditioner Functionality; IEEE Transactions on Industrial Electronics; (accepted for publication)

VIII.   T. Kerekes, R. Teodorescu, M. Liserre, C. Klumpner and M. Sumner, Evaluation of Three-phase Transformerless Photovoltaic Inverter Topologies, IEEE Transactions on Power Electronics (accepted for publication)

IX.   T. Kerekes, R. Teodorescu, P. Rodriquez, G. Vazquez and E. Aldabas, A new high-efficiency single-phase transformerless PV inverter topology; IEEE Transactions on Industrial Electronics (accepted for publication)

Chapter 2

Overview of grid connected PV systems

This chapter highlights the advantages of transformerless PV inverters compared to those with galvanic isolation. Furthermore, a summary of several transformerless PV inverter topologies is presented, followed by discussions about the parasitic capacitance of the PV array, emphasizing the safety issues regarding ground leakage currents due to varying voltages imposed over this capacitance.

2.1 Introduction

PV systems connected to the low voltage grid have an important role in distributed generation systems. In order to keep up with the current trends regarding the increase in PV installations, PV inverters should have the following characteristics:

Low cost
- Small weight and size, due to residential installations
- High reliability to match with that of PV panels
- High efficiency
- Be safe for human interaction

During the last decade PV inverter technologies have evolved a lot. As shown in Fig. 2.1, inverter prices have dropped around 50% during the last two decades and efficiency and reliability have increased considerably [1]. Depending of the power rating of the inverter, the price of inverters below *10 kW* varies between 0.2 and 1.2 euro/kW excluding VAT [8]. All this development and improvement happened especially in Europe, USA and Japan. Here one can find many small-scale, building integrated systems that are connected to the grid [9].

In order to decrease the cost-to-efficiency ratio of PV systems, new inverter designs have been developed. A general classification of grid connected PV inverters is as follows [1], [9], [10], [11], [12], [13],[14]:

- central inverters
- string inverters
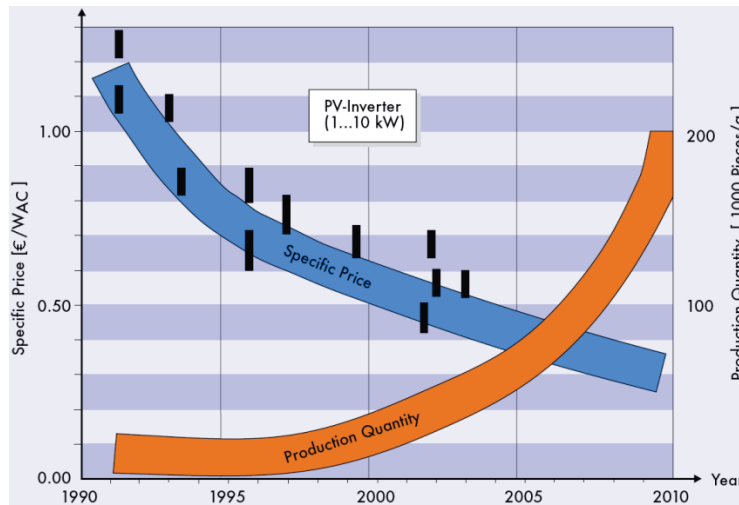- module integrated inverters
- multi-string inverters

Fig. 2.1: Development and prognoses of specific cost and production quantity for a PV-inverter of nominal power between 1 and 10kW during the last two decades [1].

2.1.1 Central inverters

PV plants bigger than *10 kWp* arranged in parallel strings, are connected to one common central inverter (as shown in Fig. 2.2(a)). At first, line commutated thyristor based inverters were used for this purpose. These were slowly replaced by force commutated inverters using IGBTs, because the efficiency of these inverters is higher and their cost is lower.

However the list of its disadvantages is significant:

- need for high-voltage DC cables between PV panels and inverter
- power losses due to common MPPT
- power loss due to module mismatch
- losses in the string diodes
- reliability of the whole system depends on one inverter

2.1.2 String inverters

String inverters, shown in Fig. 2.2(b), were introduced into the European market in 1995. They are based on a modular concept, where PV strings, made up of series-connected solar panels, are connected to separate inverters. The string inverters are paralleled and connected to the grid. If the string voltage is high enough then no voltage boosting is necessary, thereby improving efficiency. Fewer PV panels can also be used, but then a DC-DC converter or a line frequency transformer is needed for a boosting stage.

The advantages compared to the central inverter are as follows:

- no losses in string diodes (no diodes needed)
- separate MPPTs for each string
- better yield, due to separate MPPTs
- lower price due to mass production

2.1.3 Module inverters

An AC module is made up of a single solar panel connected to the grid through its own inverter, as shown in Fig. 2.2(c). The advantage of this configuration is that there are no mismatch losses, due to the fact that every single solar panel has its own inverter and MPPT, thus maximizing the power production. The power extraction is much better optimized than in the case of String inverters. One other advantage is the modular structure, which simplifies the modification of the whole system because of its "plug & play" characteristic. One disadvantage is the low overall efficiency due to the high-voltage amplification, and the price per watt is still higher than in the previous cases. But this can be overcome by mass production, leading to low manufacturing and retail costs [10].

2.1.4 Multi-String inverters

Multi-String inverters have recently appeared on the PV market. They are an intermediate solution between String inverters and Module inverters. A Multi-String inverter, shown in Fig. 2.2(d), combines the advantages of both String and Module inverters, by having many DC-DC converters with individual MPPTs, which feed energy to a common DC-AC inverter. This way, no matter the nominal data, size, technology, orientation, inclination or weather conditions of the PV string, they can be connected to one common grid connected inverter[15], [16].

The Multi-String concept is a flexible solution, having a high overall efficiency of power extraction, due to the fact that each PV string is individually controlled, as done by the Sunny Boy Multi-String 5000 by SMA.
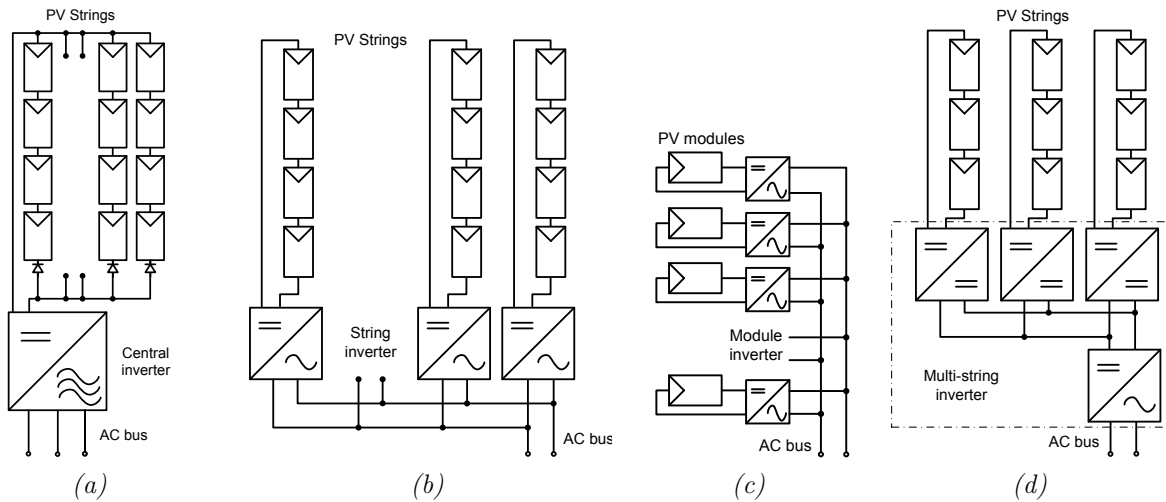
Fig. 2.2: Different grid-connected PV inverter structures: Central inverter (a); String inverter (b);

Module inverter (c) and Multistring inverter (d).

2.2 Grid requirements

If a PV system is connected to the grid, then the generated power has to comply with specific standards, which are regulated by the utility in each country. The main norms that grid connected inverters have to comply with are:

- Total Harmonic Distortion (THD) and individual harmonic current levels
- Power factor (PF)
- Level of injected DC current
- Voltage and frequency range for normal operation
- Detection of islanding operation (islanding or non-islanding functions)
- Automatic reconnection and synchronizing
- Grounding of the system

International Standards that deal with grid connected photovoltaic systems are the following:

- IEC 60364-7-712:2005. Electrical Installations of Buildings. Part 7: requirements for special installations or locations. Section 712: Photovoltaic power supply systems. [17]
- IEEE 1547.1-2005 IEEE Standard Conformance Test Procedures for Equipment Interconnecting Distributed Resources with Electric Power Systems. [18]

- UL 1741. Standard for Safety Inverters, Converters, Controllers and Interconnection System Equipment for Use with Distributed Energy Resources. 7th May 1999, updated in 2005.
- IEEE 929-2000. Recommended Practice for Utility Interface of Photovoltaic (PV) Systems. [19]
- IEC 61727 (1995-06) Photovoltaic Systems – Characteristics of the Utility Interface. [20]
- DS/EN 61000-3-2 (2001) EMC, Limits for harmonic emissions (equipment input current up to and including *16 A* per phase) [21]
- VDE0126-1-1 (2006) Selbsstättige Schaltschtelle zwischen einer netzparalellen Eigenerzeugungsanlage und dem öffentlichen Niederspannungsnetz [22]

Most of the above standards are related to the THD and to the individual harmonic levels in the injected current, the frequency deviation of the grid voltage from the standard one, the PF, the normal operating voltage range and the level of the DC current that is injected in the grid. In [10] a comparison of three different standards is made (IEC61727, IEEE1547 and EN61000-3-2), focusing on the previously enumerated issues.

Regarding DC current injection (an important issue in case of grid connected inverters) the following table can be summarized about the requirements set by each standard:

Table 2-1: Limit of the injected DC current, for different standards [10].

	IEC61727	*VDE0126-1-1*	*IEEE1547*	*EN61000-3-2*	*IEEE 929-2000*
DC current injection	*< 1 % of rated output current*	*< 1 A*	*< 0.5 % of rated output current*	*< 0.22 A corresponds to a 50 W half-wave rectifier*	*< 0.5 % of rated output current*

Furthermore, the VDE 0126-1-1 standard states, that in the case of a DC current injection greater than *1 A*, disconnection is mandatory in *0.2 s*. The other standards do not mention a requirement for disconnection time.

There is only one standard that specifically deals with transformerless PV systems regarding fault and leakage current levels: the German VDE-0126-1-1 standard.

According to the German standard, there are three different currents that have to be monitored:

- Ground Fault current, which happens in case of insulation failure when the current flows through the ground wire;
- Fault current, which represents the sum of the instantaneous values of the main currents, that in normal conditions leads to zero;
- Leakage Ground currents, which is the result of potential variations of capacitive coupled parasitic elements;

The monitoring is typically done using a Residual Current Monitoring Unit (RCMU), which measures the fault and leakage current of the whole system. The standard states that disconnection from the grid is necessary within *0.3 s* in case the leakage current is higher than *300 mA*. Furthermore, it recommends a table detailing the Root Mean Square (RMS) value of the fault/leakage current jumps and their respective disconnection times, as detailed in Table 2-2.

Table 2-2: Leakage current jumps and their corresponding disconnection times for VDE 0126-1-1

Leakage current jump value (mA)	Disconnection time (s)
30	0.3
60	0.15
100	0.04

As shown in Table 2-2, in cases where the RMS value of the fault/leakage current increases by *30 mA*, then disconnection is mandatory within *0.3 s*. This way in case of a fault/accident or too high leakage ground current, the system is disconnected and de-energized.

2.3 Transformerless PV inverters

Depending on the electrical isolation between the PV panels and utility grid, the inverter can be isolated or non-isolated. This galvanic isolation is usually realized by the means of a transformer, which has major influence on a grid-connected PV systems' DC to AC efficiency [23]. The presence of the galvanic isolation in a grid connected PV system depends on the local country regulations [24]. In some countries, like the UK and Italy, galvanic isolation is a requirement and is done either by a low-frequency step-up transformer on the grid side or by a high-frequency transformer on the DC side of the converter, as detailed in Fig. 2.3.(a) and (b), respectively.

On the other hand, there are countries like Germany and Spain, where the galvanic isolation can be left out, in case another technological solution is used to separate the PV array from the electrical grid [25]. A typical transformerless PV system is detailed in Fig. 2.4, which reduces the weight, size, cost and installation complexity of the whole PV system.

One disadvantage of transformerless systems is that the missing line-frequency transformer can lead to DC currents in the injected AC current by the inverter, which can saturate the core of the magnetic components in the distribution transformer, leading to overheating and possible failure [26],[27].

An important advantage of the transformerless solution is the increase in the total efficiency of the system by approximately *2%* [12], [28],[29],[30],[31],[32].

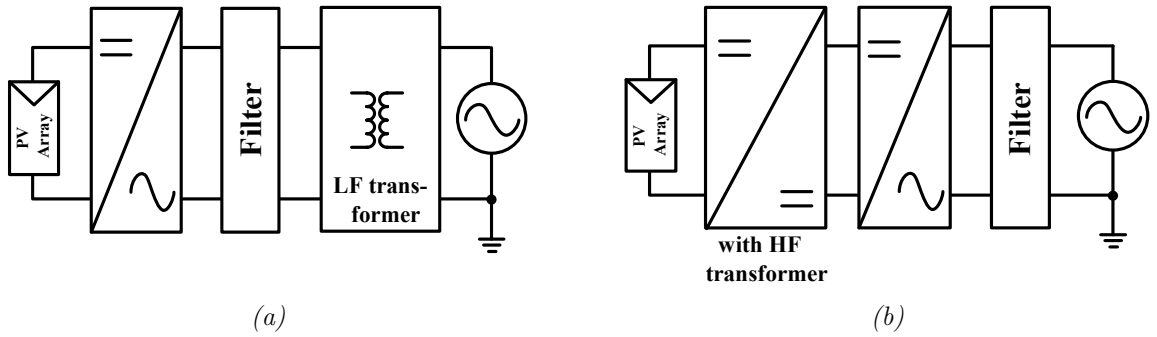
(a)   (b)

Fig. 2.3: Grid-connected PV system using an inverter with galvanic isolation: grid-side low-frequency

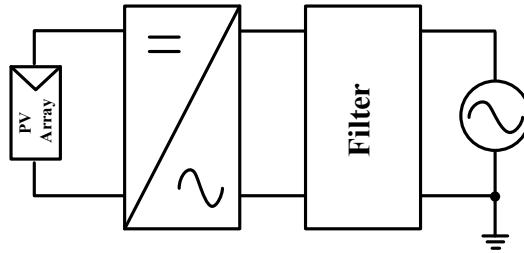(LF) transformer (a) or DC side high-frequency (HF) transformer (b).

Fig. 2.4: Grid connected PV system with transformerless inverter.

PV inverters usually have two efficiencies reported by the manufacturer: the highest DC-AC conversion efficiency, also called as "Maximum Efficiency", and a weighted efficiency dependent on efficiencies at different irradiation levels, called "European efficiency", based on the formula below [29]:

$$\eta_{EU} = 0,03\eta_{5\%} + 0,06\eta_{10\%} + 0,13\eta_{20\%} + 0,1\eta_{30\%} + 0,48\eta_{50\%} + 0,2\eta_{100\%} \qquad (2.1)$$

Fig. 2.5 has been made from a database of more than 400 commercially available PV inverters, presented in a commercial magazine about the photovoltaic industry [33], giving details of, amongst other things, the maximum efficiency, weight and size of the different inverters.
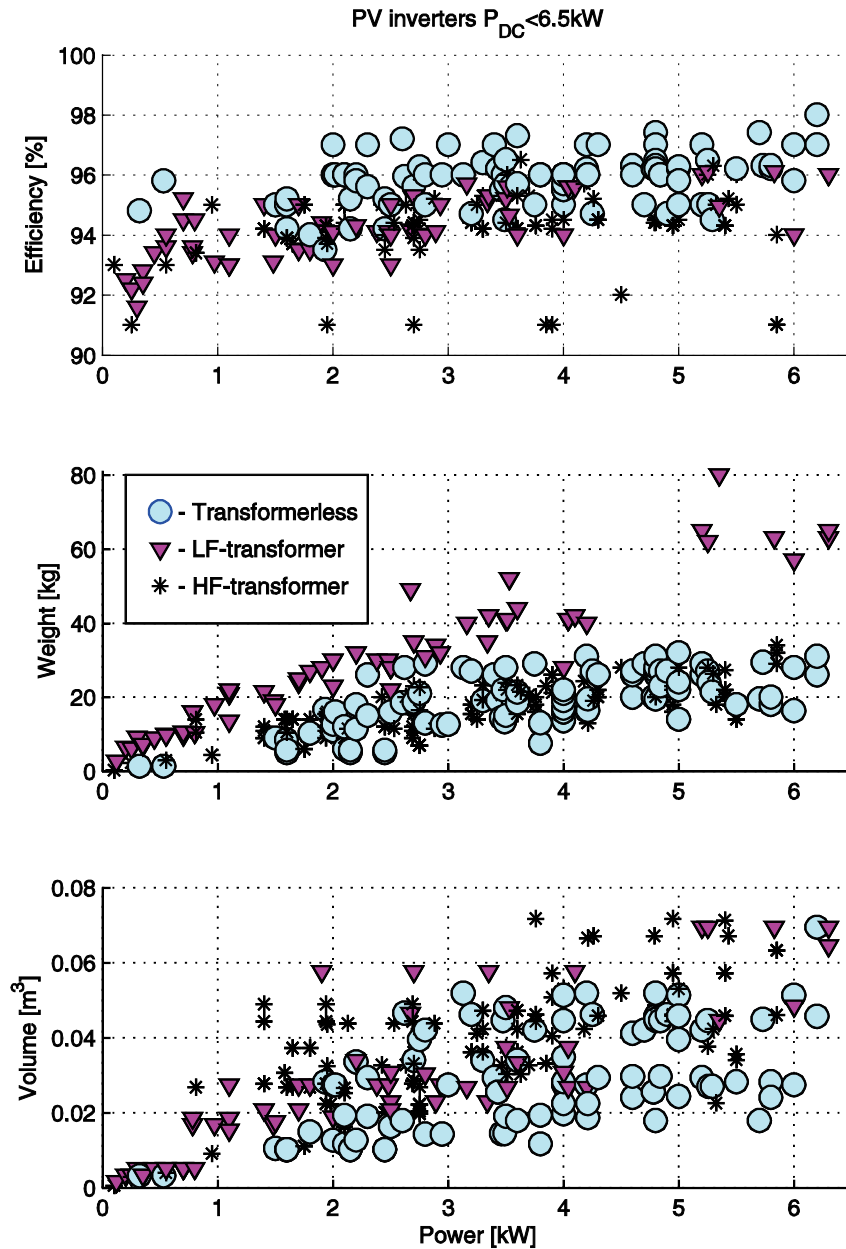

Fig. 2.5: PV inverter comparison, based on PHOTON database.

Transformerless inverters are represented by the dots (O), while the stars (✱) represent the topologies including a high-frequency DC-DC transformer and last the triangles (▼) represent the inverters that have a low-frequency transformer on the grid side, adding a galvanic isolation between the PV and grid. It is shown that in the case of PV systems up to *6.5kW*, transformerless inverters can reach maximum efficiencies

up to *98%*, while inverters with galvanic isolation only have maximum conversion efficiency around *96-96.5%*.

The conclusion drawn from these graphs is that the majority of transformerless inverters have higher efficiency, smaller weight and size than their counterparts with galvanic separation.

In the case of Fig. 2.5, the reason for limiting the power up to *6.5kW* was the fact that there were only 20 inverters between *6.5* and *15kW* and including these in the graph would have influenced the readability of the results.

2.4 Transformerless inverter topologies

Inverters, according to the levels of power conversion, can have one or more stages. A single and double stage topology for a single-phase grid connection is presented in Fig. 2.6 [34].
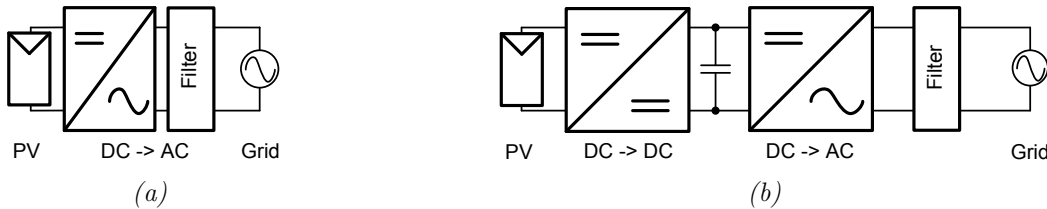

Fig. 2.6: Single stage (a) and double stage including voltage boost (b) grid connected PV inverters.

Depending on the voltage level of the PV array, a voltage-boosting stage can be present, which raises the DC-link voltage of the inverter to the required level. This is the case of the two stage topology, where the PV system includes either a DC-DC boost converter, followed by a DC-AC grid side inverter or a step-up transformer on the AC side [35].

The first PV inverters were based on the technologies used in electrical drives from the beginning of the 1980s. As seen in Fig. 2.7(a), they were line commutated inverters with power ratings of several kW. The major advantages were high efficiency, cheapness and robustness, but the power factor was a major drawback with values between *0.6* and *0.7*.

Nowadays inverters are force commutated inverters having power ranges above *1.5kW*. A "classic" transformerless topology can be seen on Fig. 2.7(b), having an H-Bridge configuration, usually with switching frequencies greater than *16 kHz* to avoid acoustic noise. The efficiency is lower than the line commutated topology, due to the high switching losses. But it is still a robust, cheap and well known technology [36].
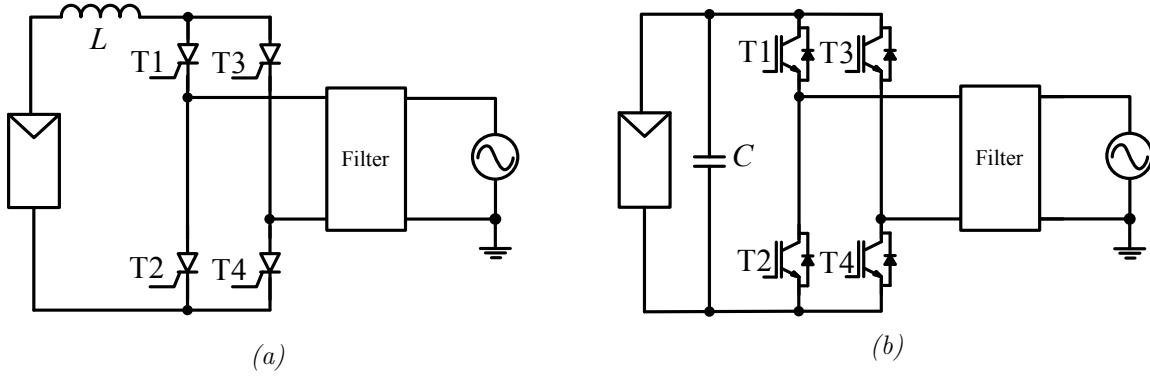
Fig. 2.7: Typical single-phase PV inverter, past and present topology, showing a line commutated inverter(a) and an H-Bridge (force commutated) inverter (b) [36].

In case the voltage level from the PV is lower than the required minimum, then a boost converter is added between the PV array and the inverter. This boosts the input voltage from the PV so the inverter has a DC-link voltage around *400 V* for single-phase systems and up to *700 V* for three-phase grid connection in the European case. Such a single-phase topology can be seen on Fig. 2.8, which differs from Fig. 2.7(b) only by the added boost stage.
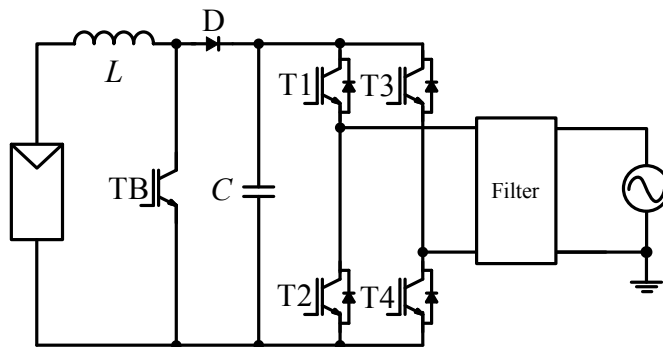

Fig. 2.8: Transformerless PV inverter with voltage boost stage [37].

In [38], a similar topology to Fig. 2.8 is proposed for a grid connected PV system. As presented in Fig. 2.9, it is made up of a boost rectifier that raises the voltage of the PV array from *100 V* to above *680 V*. This half-bridge topology uses the upper switches in case positive output voltage and the lower switch in case when negative output voltage is required. This topology is used by SMA in their old transformerless inverter Sunny Boy 5000TL Multi-String[16].
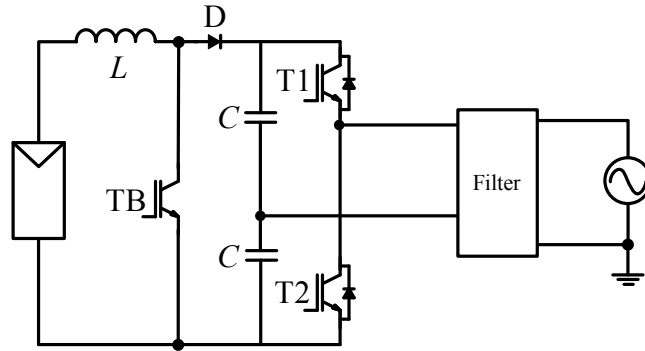
Fig. 2.9: Half-bridge topology with voltage boost stage [38].

Having fewer switches in this topology it implies:

- lower conduction losses
- fewer number of components

The disadvantage is that higher input voltage is needed, which increases the rating of the components.

There are also other, more complicated topologies that were summarized in [38] and are a combination of multiple boost or buck-boost single stage inverters.

The first topology can be seen on Fig. 2.10 and was proposed by Cáceres and Barbi [39]. The DC inputs of the two identical boost DC-DC converters are connected in parallel with a DC source, such as a PV panel for example. Each one of the converters is modulated to produce a unipolar DC biased sinusoidal output, having a *180°* phase-shift between each other. This way the output across the load is a pure sinusoidal waveform.
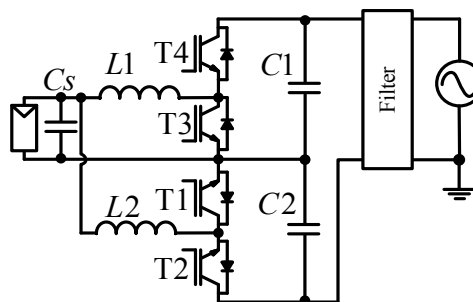

Fig. 2.10: Boost inverter by Cáceres and Barbi [39].

Similarly to the previously presented solution, Vásquez proposed a buck-boost inverter, connecting two buck-boost converters in parallel, the same way as in Fig. 2.10, thereby generating an output voltage either lower or higher than the input. See Fig. 2.11 for details.
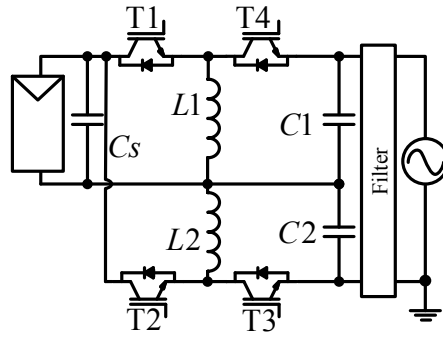
Fig. 2.11: Buck-boost inverter topology by Vásquez [40].

Another buck-boost inverter topology, proposed in [41] for a residential PV power system, is able to operate with a wide input voltage range but needs a split DC input source [42]. The topology can be seen in Fig. 2.12. The two converters share the output and operate each half cycle with their own voltage supplies. It is emphasized in [43], that this topology has the inherent nature of common ground for the DC and AC, which makes it suitable for systems where the grounding is required both for the grid neutral and for the distributed power generation resource.
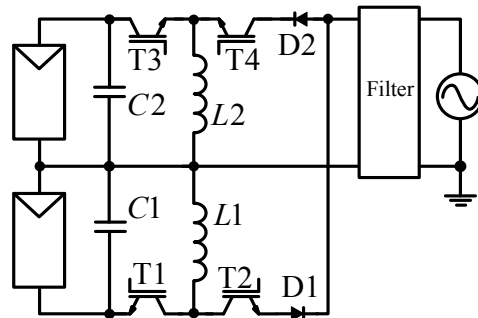

Fig. 2.12: Buck-boost inverter by Kasa [41],[44].

Furthermore, Wang proposed a four-switch resonant buck-boost inverter. The topology can be seen in Fig. 2.13. This zero-current-switching buck-boost inverter operates with switches T1 and T4 and diode D2 in the positive half cycle together with L_{r1} and C_r and with T2, T3 and D1 in the negative half cycle together with L_{r2} and C_r.
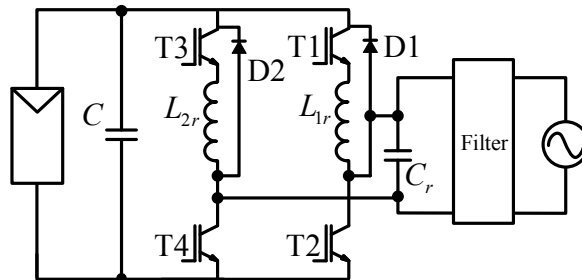

Fig. 2.13: Four-switch resonant buck-boost inverter by Wang [45].

The flying inductor topology patented in [46], reviewed in [37], is shown in Fig. 2.14. It has the advantage of being able to operate in different modes. The positive output current waveform is generated by the converter operating in either buck or boost modes. When the input voltage is higher than the grid voltage, then the inverter operates in buck mode.
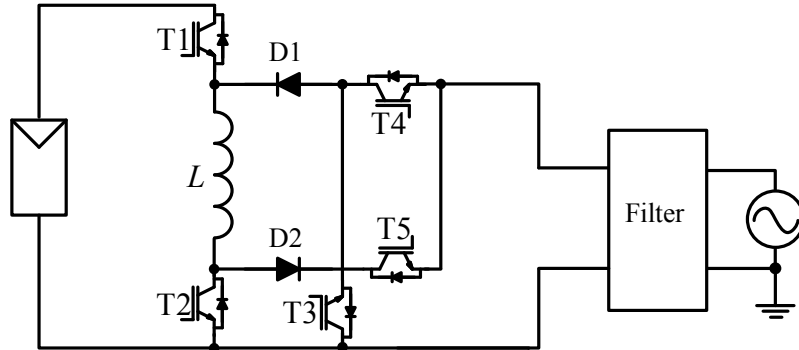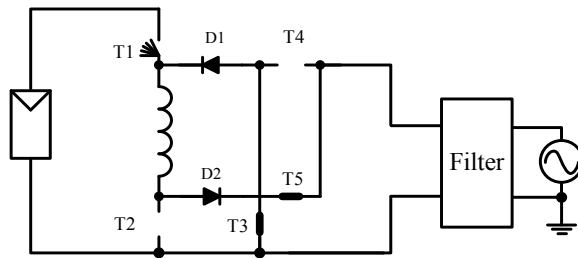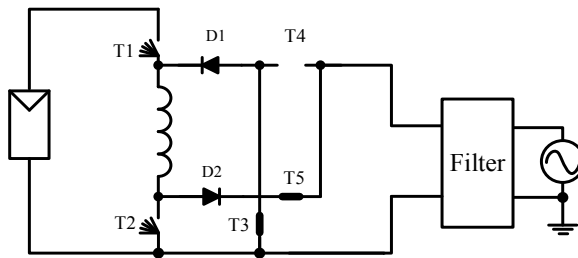

Fig. 2.14: Flying inductor inverter[46].

As shown in Fig. 2.15(a), T1 is sine modulated, T2 and T4 are open all the time, T3 and T5 are permanently closed and D1 acts as a freewheeling diode. In the other case, when the input voltage is below the grid voltage, then (as detailed in Fig. 2.15(b)), T1 and T2 are simultaneously sine modulated, T3 and T5 are permanently closed and T4 is open and D1 acts as a freewheeling diode. The negative current waveform is generated by operating the inverter in buck-boost configuration, as shown in Fig. 2.15(c). T1 is sine modulated, T2 and T4 are permanently closed and T3 and T5 are open. D1 acts as a freewheeling diode.

(a) Buck mode.

(b) Boost mode.
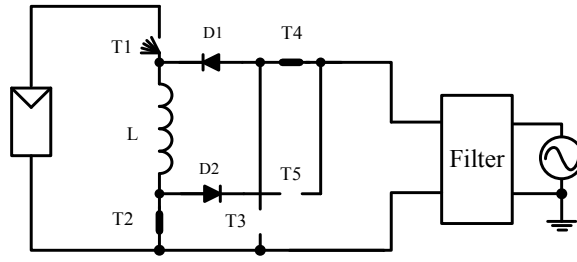
(c) Buck-boost mode.

Fig. 2.15: Three different operation modes of the flying inductor inverter.

The main disadvantage of the above topology is the design requirements for the inductor (L), which serves as an energy storage. Magnetic components add to the size and cost of the converter and reduce the overall efficiency. The advantage of this topology is that the negative terminal of the PV array is always connected to grounded grid neutral, thereby fixing the potential of the PV [37]. This topology is used by Siemens in their Sitop Solar Master 1100 PV inverter.

A similar topology to the flying inductor topology is shown in Fig. 2.16 and has been presented in [47]. During the inverting period, when the grid voltage is negative, T1, T3 and T6 are in their conducting state, while T4 and T5 are in their blocking state. T2 is used to shape the output voltage over L2 into a sinusoidal form, using PWM modulation. When the grid voltage is positive, the inverter is in the non-inverting period and T2, T4 and T5 are in their conducting state, while T3 and T6 are blocking. T1 is used to shape the output voltage over L2 using a sinusoidal PWM.
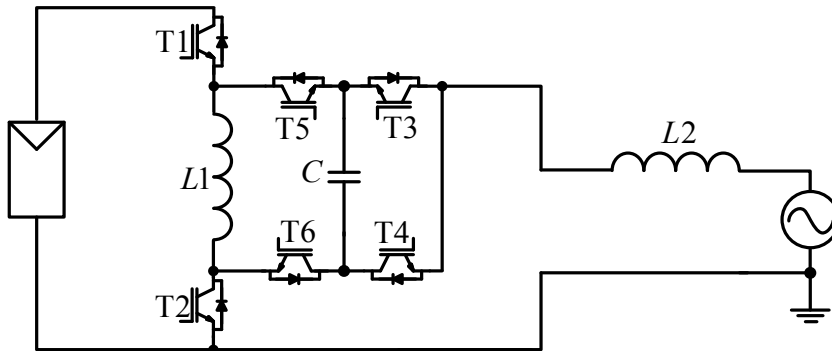
Fig. 2.16: Transformerless PV inverter topology patented by Schekulin [47].

Fig. 2.17 shows a grid connected neutral point diode clamped inverter having a boost stage at its DC input. For the positive current half-wave switches T1 and T2 are used. Turning T2 and T3 ON generates the zero output voltage. And finally, the negative half wave is generated by the pulse-width modulation of T3 and T4. This topology allows the connection of the midpoint of the DC bus to grid neutral, thereby reducing the voltage fluctuations between the PV array and ground [37], [48].

Fig. 2.17: Neutral point diode clamped inverter [37], [49] and [50].
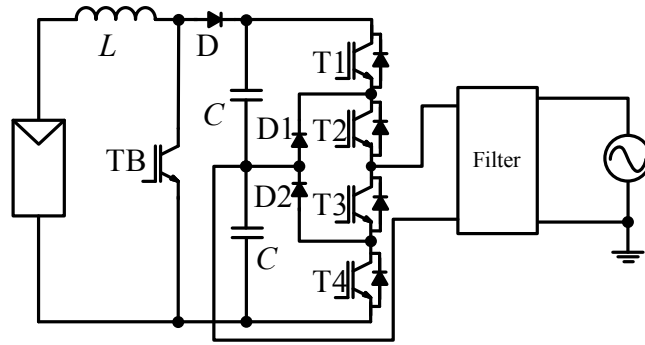
A patented topology shown in [51], called the Highly Efficient and Reliable Inverter Concept (HERIC), uses a modified version of the H-Bridge, by adding two extra switches connected in series with two diodes as shown in Fig. 2.18. The two extra switches (T5 and T6) are used for the freewheeling period and increase the efficiency of the inverter due to the fact that the freewheeling current will not go back to the DC-link capacitor, but it finds a path through T5 or T6 and the respective diode, depending on the sign of the current.
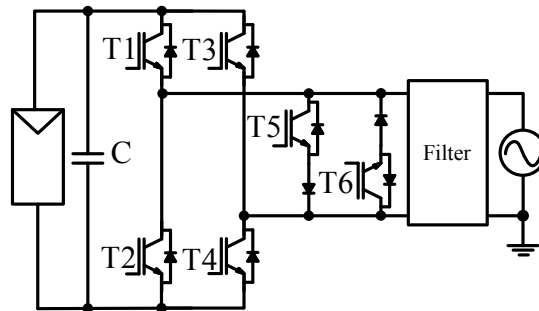
Fig. 2.18: Highly Efficient and Reliable Inverter Concept from Sunways [51].

Another patented inverter topology is again an H-Bridge hybrid. SMA calls it the H5 topology. As detailed in Fig. 2.19, it is made up of a standard H-Bridge topology with an added fifth switch on the DC side. Using this circuit configuration, maximum conversion efficiencies of up to *98%* have been reported, depending on the input voltage.
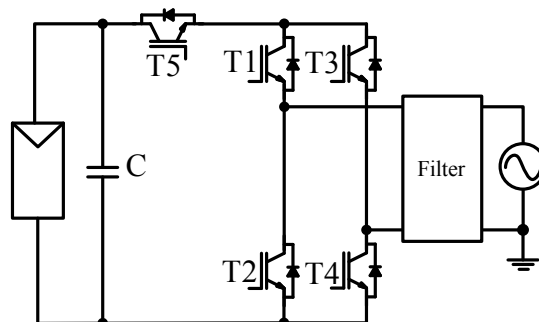

Fig. 2.19: H5 topology from SMA [52].

A similar topology to the previous one is presented in Fig. 2.20, which also uses a modified H-Bridge topology, and adds two extra switches and two diodes. In [53] it is shown that the conversion efficiency of this topology is in the range of *97%*, decreasing only in case the input DC voltage is increased above *350V*, but even in those cases it stays above *95%*.
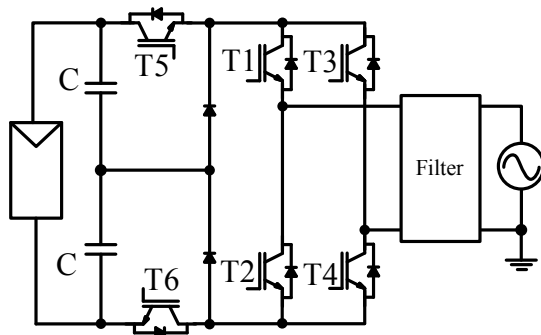

Fig. 2.20: Transformerless topology by Gonzales et al. [53].

There are several more topologies that have been proposed for transformerless PV inverters in [54],[55],[56], [57], [58] and [59], although their major disadvantage is that they have several conversion stages and need a complex control structure, thereby decreasing the overall conversion efficiency and increasing the complexity and the component count of the inverter.

The PV inverter industry has developed a lot in the last few decades. During these years many transformerless topologies have been proposed, but only a few have been accepted by the industry as suitable topologies for grid-connected PV systems. Therefore, inverters available on the commercial market include the most promising topologies, from the point of view of the structure, complexity, safety, price and efficiency.

2.5 Parasitic capacitance of PV arrays

Nowadays most photovoltaic panels have a metallic frame, which is required to be grounded in almost all countries, in order to comply with the safety regulations and standards. Since PV panels have a considerable surface area, this with the metallic frame forms a parasitic capacitance, shown as $C_{G\text{-}PV}$ in Fig. 2.21. The value of this parasitic capacitance depends on the:

- Surface of the PV array and grounded frame
- Distance of PV cell to the module
- Atmospheric conditions
- Dust and humidity, which can increase the electrical conductivity of the panel's surface [2].

In [60] the parasitic capacitance of certain PV panels has been measured to be around *150 pF*. If the surface of the panel is fully covered with tap water, the parasitic capacitance increased to *9 nF*, approximately 60 times its previous value. According to the measurements the parasitic capacitance varies between *50 nF* and *150nF* for each *kW* of installed PV panels. In [60],[61] and [62] the parasitic capacitance has been measured for different PV panels, varying from *100 pF* to *3.6 μF*. It is also mentioned that in the case of thin film modules the measured parasitic capacitance reaches values up to *1 μF/kW*, due to the metallic sheet on which the cells have been deposited.

In order to have a fairly precise value for simulations, the parasitic capacitance has been also measured for the following multicrystalline PV panels: Soleil FVG 36-125, Kyocera KS10 and BPSolar MSX120.

An HP/Agilent 4284A Precision LCR Meter has been used to measure the series capacitance value, using the following output voltage settings: f_{sw-LCR}=10 kHz, $V_{out-LCR}$=5 V. The measurements, shown in Table 2-3, have been done by connecting the first terminal of the LCR meter to the output terminal of the PV panel (positive, negative or both short-circuited) and the second terminal of the LCR meter to the frame of the PV panel.
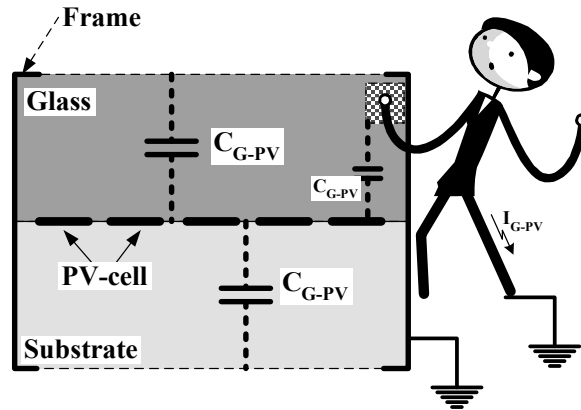

Fig. 2.21: Parasitic capacitance in PV panels [2].

In case of the measurement using someone's palm, the second terminal of the LCR meter was connected to the palm directly, while the whole palm touched the surface of the PV panel. In this case there were two different palms: a copper palm, represented by a copper plate, having the size of an average palm and a normal human palm.

The frequency of the output voltage has been changed for the following values: *1kHz, 10 kHz, 20 kHz* and *50 kHz*. No difference has been observed in case of the first set of measurements, representing the case when the PV panels and the palm were dry. The measured parasitic capacitance values were not influenced by the frequency of the voltage.

Furthermore, the atmospheric conditions were changed by covering the surface of the PV panels with moisture and the measurements were repeated, in order to take the readings for the wet case too.

The results are summarized also in Table 2-3, and it can be seen that in humid atmospheric conditions the measured values of the parasitic capacitance have significantly increased, in some cases by a factor of 10 or more, depending on the frequency of the imposed voltage.

Table 2-3: Parasitic capacitance measurements.

	Soleil FVG 36-	Kyocera KS10	BPSolar MSX120
Surface of PV panel	204 **x** 352 mm^2	1197 **x** 535 mm^2	1108 **x** 991 mm^2
Power at MPP (STC)	80 W	10 W	120 W
$C_{G\text{-}PV}$(1 panel)	130 pF	57 pF	21 pF
$C_{G\text{-}PV}$(1panel) wet	2.58 nF @ 1 kHz 1.38 nF @ 10 kHz 1.12 nF @ 20 kHz 770 pF @ 50 kHz	3.44 nF @ 1 kHz 2.39nF @ 10 kHz 1.99nF @ 20 kHz 1.37 nF @ 50 kHz	9 nF @ 1 kHz 3 nF @ 10 kHz 2 nF @ 20 kHz 1.15 nF @ 50 kHz
$C_{G\text{-}PV}$(2panels)	247 pF	101 pF	not available
$C_{G\text{-}PV}$(1panel+ palm)	140 pF	150 pF	200 pF
$C_{G\text{-}PV}$ (1panel+palm) wet	215 pF @ 1 kHz 185 pF @ 10 kHz 175 pF @ 20 kHz	350 pF @ 1 kHz 230 pF @ 10 kHz 180 pF @ 20 kHz	320 pF @ 1 kHz 200 pF @ 10 kHz 185 pF @ 20 kHz
$C_{G\text{-}PV}$(1panel+ copper plate)	160 pF	140 pF	150 pF
$C_{G\text{-}PV}$(1panel+ copper plate) wet	219 pF @ 1 kHz 210 pF @ 10 kHz 208 pF @ 20 kHz 205 pF @ 50 kHz	235 pF @ 1 kHz 212 pF @ 10 kHz 207 pF @ 20 kHz 200 pF @ 50 kHz	276 pF @ 1 kHz 257 pF @ 10 kHz 251 pF @ 20 kHz 244 pF @ 50 kHz

This parasitic capacitance is present in every PV installation and may or may not lead to leakage ground current, depending on the existence of the return path within the circuit. Since the value of this parasitic capacitance changes within wide ranges depending on construction, atmospheric conditions, etc., a value of *100 nF/kW* has been chosen to be used in simulations, in order to accurately simulate the behavior of the whole PV system, with regards to the ground leakage current. The *100 nF/kW* value has been chosen taking into account the worst case scenario in case of a *5 kW* PV installation, made up of 40 BPSolar 120MSX panels.

2.6 Leakage ground current

A transformerless topology lacks the galvanic isolation between the PV array and grid. This way the PV panels are directly connected to the grid, which means that

there is a direct path for the leakage ground currents caused by the fluctuations of the potential between the PV array and the grid. These voltage fluctuations charge and discharge the parasitic capacitance formed between the surface of the PV and grounded frame, shown as $C_{G\text{-}PV}$ in Fig. 2.22. The parasitic capacitance together with the DC lines that connects the PV array to the inverter, form a resonant circuit and the resonance frequency of this circuit depends on the size of the PV array and the length of the DC cables [63],[64].

A study, presented in [60] discusses the electrical hazards when a person touches the surface of the PV array. Based on the inverter topology, PV panel structure and modulation strategy, when touching the surface of the panels, a ground current could flow through the human body and if the current is above a certain levels it could lead to a shock or resulting in personal injury, as also discussed in [65], [66]. The path of the ground current ($I_{G\text{-}PV}$) flowing through the parasitic capacitance of the PV array is shown with a grey intermittent line in Fig. 2.22.
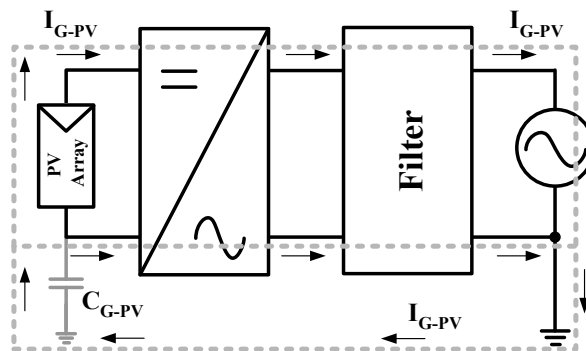

Fig. 2.22: Transformerless PV system showing the parasitic capacitance between the PV and the grounded frame of the array and the path of the alternating ground leakage current.

In [60] several recommendations are given, which lead to the minimization of the before mentioned leakage current, by:

- grounding the frame of the PV array, which reduces the capacitance, thereby minimizing the ground leakage current.
- carefully choosing the topology and the modulation strategy, thereby reducing the voltage fluctuations between the PV array and ground.
- disconnecting the inverter under service maintenance.

The VDE0126-1-1 standard recommends the use of a Residual Current Monitoring Unit (RCMU) in order to monitor the safe operation of the grid connected PV system. Several experimental tests have been done in order to test two commercially available current sensors that could be used for ground leakage current measurement.

The **LEM CT 0.2-P** [67] sensor is a differential current sensor used for current measurements up to *400 mA*. The step response tests showed that using this sensor the readings are accurate in all conditions. There are some high frequency oscillations in the sensor output in the case of the high frequency capacitive discharge test, but otherwise the sensor was very accurate and had a steady state error below *5%* of the reading. Step response tests had less than *20%* overshoot above the reference level and the output stabilized after *0.2 s*.

The **Telcon HES 25VT** [68] sensor was also tested for differential current measurement, by modifying the auxiliary circuit based on the suggestions on the supplier's webpage, in order to be able to measure mA currents. Direct currents could be measured accurately. On the other hand, the *50 Hz* current influenced the reading and a *50 Hz* component was present in the sensor output having amplitude proportional to the level of the *50 Hz* current. The influence was further investigated and it was found out that the position of the wires relative to the Hall sensor is very important and the output of the sensor is very sensitive to this position.

The details regarding these tests are included in Appendix A.

2.7 Summary

This chapter shows the advantages of transformerless PV inverters compared to topologies with galvanic isolation. It is shown that transformerless topologies are smaller in size and have higher efficiencies than inverters with high-frequency or low-frequency transformers. Furthermore, a summary of several transformerless PV inverter topologies is presented, detailing the many different topology structures that are used by the PV industry or have been proposed as transformerless PV inverters. Finally the parasitic capacitance of the PV array is discussed and measured in case of several commercial PV panels, emphasizing the safety issues regarding ground leakage currents due to varying voltages imposed over this capacitance.

Chapter 3

Investigation of transformerless topologies

In this chapter the modeling of several transformerless grid connected topologies is done. For each case the voltage to ground and leakage ground current is measured and, based on the result, a conclusion is given regarding the use of such a topology in transformerless grid-connected PV systems.

3.1 Introduction

The voltage to ground is measured across $C_{G\text{-}PV}$, between the DC+ and ground respectively, DC- and ground terminals of the PV array, as shown in Fig. 3.1. The parasitic capacitance of the PV array is modeled using a simple capacitor, through which the leakage current finds its path to ground. This leakage current is measured and, based on these results, an individual conclusion is drawn for each topology.
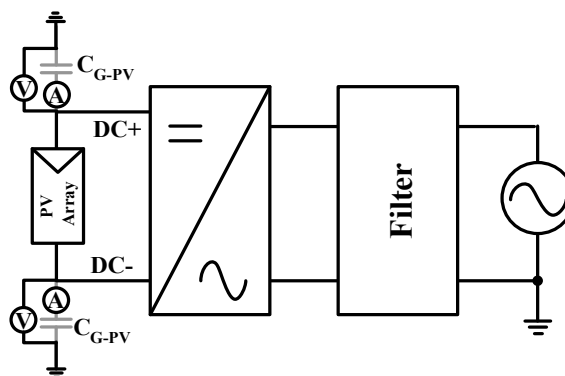

Fig. 3.1: Voltage to ground and leakage ground current measurement setup.

Simulations were done in MATLAB Simulink with the PLECS toolbox, used to model the electrical part of the system, as detailed in Publication II. The implemented control strategy is described in Publication I. The simulation parameters are given in Table 3-1.

Table 3-1: Parameters used in case of the simulation.

Simulation step size	$T_s=2{,}5e\text{-}7$ s (250 ns)
Switching frequency	$f_{sw}=10$ kHz
Single phase DC voltage	$Vdc1=400$ V
Three-phase DC voltage	$Vdc3=700$ V
DC-link capacitance	$C_{dc}=1$ mF
Output filter inductance	$L_f=1.8$ mH
Output filter capacitance	$C_f=2$ μF
Grid voltage (peak of phase to neutral voltage)	$V_g=325$ V
Grid frequency	$f_g=50$ Hz
Grid inductance	$L_g=50$ μH

Two LCL filter configurations can be considered for the grid side filter, as presented in Fig. 3.2, having inductor L_f only in the line branch or like in Fig. 3.3, having inductor L_f split equally between the line and neutral branches. The current ripple is identical for both, although the leakage current is greatly influenced by the filter configuration, as will be shown in the simulations. Only the LCL configuration has been used for the grid side filter, because it has the advantage over the L_f and LC filter configurations that it reduces the dependence on grid parameters by providing a better decoupling between the filter and grid impedance [69].
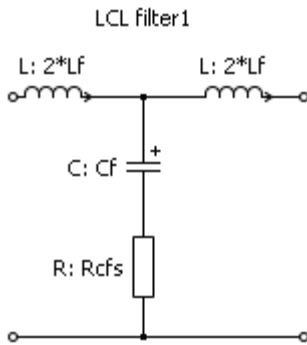

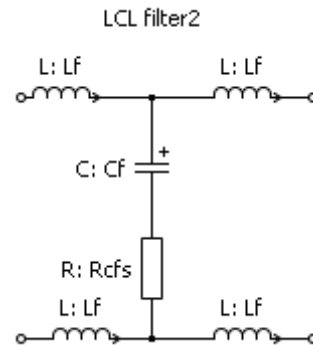Fig. 3.2: LCL filter configuration (case 1).

Fig. 3.3: LCL filter configuration (case 2).

The simulations include the following topologies:

- Single-phase:
  - H-Bridge with bipolar modulation

- o H-Bridge with unipolar modulation
- o H-Bridge with hybrid modulation
- o H-Bridge with AC bypass (HERIC)
- o H-Bridge with DC bypass (H5-SMA)
- o H-Bridge with DC bypass (6 switches)
- o Half-Bridge
- o Neutral Point Clamped
- Three-phase inverter
  - o Three-phase Full-Bridge
  - o Three-phase Full-Bridge with split capacitor
  - o Three-phase Full-Bridge with split capacitor using staggered modulation
  - o Three-phase Neutral Point Clamped

3.2 Single-phase topologies

Single-phase systems are mostly used in the private sector. The majority of such PV systems can have up to *5kW* and are roof mounted with a fixed tilt and a southward orientation.

3.2.1 H-Bridge topology with Bipolar PWM

The H-Bridge is a well-known topology and it is made up of two half bridges. This topology has also been used in motor drives or UPS applications. To control the four switches of this topology several PWM techniques can be implemented. The simplest one is the bipolar PWM [70], which modulates switches T1-T4 (Fig. 3.4) complementary to T2-T3 (Fig. 3.5), resulting in a two level output voltage $(+V_{DC}$ and $-V_{DC})$. The conversion efficiency is reduced due to the fact that during the freewheeling period the grid current finds a path and flows back to the DC-link capacitor.
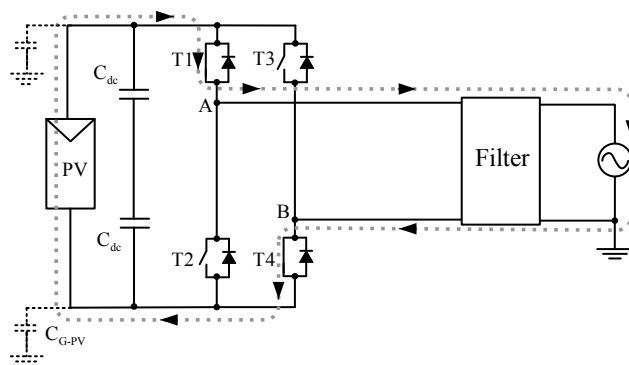

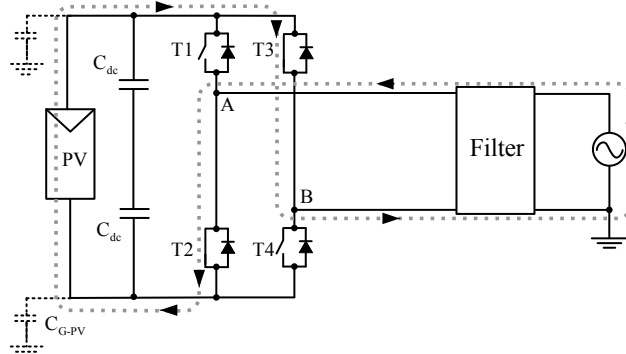*Fig. 3.4: T1-T4 turned-ON, for $+V_{DC}$ output voltage.*

Fig. 3.5: T2-T3 turned-ON, for -V_{DC} output voltage.

Fig. 3.6 shows an FFT of the voltage to ground of the PV array when the grid side filter has the inductors only in the line side. In this case there are high frequency components at the switching frequency and multiples of it, having very high amplitudes. If these high frequency voltage fluctuations are imposed on the parasitic capacitance of the PV array, then the leakage current will be very high and the exact value of the current will depend only on the value of the parasitic capacitance ($C_{G\text{-}PV}$). Therefore it can be said, that this particular case with such a filter configuration is not suitable for transformerless PV systems.
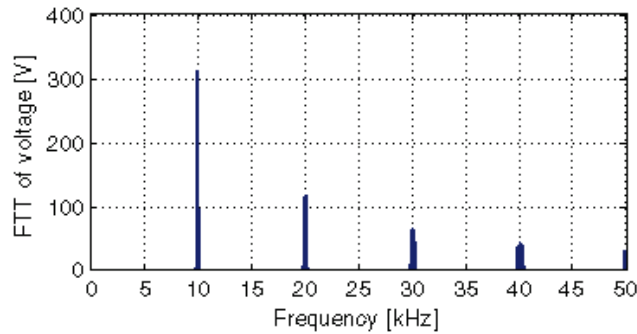

Fig. 3.6: Simulation results, FFT of voltage to ground having a bipolar PWM (grid side filter is according to case 1 from Fig. 3.2).

On the other hand, when the grid side filter inductors are equally distributed in both line and neutral connections, case 2 presented in Fig. 3.3, the bipolar PWM strategy will result in a constant common-mode voltage and the voltage to ground of the PV array will only fluctuate with the grid frequency with an amplitude half of the peak value of the grid voltage, as also shown in Fig. 3.7 for the simulated waveforms and in Fig. 3.8 for the experimental measurements. This means that the H-Bridge with bipolar modulation, having a grid side filter with inductors equally distributed between both line and neutral, is suitable for transformerless PV systems. The only drawback is the conversion efficiency, as discussed earlier.
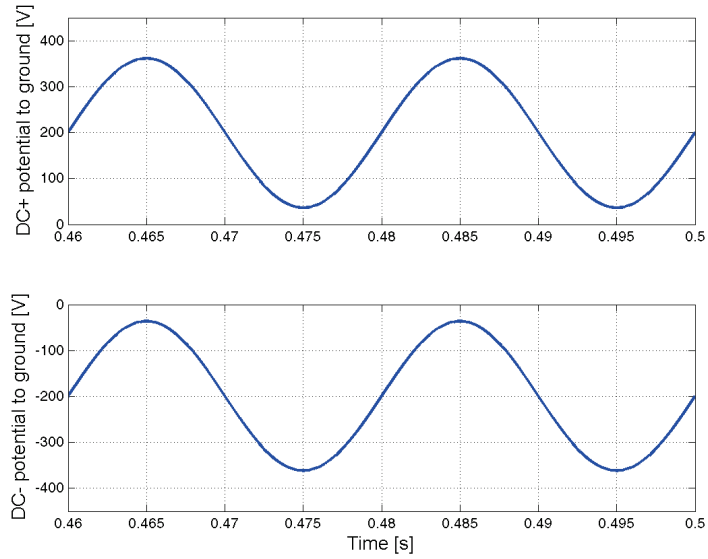
Fig. 3.7: Simulation results, voltage to ground for both terminals of the PV array with bipolar PWM (grid side filter is according to case 2 Fig. 3.3).
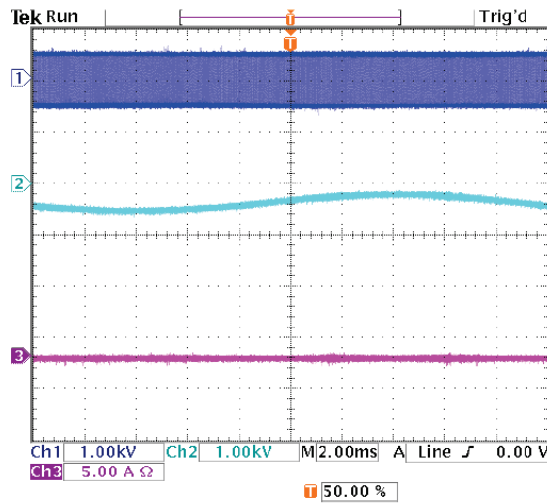

Fig. 3.8: Experimental measurements showing, on Channel 1 the bipolar output of the converter, on Channel 2 the voltage to ground (DC- terminal of the PV array) and on Channel 3 the leakage ground current for the single-phase inverter with bipolar PWM (grid side filter is according to case 2 Fig. 3.3).

3.2.2 H-Bridge topology with Unipolar PWM

This H-Bridge topology uses a different PWM than the bipolar one, which results in unipolar output voltage *(+Vdc, 0* and *-Vdc)* that has twice the switching frequency. The advantage of this method is that the grid side filter elements need to be much smaller due to the unipolar output of the converter and also due to the fact that the

frequency of the output voltage is twice the switching frequency. Therefore, the switching frequency in this case has been set at *5 kHz*. Furthermore, during the freewheeling period, the grid current finds a path through the short-circuited output of the converter, either through T1-T3, as shown in Fig. 3.9 or similarly through T2-T4.
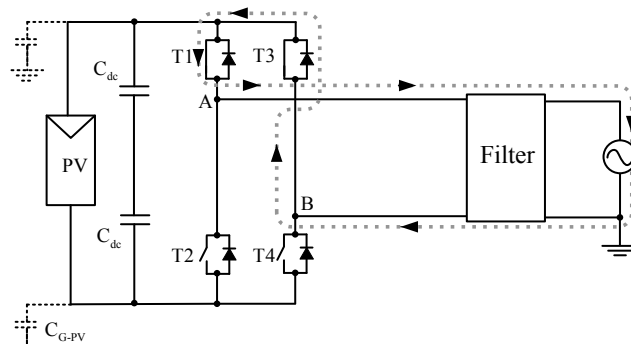

Fig. 3.9: Zero voltage vector, using T1-T3 as free-wheeling path.

On the other hand, there is a big disadvantage in case the unipolar PWM is used for transformerless PV systems, regarding the voltage to ground of the PV array and the ground leakage currents. As shown in Fig. 3.10, the modulation strategy generates a varying common-mode voltage. The FFT of the voltage shows that components at the switching frequency have very high amplitudes in the range of V_{DC}.
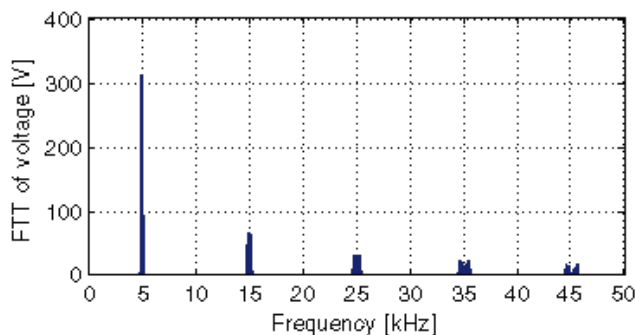
Fig. 3.10: FFT of simulated voltage to ground having a unipolar PWM.
(grid side filter is according to case 2 Fig. 3.3).

Also the experimental measurements, shown in Fig. 3.11, confirm the high frequency voltage components present in the voltage to ground measured between the DC- terminal and the ground connection, leading to very high leakage ground current, with peaks well above *5 A*. Knowing this fact, it can be stated that the H-Bridge with unipolar PWM cannot be used in transformerless PV systems.

Fig. 3.11: Experimental measurements showing, on Channel 1 the unipolar output of the converter, on Channel 2 the voltage to ground (DC- terminal of the PV array) and on Channel 3 the leakage ground current for the single-phase inverter with unipolar PWM (grid side filter is according to case 2 from Fig. 3.3).
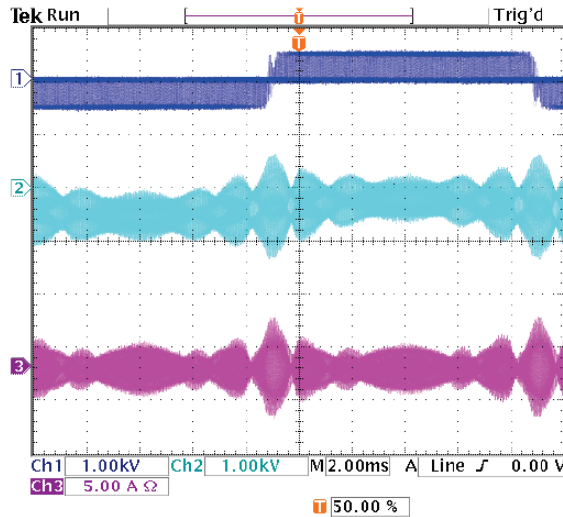
3.2.3 H-Bridge topology with hybrid modulation

Another type of modulation that can be used in case of an H-Bridge is a hybrid modulation, also called single-phase chopping [60],[71]. In this case, one leg of the inverter is modulated with the switching frequency, while the second leg is switched with the grid frequency. This way the neutral line of the topology is connected either to the positive or the negative DC terminal, depending in which half period the reference signal is.

In case the filter inductor is only placed in the phase connector and the neutral connector is left inductance free, as shown in Fig. 3.2, the simulated voltage to ground of the PV array will look as presented in Fig. 3.12, having a square waveform with *50 Hz frequency*. Due to the sharp changes in the voltage that happens every *10 ms*, the leakage ground current will have *100 Hz* spikes. The amplitude of these spikes will depend on the value of the parasitic capacitance and therefore it might lead to a leakage ground current that is above the allowed limit set in the VDE 0126 standard. Besides the square wave shape of the voltage to ground, this modulation technique has another drawback, which is the two quadrant operation, making it impossible to have reactive power flow [60].
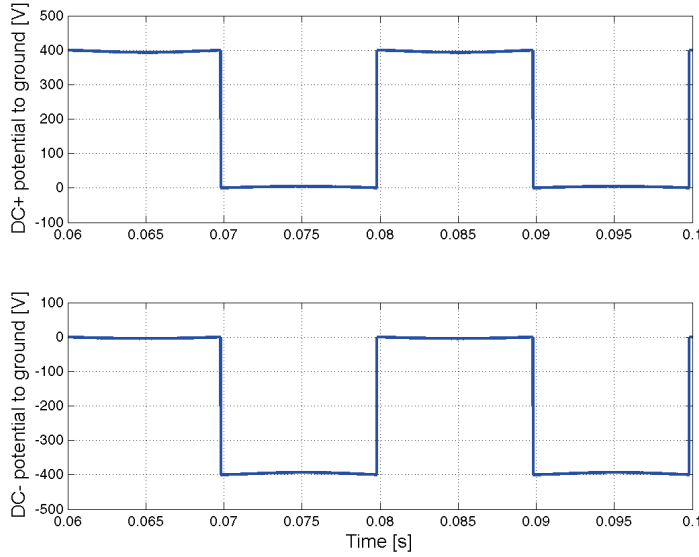
Fig. 3.12: Voltage to ground for both terminals of the PV array (H-Bridge topology; output filter according to case 1 from Fig. 3.2).

3.2.4 HERIC topology from Sunways

To keep the high efficiency and all the advantages given by the unipolar PWM, but still have the common-mode behavior as in case of the bipolar PWM, the H-Bridge topology has been modified as presented in[51], the Highly Efficient and Reliable Inverter Concept (HERIC). The modification includes two extra switches (T5-T6) each connected in series with a diode. During the zero voltage vector, depending on the sign of the reference voltage, either T5 of T6 are turned ON, while T1, T2, T3 and T4 are all in their OFF state and the PV array is disconnected from the grid, as shown in Fig. 3.13. This way there is a possibility of achieving the zero voltage vector and the output voltage will be unipolar, having the same frequency as the switching frequency and there will be no high frequency fluctuations present at the DC terminals of the PV array. Furthermore, the efficiency of the inverter is still kept high, because during the freewheeling period, the load current is short-circuited through T5 or T6, depending on the sign of the grid current.
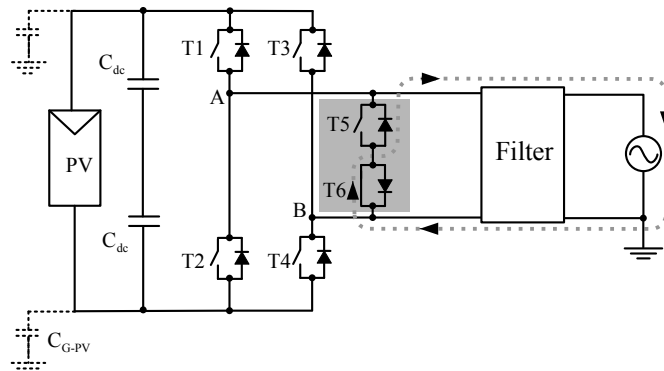

Fig. 3.13: Path of the current during the zero voltage vector, for positive load current (HERIC).

As seen in Fig. 3.14, the common-mode behavior of the HERIC topology is similar to the H-Bridge with bipolar PWM. The voltage to ground of the PV array terminals will only have a sinusoidal shape, while having the same high conversion efficiency as the H-Bridge with unipolar switching.

Based on these results, it can be stated that the HERIC topology is suitable for transformerless PV systems. Unipolar output voltage is achieved and the PV array is disconnected from the grid during the period of the zero voltage vector, using a method called AC decoupling.

Fig. 3.14: Voltage to ground for both terminals of the PV array for the single-phase HERIC topology (output filter according to case 2).

3.2.5 H5 topology from SMA

The H5 topology [52], used by SMA in many of their transformerless inverters, uses the same idea for the generation of the unipolar output voltage: disconnection of the PV array from the grid during the zero voltage vector. The used PWM is a hybrid one. T1 and T3 are switched with the grid frequency; T1 is continuously ON during the positive half, while T3 is continuously ON during the negative half of the reference voltage. To make the positive voltage vector, T5 and T4 are switched simultaneously with high frequency, while T1 is ON and the current will flow through T5-T1 returning through T4, as shown in Fig. 3.15.
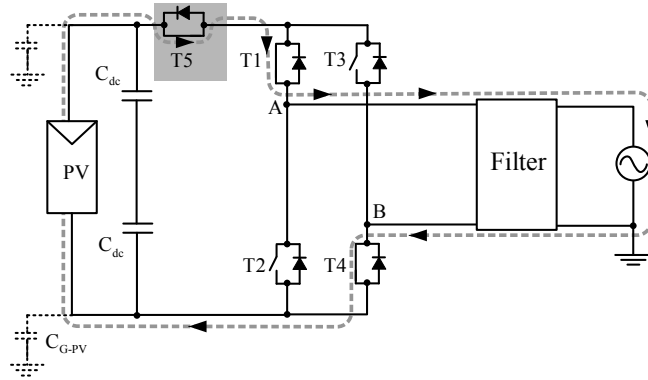
Fig. 3.15: Path of the current in case of the positive voltage vector, for positive load current (H5-SMA).

During the zero voltage vector, T5 and T4 are turned OFF and the freewheeling current finds its path through T1-T3, as detailed in Fig. 3.16. The negative voltage vector is done by switching T5 and T2 simultaneously with high frequency, while T3 is ON, during the corresponding half period of the reference voltage and the current will flow through T5-T3 returning through T2.
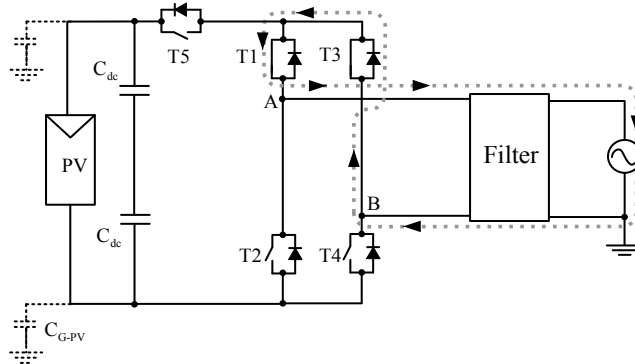
Fig. 3.16: Path of the current in case of the zero voltage vector, for positive load current (H5-SMA).

As seen in Fig. 3.17, the common-mode behavior of the H5 topology is similar to the H-Bridge with bipolar PWM. The voltage to ground of the PV array terminals will only have a sinusoidal shape, while having the same high conversion efficiency as the H-Bridge with unipolar switching.

Based on these results it can be stated that the H5 topology is suitable for transformerless PV systems. Unipolar output voltage is achieved by disconnecting the PV array from the grid during the period of the zero voltage vector, using a method called DC decoupling.
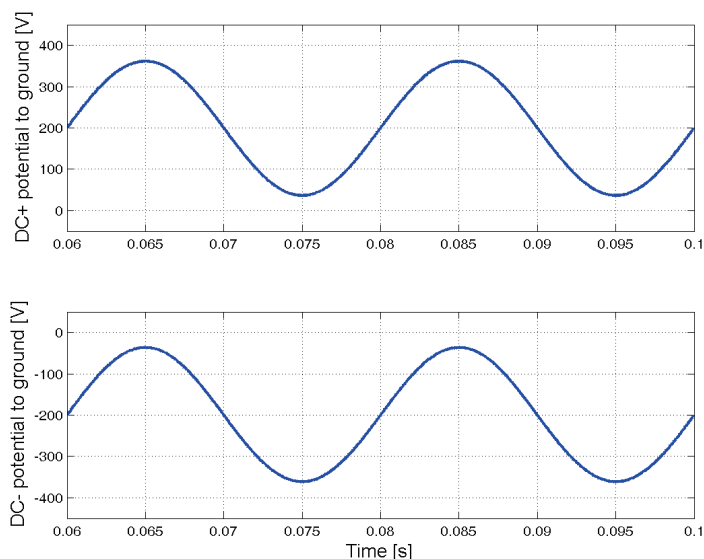
Fig. 3.17: Voltage to ground for both terminals of the PV array for the single-phase H5 topology (output filter according to case 2).

3.2.6 Single-phase topology with DC decoupling (Ingeteam)

Another topology using the DC decoupling method is the one presented in [53], which adds two extra switches and two extra diodes to the H-Bridge topology. The modulation strategy in case of this topology is also a hybrid one. The active voltage vector is achieved by switching T5-T6 with high frequency. Switches T1-T4 are switched with the grid frequency and in antiparallel to T2-T3, depending on whether the reference voltage is in the positive or negative half period. This way the output of the converter will be a unipolar voltage, like in case of the HERIC and H5 topologies.

Fig. 3.18: Single-phase topology with DC decoupling used for transformerless PV systems.

The common-mode behavior of the topology is also similar to the HERIC and H5 topologies, since the voltage to ground of the PV array has only a sinusoidal shape and the frequency is the grid frequency, as shown in Fig. 3.19.

Based on these results it can be stated that this topology is also suitable for transformerless PV systems. Unipolar output voltage is achieved by disconnecting the PV array from the grid during the period of the zero voltage vector, using DC decoupling.
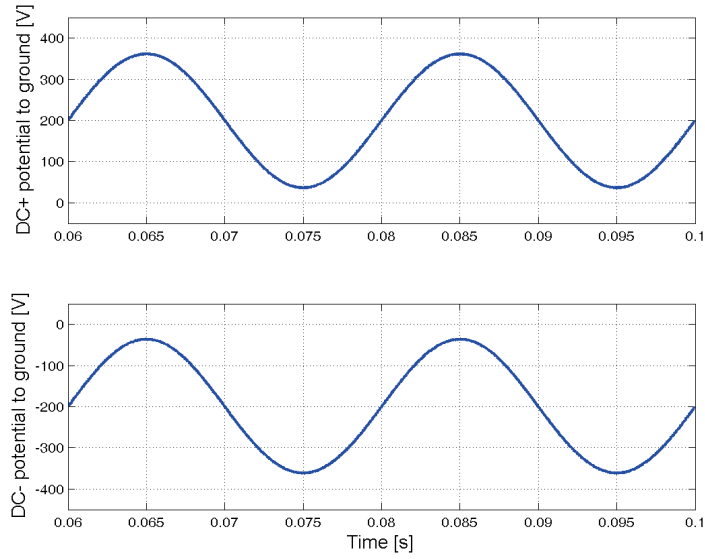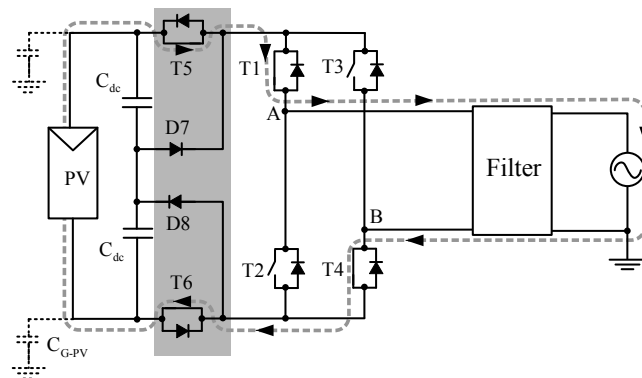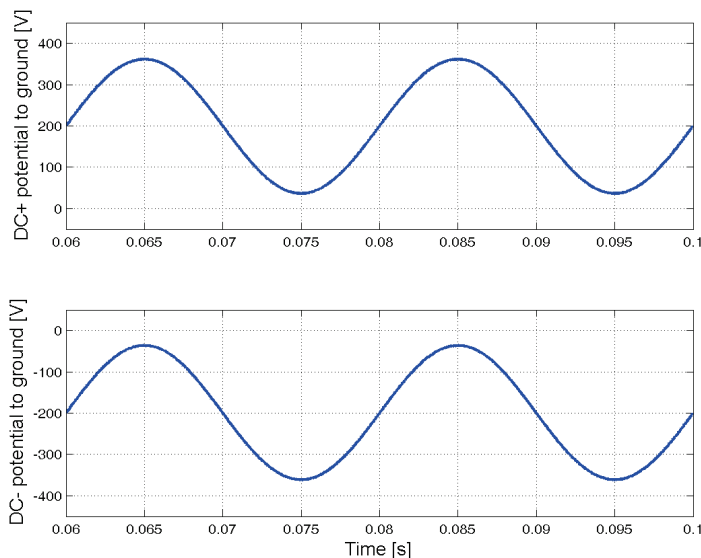

Fig. 3.19: Voltage to ground for both terminals of the PV array (topology with DC decoupling; output filter according to case 2).

3.2.7 Half bridge topology

The half bridge topology uses only two switches to connect either the upper or the lower half of the DC-link to the phase connection of the grid, while the neutral wire is always connected to the middle of the DC-link capacitors [72]. The major disadvantages of this topology are that the DC-link needs to be twice the grid peak voltage and that the switches have to block the full DC-link voltage, while in case of the H-Bridge topologies the same DC-link voltage was shared between two series-connected switches. The output of the converter will be a bipolar voltage, since T1 is controlled with high frequency in antiparallel with T2. This means that bigger filtering elements are needed and the conversion efficiency of the converter will be lowered. A major advantage, on the other hand, is the fact that the middle of the DC-link is always connected to the neutral, thereby fixing the potential of the PV array, and the voltage to ground will be constant, as shown in Fig. 3.20, when the switching ripple on the DC side is not taken into consideration.

Based on the common-mode behavior, the half bridge topology is suitable for transformerless PV systems. The only drawback is the high DC-link voltage, which will need a boost stage to keep the DC-link voltage above *650 V*. Otherwise, in a single-stage system, the voltage at the maximum power point (V_{MPP}) has to be above *650 V*, which could give an open circuit voltage (V_{OC}) above *1000 V* [73]. This is not allowed

according to the datasheet rating of most PV panels (maximum system voltage based on TÜV Rheinland rating or IEC61216 - paragraph 10.3.4.).
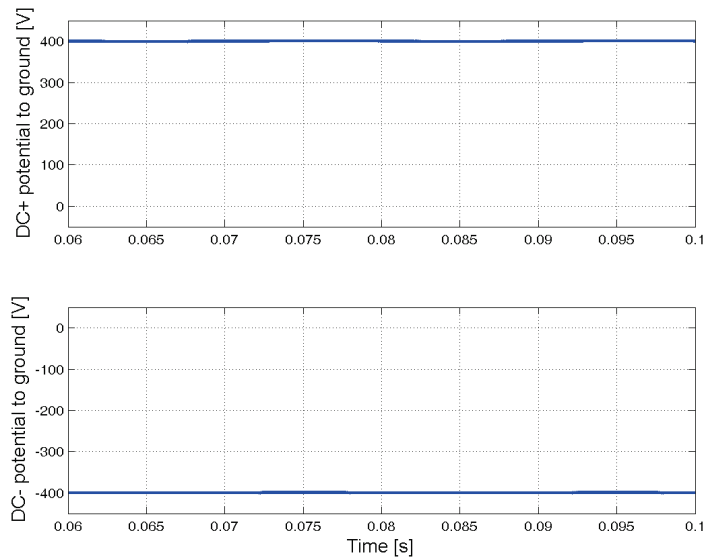
Fig. 3.20: Voltage to ground for both terminals of the PV array for the half bridge topology.

3.2.8 Neutral Point Clamped topology

The Neutral Point Clamped (NPC) topology was introduced some years ago in [74] and has mostly been used for applications in AC drives. In Publications III and IV the advantages of the NPC topology have been detailed, together with simulation results. As seen in Fig. 3.21, the voltage to ground measured at both PV array terminals is constant, when the switching ripple is not taken into consideration. This is due to the connection to the neutral line of the middle point of the DC-link that fixes the potential of the PV array to the grounded neutral.

Based on the shown common-mode behavior, the NPC topology is suitable for transformerless PV systems, since the voltage to ground is constant in case of both terminals of the PV. The only drawback for the single-phase NPC topology is the high DC-link voltage, which has to be twice the grid peak voltage. and might reach voltages higher than the allowed maximum system voltage, therefore needing a boost stage before the inverter, which decreases the overall efficiency of the whole PV system.

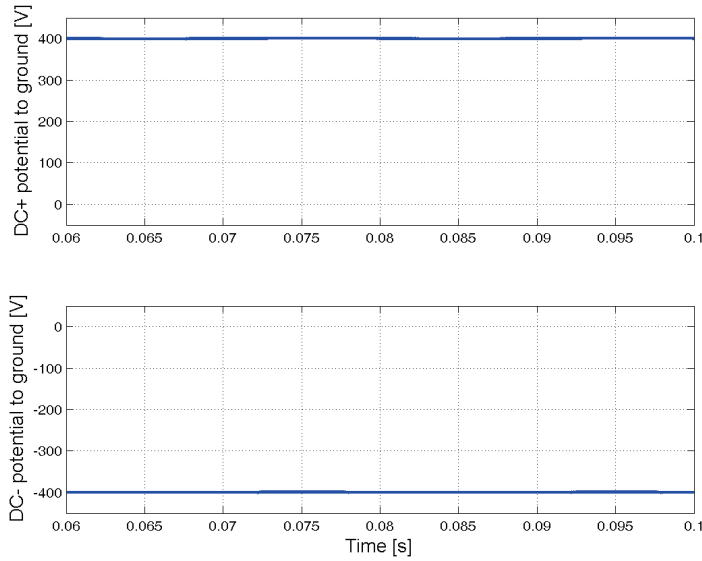*Fig. 3.21: Voltage to ground for both terminals of the PV array for the NPC topology.*

3.3 Three-phase topologies

In single-phase systems the output power on the AC side is not constant since both the grid voltage and current are sinusoidal. These pulsations in the power on the AC side are also present on the DC side and, to compensate for them, huge DC-link capacitors are needed to decrease the oscillations, which will also be present around the maximum power point (MPP). In a three-phase system on the other hand, the injected power is constant in a symmetrical three-phase system, since the sum of the currents from all three phases is zero. This means that smaller DC-link capacitors are needed, making the inverter more compact. The power output of three-phase systems is higher than was in the single-phase case and can go up to *20 kW* in case of the low voltage grid.

3.3.1 Three-phase Full Bridge

The Three-phase Full Bridge (3FB) topology is the simplest and most widely-used one for general applications in three-phase systems. As shown in the simulation and experimental results detailed in Publications III and IV, the common-mode voltage generated by this topology is not constant. An FFT of the simulated ground voltage shows high frequency components at the switching frequency and multiples of it, having high amplitude.
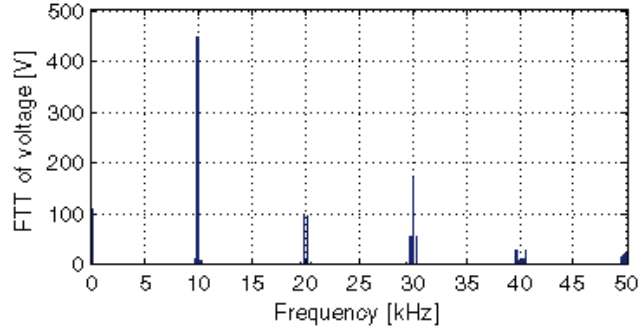
Fig. 3.22: FFT of voltage to ground for the 3FB topology.

As also shown by the experimental measurements in Fig. 3.23, the voltage to ground varies with the switching frequency and changes according to the PWM strategy. Depending on the state of each leg, it has four different values: V_{DC}, $\frac{2}{3}V_{DC}$, $\frac{1}{3}V_{DC}$, 0.

This means that the leakage ground current will only be limited by the parasitic capacitance of the PV array, which, in a kW size PV system, will be in the range of 100nF, leading to very high leakage ground current, well above the limit stated in the VDE 0126.
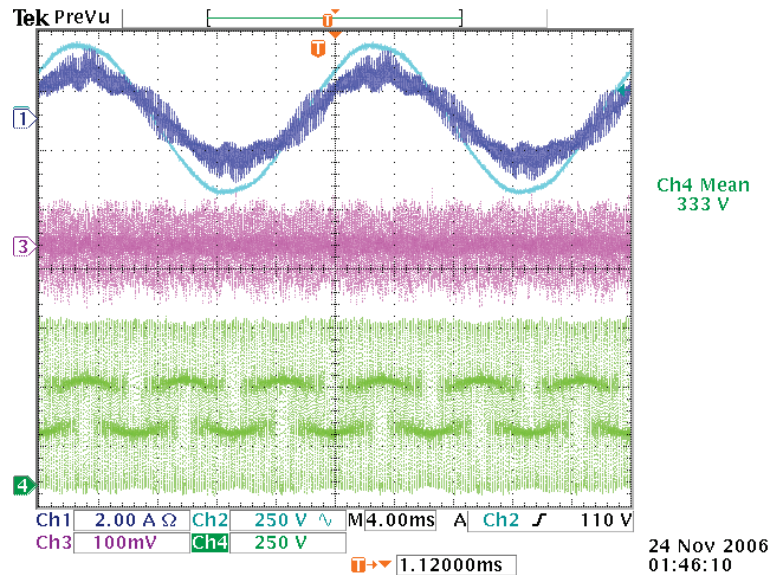
Fig. 3.23: Experimental measurements for 3FB topology. Channel 4 shows the voltage to ground of the DC+ terminal [250V/div].

Therefore, it can be stated that the 3FB topology is not suitable for transformerless PV systems, due to the common-mode behavior of the topology. Nevertheless, choosing a different PWM strategy it is possible to reduce the leakage current as shown in [75], although for high power applications with a huge PV array surface, the leakage current will still be too high, well above the level given by the VDE 0126-1-1.

3.3.2 Full Bridge with Split Capacitor

The Full Bridge with Split Capacitor (3FBSC) topology is similar to the 3FB one, with the difference that the input DC-link capacitor is split in two halves and the middle point is connected to the grounded neutral line of the grid, as detailed in Publication IV. Since the middle point of the DC-link is always connected to the grounded neutral of the grid, the PV array will be fixed to the potential of the neutral. Therefore, the measured voltage to ground of the PV array will be constant. According to the simulation results presented in Publication IV, this topology is a suitable solution for transformerless PV systems.

3.3.3 Full Bridge with Split Capacitor using staggered modulation

In case of the 3FBSC topology the standard PWM strategy has been used, where all the gate signals have been synchronized to a single PWM timer. Another solution is to have three separate timers, one for each leg of the inverter displaced by 120°. This PWM strategy is also known as staggered or interleaved modulation [76]. As shown the simulation results presented in Publication IV, using this method both the ripple in the grid current and the leakage ground current can be minimized.

Based on the detailed results it can be stated that the performance of the 3FBSC topology can be improved, using the staggered PWM strategy.

3.3.4 Three-phase Neutral Point Clamped

The single-phase NPC topology has proven to be a very good solution for transformerless PV systems. The three-phase version of the NPC topology (3xNPC) has been simulated and the results are detailed in Publication IV. In this topology the midpoint of the DC-link can connected to the neutral of the grid. Therefore the PV array is fixed to the potential of the neutral and there are no high frequency components in the ground voltage measured between the terminals of the PV array and the ground connection. The generated leakage ground current will be very small and taking into account the high conversion efficiency of up to *98%*, it can be concluded that this topology is a very good solution for transformerless PV systems [77].

3.4 DC current injection control in case of transformerless systems

In grid-connected PV systems, DC current injection is limited by standards, as detailed in subsection 2.2 Grid requirements, and needs to be monitored during the functioning of the inverter, by the means of a DC sensitive current sensor or the RCMU of an inverter also used for leakage ground current measurements [26].

In [78] it is mentioned that DC injection into the electrical grid is undesirable due to the impact on electrical equipment, and therefore a study is made regarding the effects and risks associated with DC current injection on various components in the electrical grid.

Table 3-2: Effects and risks associated with DC current injection [78].

Equipment	Technical effects of DC injection	Impacts and risks associate with DC injection
Distribution transformer	− *Saturation* − *Harmonic distortion increases* − *Losses increase* − *Heating (thermal stress) increase* − *Noise increase*	− *Premature ageing* − *Premature failure (risk of fire, service interruption…)* − *Inefficient operation* *Environmental impact (noise)*
RCD*	− *Modification of the tripping characteristic*	− *Sensitivity reduction*
Current transformers	− *Saturation*	− *Erroneous measurement*
Energy meters		− *Erroneous metering*

In grid-connected PV inverters, DC current injection is another critical issue, due to its effect on distribution transformers. As detailed in [78], losses, temperature and noise increase in transformers when DC currents are injected. All these affect the lifetime of the transformer. Therefore special care should be taken to prevent DC injection in case of transformerless PV inverters.

An inverter topology is proposed in [79] that reduces the DC current injection. According to the authors, the non injection of DC current into the grid is topologically guaranteed by adding a second capacitive divider to which the neutral terminal of the

grid is connected. An extra control loop is introduced that compensates for any DC current injection, by controlling the voltage of both capacitive dividers so that they are equal.

Another solution could be to control the voltage over the output filter capacitor in the grid side LCL filter so that the DC component is *0*, thereby ensuring that the injected current is pure AC. Such a control is detailed in Publications V and VII, which present a voltage control in case of a grid-connected PV inverter.

3.5 Summary

In this chapter several single-phase and three phase topologies have been investigated, focusing on the ground voltage measured at the terminals of the PV array as well as the suitability of each topology in transformerless grid connected PV systems. It has been shown that the single-phase topologies, the H-Bridge with unipolar PWM is not suitable for transformerless PV systems, due to the way the zero voltage vector is achieved, leading to very high leakage ground currents, limited only by the parasitic capacitance of the PV array. Unipolar output voltage is still possible to achieve, as was the case of the HERIC, H5, NPC and other topologies, by either disconnecting the PV array from the grid during the zero voltage vector or by connecting the midpoint of the DC-link to the neutral of the grid. The ground leakage current can be further reduced in certain cases, by choosing a modulation strategy like the staggered PWM, as was the case for the 3FBSC topology.

It can therefore be concluded that the common-mode behavior of a PV system is influenced by the chosen topology and modulation strategy.

Chapter 4

Common mode voltage in PV
inverter topologies

*This chapter offers a comprehensive analysis of the single- and three-phase trans-
formerless converter with respect to the problem of the leakage current that flows
through the parasitic capacitance of the PV array.*

4.1 Introduction

PV systems usually have an isolation transformer between the PV panels and the
grid. Fig. 4.1 shows such a system, including the parasitic capacitance of the PV array
($C_{G\text{-}PV}$) connected between ground and each terminal of the PV array.
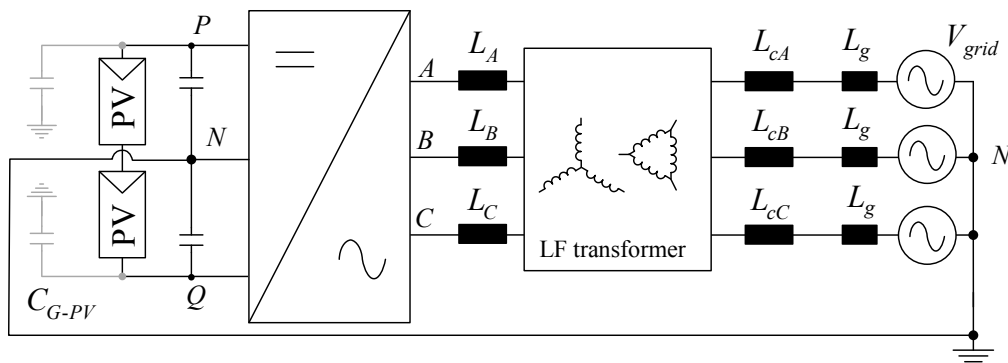

Fig. 4.1: Grid-connected PV system including the PV array parasitic capacitance to ground.

In order to show the path for the common-mode current the stray elements are
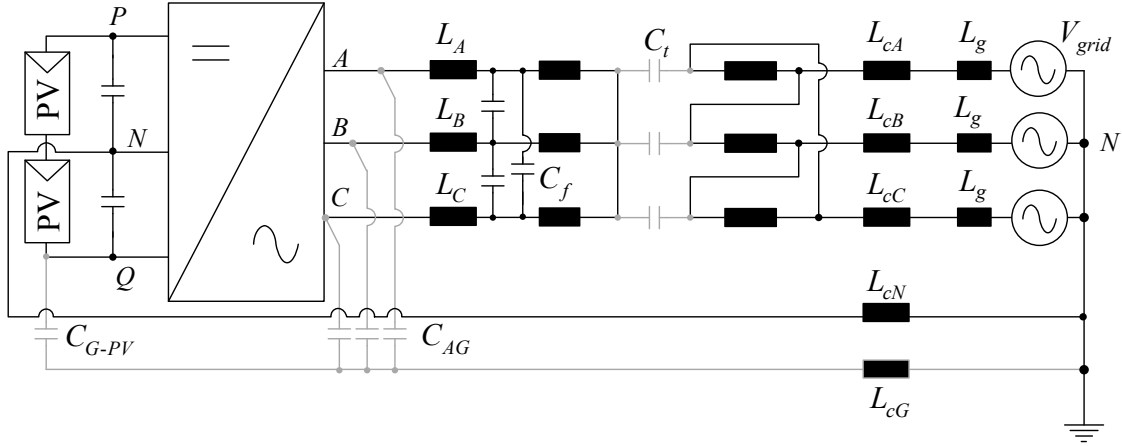added to the system in Fig.4.2 [80].

Fig.4.2. Three-phase grid-connected PV system showing the parasitic capacitance of the PV array, the parasitic capacitance of the converter, the cable inductance of the phases, and the stray capacitance of the transformer in a system with galvanic isolation.

- C_{AG}, C_{BG} and C_{CG} are the stray capacitances between the converter output points and the ground, present for all three-phase legs of the inverter; these capacitances depend on the connection between the switches and the grounded heatsink.

- $C_{G\text{-}PV}$ is the parasitic capacitance, also known as leakage capacitance;

- C_t represents the stray capacitance between the transformer primary and secondary windings.

- L_A, L_B and L_C are the output inductors used to control the current injected into the grid.

- L_{cA}, L_{cB} and L_{cC} represent the series inductance of each phase.

- L_{cN} represents the series inductance of the neutral when connected to the midpoint of the DC-link.

- L_{cG} represents the inductance between the ground connection of the inverter and the grid neutral.

In a grid-connected PV system with an isolation transformer, the common-mode current can only find its path through the stray capacitances of the transformer (C_t). Due to the fact that this capacitance has values in the order of *100 pF*, the common-mode current at frequencies lower than *50 kHz* will be strongly reduced and the higher frequencies can be filtered by the EMI filter [80]. This is mainly the reason why when PV systems have a galvanic isolation in the form of a transformer, the low frequency leakage current behavior is not influenced by the converter topology or modulation technique.

On the other hand, in transformerless PV systems, the common mode behavior is greatly influenced by the chosen topology or PWM. In this case, as also shown in Fig.4.3, the PV array is directly connected to the grid and common mode voltages present at the PV panel terminals lead to leakage ground current.
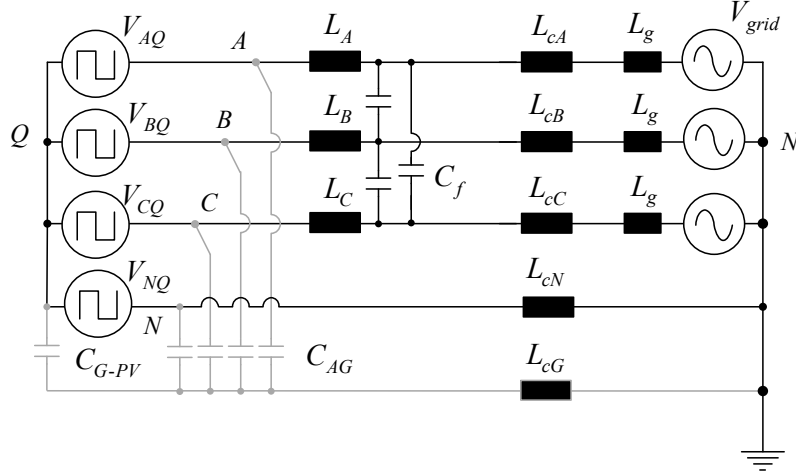
Fig.4.3. Three-phase grid-connected PV system with the inverter modeled as a voltage source (without galvanic isolation).

4.2 Common-mode voltage in three-phase systems

4.2.1 Model of common-mode and differential-mode voltages

In order to analyze the system regarding common-mode and differential-mode behavior, an analysis has been done in Publications VI and VIII.

The equation for the total common-mode voltage, including the contribution from inductor imbalance, is defined by (4.1):

$$V_{cmm-tot} = V_{cmm3\sim} + \frac{V_{ab1} + V_{bc1} + V_{ca1}}{3} \tag{4.1}$$

where:

$$V_{cmm3\sim} = \frac{V_{cmm-AB} + V_{cmm-BC} + V_{cmm-CA}}{3} = \frac{V_{AQ} + V_{BQ} + V_{CQ}}{3} \tag{4.2}$$

Equation (4.1) is used to predict the total common-mode voltage, due to the modulation strategy and unbalance of the system. Fig.4.4 presents the simplified model, showing the common-mode voltage sources for the three-phase system.

The common-mode voltage described by (4.1) charges and discharges the parasitic capacitance C_{G-PV}, and there will be a leakage current flowing towards ground. The level of the leakage current depends on the amplitude and frequency content of the voltage fluctuations, as well as the value of the leakage capacitance [81].
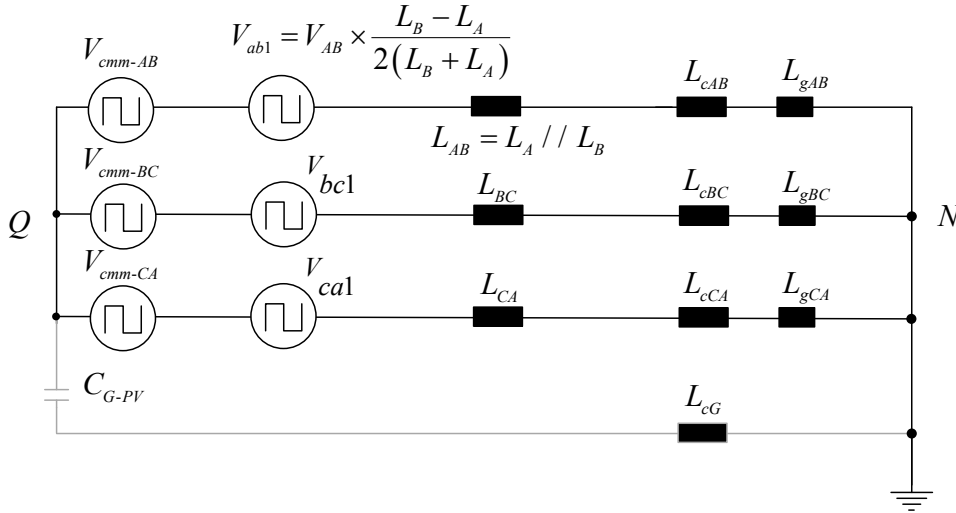
Fig.4.4. Simple model showing the common mode voltage for the three-phase system.

4.2.2 Leakage current in case of imbalance filter inductance condition

The total common-mode voltage is also influenced by the output filter inductors. Unbalance between the phases leads to a common-mode voltage component influenced by the difference between the inductors on the phases.

Fig.4.5 presents the two cases: no unbalance in (a), while in (b) the common-mode voltage in case of the simulation is presented and (c) shows the calculated value of the common-mode voltage, based on the equations describing the common-mode voltage. As seen in Fig.4.5, the simulated voltage closely matches the modeled common-mode voltage, in unbalanced conditions, when $L_A = 1.3 \cdot L_B$.

When the neutral line is connected, from the point of view of the common-mode model, the three-phases with the neutral connection of the inverter can be modeled as three individual single-phases, and the result is a constant total common-mode voltage, leading to very low leakage ground current, as shown in Fig.4.6(a), which represents the simulation results for the 3FB-SC and 3xNPC topologies.

When there is some inductance present in the neutral line, for example due to the EMI filter, the total common-mode voltage is not constant any more. A small inductance of $L_N = 10 \ \mu H$ present in the neutral can lead to high frequency common-mode voltage, that would generate leakage ground currents that could reach amplitudes greater than the threshold stated in the German standard regarding grid connection of PV systems: VDE-0126-1-1. Fig.4.6(b) and (c) show the simulated and calculated common-mode voltage when *10 μH* inductance is present in the neutral line. This results in a common-mode voltage which is not constant any more, leading to an increase in the leakage current flow to ground. Much attention should be paid to the design of an inductance-free neutral connection.

Fig.4.5. Total common-mode voltage 3FB topology, (a) common-mode voltage in case of NO unbalance; (b) common-mode voltage in case of unbalance (simulation); (c) common-mode voltage in case of unbalance (calculated).
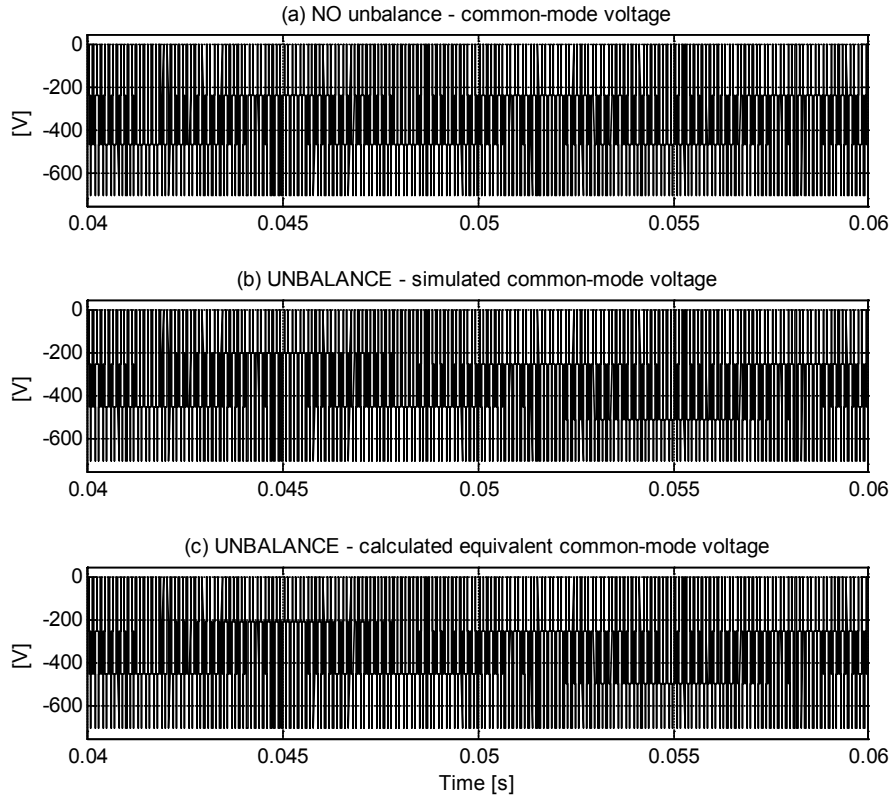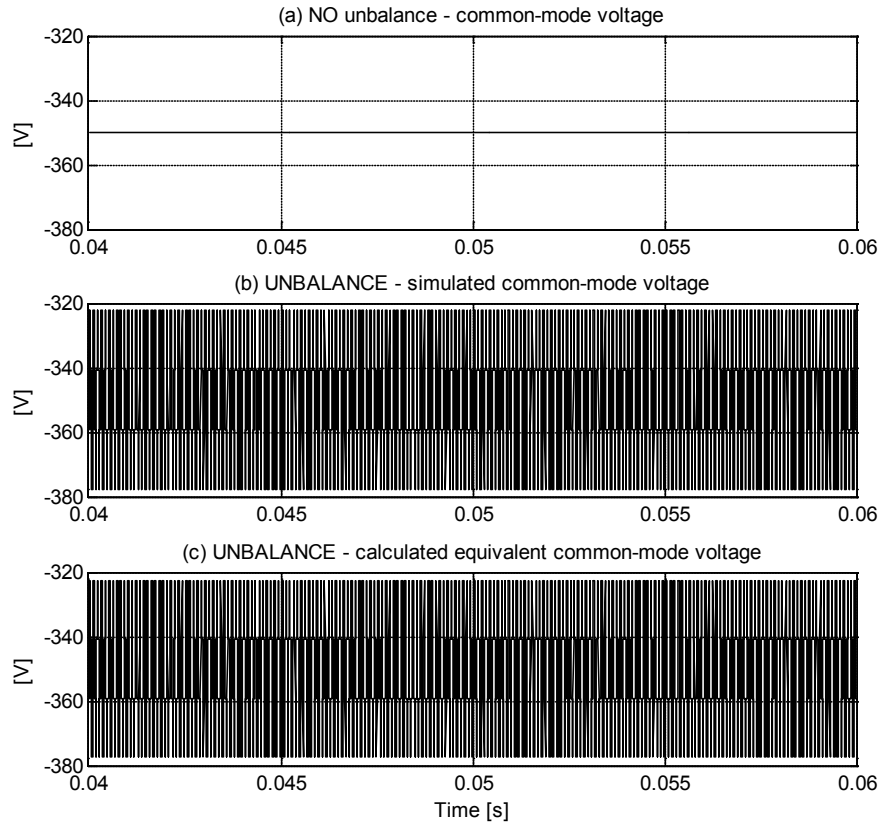

Fig.4.6. Total common-mode voltage 3FBSC topology, (a) common-mode voltage in case of NO unbalance; (b) common-mode voltage in case of unbalance (simulation) and (c) common-mode voltage in case of unbalance (calculated), having $L_1=10\,\mu H$ in the grid neutral.

4.2.3 Experimental results (inverter mode)

To verify the simulation results, an experimental setup has been realized, made up of a single-phase NPC leg connected to the grid, tested as an inverter. In fact, the three-phase NPC topology can be obtained using three independent single-phase inverters, connected through the common neutral. The experimental setup and the obtained results are detailed in Publication VIII.
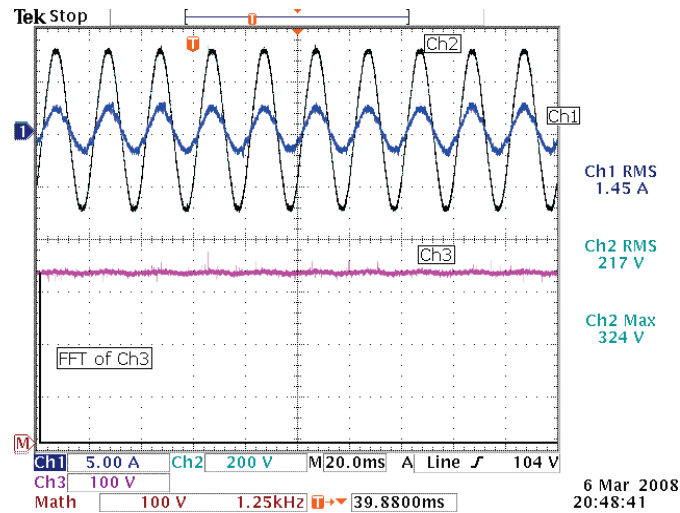

Fig. 4.7. Experimental results for single-phase NPC inverter: Channel 1: grid current [5A/div]; Channel 2: grid voltage [200 V/div]; Channel 3: voltage between DC+ terminal and ground [100 V/div]; Channel M: FFT of Channel 3 [100 V/div and 1.25 kHz/div].

An FFT of the common-mode voltage, shown with Chanel 3 in Fig. 4.7, confirms that the measured common-mode voltage has only a DC value with no high frequency components. This means that the leakage ground current generated by this topology is very low, as also shown in the simulations in the previous chapter.

4.2.4 Experimental results (rectifier mode)

In order to further verify the simulation results, another experimental setup has been done, made up of the same NPC leg connected to the grid tested as a rectifier. For a grid connected inverter a DC power supply is needed, and it is very hard to determine the parameters of the EMI filter of a switched mode power supply. In the rectifier mode, the topology is connected to a resistive load, which being a passive one, gives better control over the parasitic components in the whole circuit.

Fig. 4.8 and Fig. 4.9 show the components and the equivalent circuit of the experimental setup, made up of the grid-connected NPC rectifier, together with the resistive load. For the filter on the grid side a *3 mH* inductor was used. Furthermore, in Fig. 4.8 the sensors, gate drivers and the TI eZdsp used for the control of the system are shown.

The experimental setup has the following main components, listed in Table 4-1:

Table 4-1: Parameters of the experimental test setup.

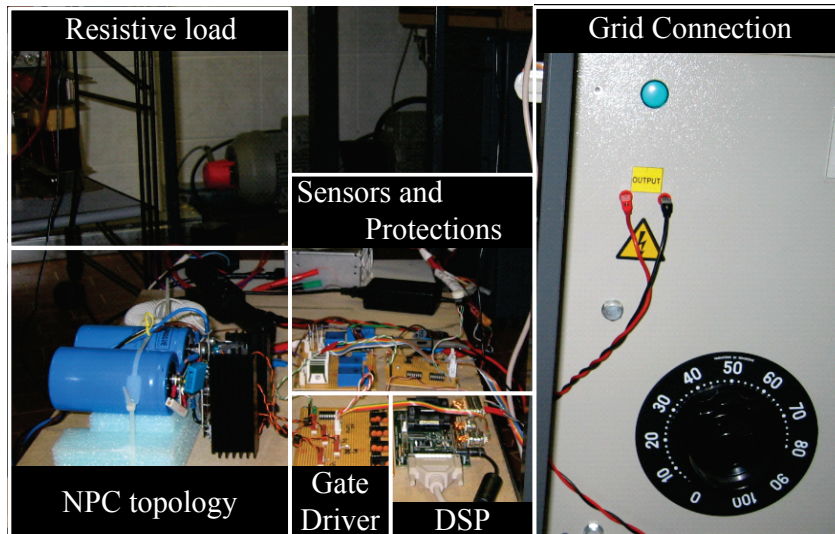| Digital control	TI TMS320F2812 eZdsp kit
MOSFET (T1-T4)	IXYS 82N60P (600 V, 82 A)
Diode (D)	IXYS DSEP 30-06BR (600 V, 30 A)
DC capacitor (C_{dc})	C_{dc}=1 mF, 450 V
Filter	L_f=3 mH
Grid	Vg=110V (RMS), f_g=50 Hz
DC load	R=246 Ω, 1.2 kW

Fig. 4.8: The components of the experimental setup for the test of the NPC single-phase rectifier.
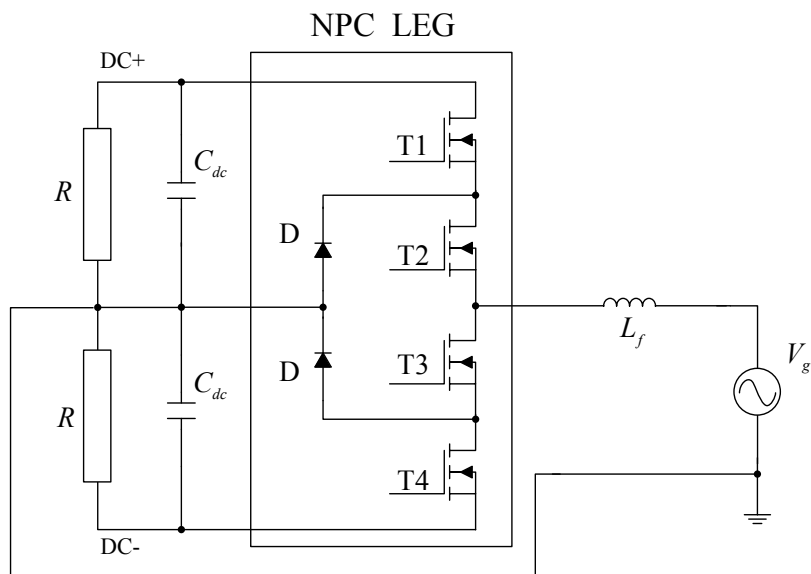
Fig. 4.9: Electrical circuit of the experimental setup using the NPC rectifier.

The experimental tests were done at grid voltage V_g=110V (RMS) and the grid current was set to I_g=5.1 A (RMS), as seen in Fig. 4.10.
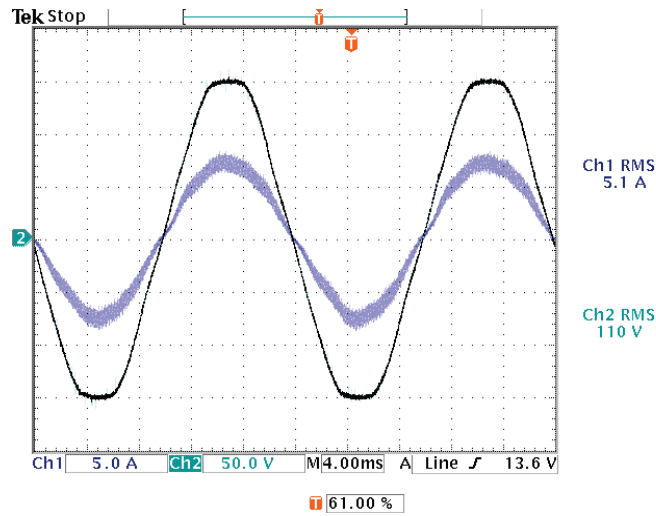
Fig. 4.10: Experimental results for single-phase NPC inverter Grid voltage (V_g) [50V/div] and grid current (I_g) [5A/div] for NPC rectifier.

For the previously mentioned conditions, the resulting DC voltage was V_{dc}=300 V, as it can also be seen in Fig. 4.11 and Fig. 4.12. In Fig. 4.11 the 50 Hz ripple of the DC voltage can be clearly seen and is due to the single-phase pulsating power.

As can be observed on the FFT of the measured DC to ground voltage, only components at low frequencies are present.
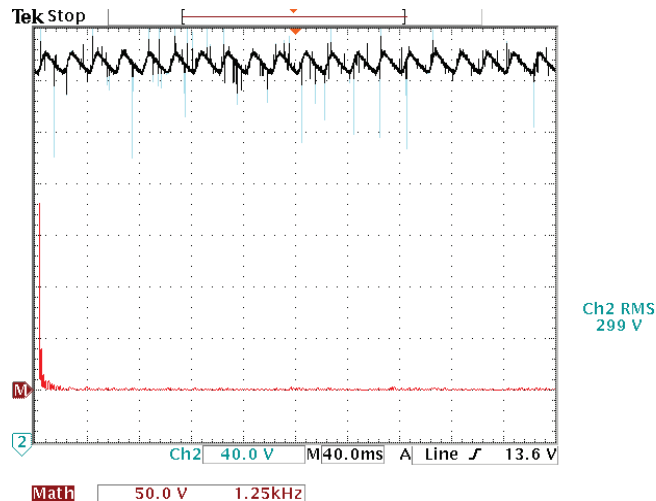
Fig. 4.11: DC to ground voltage (Channel 2) [40V/div] and FFT of the same voltage (Channel M) having 1.25 kHz per division on the FFT.

The experimental tests confirmed the simulation results. As seen on the FFT of the DC to ground voltage there are no high-frequency components present. This means that the leakage ground current is very low for the NPC topology. Therefore it can be stated that this topology can be used in transformerless PV applications.
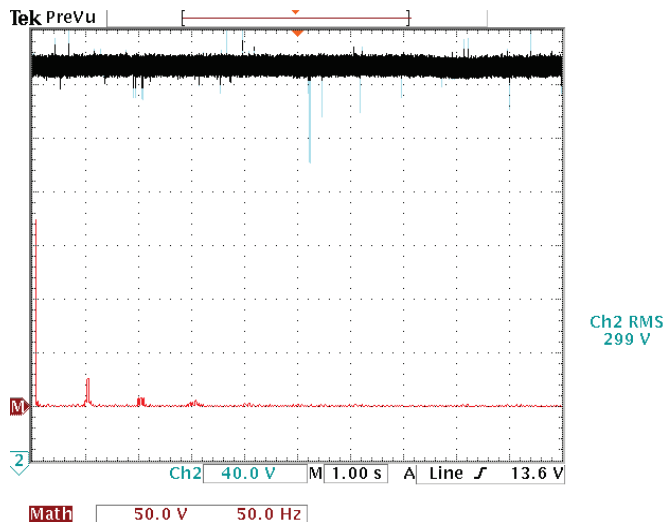
Fig. 4.12: DC to ground voltage (Channel 2) [40V/div] and FFT of the same voltage (Channel M) having 50Hz per division on the FFT.

4.3 Common-mode voltage in single-phase systems

The model of the common-mode voltage in the single-phase case is very similar to the three-phase case, with the difference that in single-phase, there is only a phase and a neutral line, for which the common-mode calculations have to be done. The single-phase case has been discussed in [80] and, based on the equations presented there, the total common-mode voltage can be similarly calculated, as has been done for the three-phase system.

The total common-mode voltage, when there is an inductor unbalance, has been calculated for the single-phase H-Bridge topology with bipolar PWM. As seen in Fig. 4.13(a), the common-mode voltage is constant when both inductors have the same value. When the inductor in the neutral (L_N) differs from the one in the phase (L_A): $L_N=0.95 \cdot L_A$, then the total common-mode voltage will not be constant anymore. The amplitude of these voltage fluctuations will depend on the difference between these two inductors and the frequency will be the switching frequency. As shown in Fig. 4.13(b) the simulation results and Fig. 4.13(c) the calculated results, for a *5%* difference be-

tween the inductors, the amplitude of the common-mode voltage will have a *10 V* component at the switching frequency and the leakage current will depend only on the parasitic capacitance of the PV array.
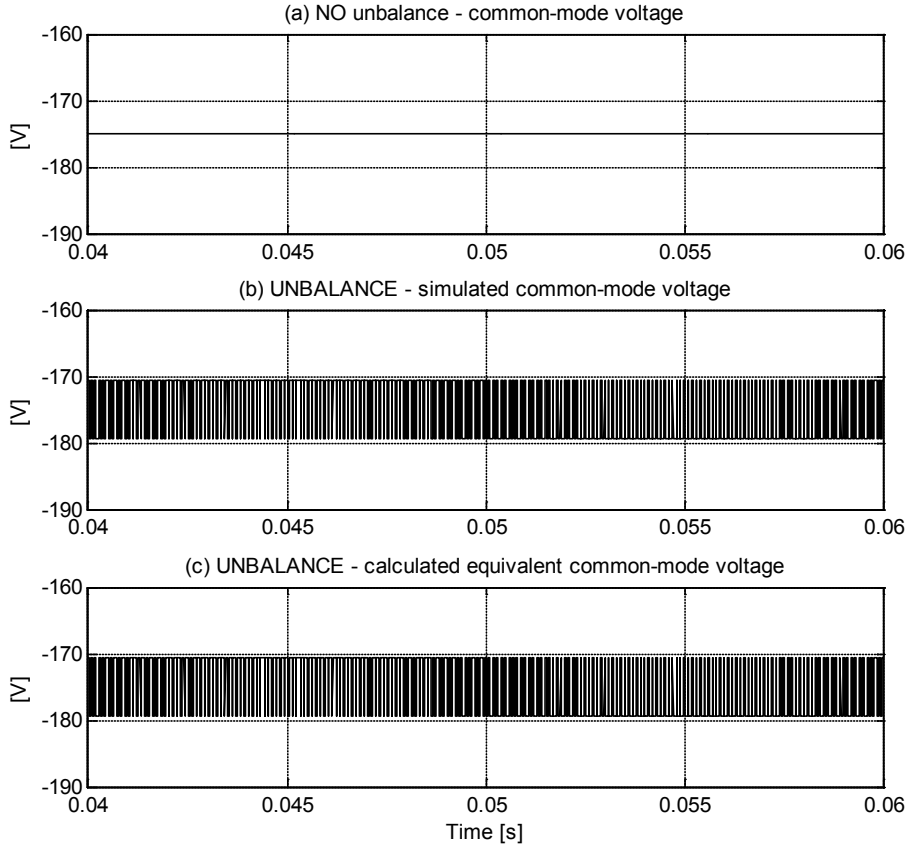
Fig. 4.13: Total common-mode voltage H-Bridge topology with bipolar PWM, (a) common-mode voltage in case of NO unbalance; (b) common-mode voltage in case of unbalance (simulation) and (c) common-mode voltage in case of unbalance (calculated) having $L_N=0.95 \cdot L_A$ in the grid neutral.

4.4 Summary

In this chapter a detailed analysis of the problem of the leakage current in transformerless converters has been carried out. The adopted common-mode model of the system has revealed that connecting the supply neutral to the middle of the DC-link capacitors will result in low-ripple voltage at both DC-link terminals of the array leading to a very low leakage current level, below the VDE 0126-01-01 standard requirement of *300mA*. However the presence of inductance in the neutral line can lead to high frequency components in the common-mode voltage, leading to leakage ground currents, higher than the allowed level given in the standard. Therefore, it is crucial that the neutral line has very low inductance, in transformerless PV systems, where the neutral line is connected to the middle of the DC-link.

Chapter 5

H-Bridge Zero Voltage Rectifier topology

This chapter introduces a novel transformerless topology derived from HERIC, but with an alternative solution for the bidirectional switch, used to generate the zero voltage state. It will be shown, that the constant common-mode voltage and the high efficiency of the proposed topology makes it an attractive choice for transformerless PV applications.

5.1 Introduction

A new topology called H-Bridge Zero Voltage Rectifier (HB-ZVR) is proposed, where the zero voltage is achieved by short-circuiting the grid voltage through the LCL filter, using a diode rectifier bridge and one switch. During the zero voltage vector the mid-point of the DC link is clamped to the short-circuited grid.

A comparison of known transformerless topologies and the HB-ZVR is performed using simulations, focusing on the voltage to earth and ground leakage current. Furthermore, experimental results are shown, confirming the simulations. And, finally, the efficiency curve of the compared topologies is detailed.

5.2 Transformerless topology analysis

As previously discussed, as well as in [80] and Publication VI, the common mode voltage generated by a topology and modulation strategy can greatly influence the ground leakage current that flows through the parasitic capacitance of the PV array. Generally, the grid does not influence the common-mode behavior of the topology, so it

can be concluded that the generated common-mode voltage of a certain inverter topology and modulation strategy can be shown using a simple resistor as a load. Of course in case of transformerless PV systems connected to the grid, the common-mode voltage will have a sinusoidal shape with the grid frequency and having an amplitude half of the grid voltage peak. Therefore, in case of the simulations, only a resistive load is used and the common-mode voltage is measured between the DC+ terminal of the DC source and the grounded middle-point of the resistor, as shown in Fig. 5.1.

In the following simulation results obtained using Matlab Simulink with the PLECS toolbox are shown. The simulation step size is *0.1 μs*, with an *8 kHz* switching frequency, in order to have the same switching frequency both in the simulations and experimental results. This is because the digital implementation of the current control was limited to *8 kHz* due to the chosen DSP hardware, as detailed in Publication I.
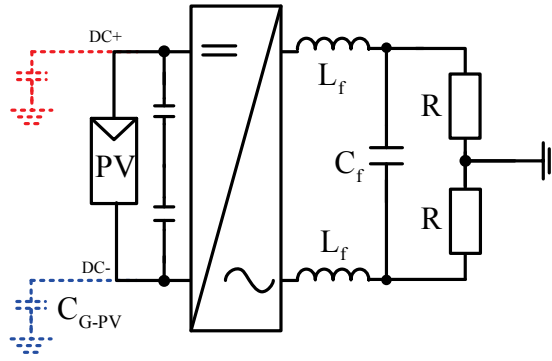
Fig. 5.1: Test setup used for common-mode voltage measurement.

Simulation parameters:

L_f=1.8 mH, filter inductor
C_f=2 μF, filter capacitor
R=7.5 , load resistor
V_{dc}=350 V, input DC voltage
C_{dc}=250 μF, DC-link capacitor
$C_{G\text{-}PV}$=100 nF, parasitic capacitance of PV array in case of simulations
f_{sw}=8 kHz, switching frequency for all cases except that the switching frequency for unipolar PWM has been chosen to be f_{sw}=4 kHz, so that the output voltage of the inverter has the same frequency in all cases.

5.2.1 H-Bridge with unipolar switching

Most single-phase H-Bridge inverters use unipolar PWM in order to improve the injected current quality of the inverter, which is done by modulating the output voltage to have three levels with twice the switching frequency. Moreover, this type of modulation reduces the stress on the output filter and decreases the losses in the inverter.

The positive active vector is applied to the load by turning ON T1 and T4, as shown in Fig. 5.2. The negative active vector is done similarly, but in this case T2-T3 is turned-ON.

In a unipolar switching pattern, the zero voltage state, during the positive voltage, is achieved by short circuiting the output of the inverter, as detailed in Fig. 5.3, which introduces high frequency content in the generated common-mode voltage.

As seen in Fig. 5.5, in a transformerless PV system using this type of topology and modulation, the high-frequency common-mode voltage, measured across C_{G-PV}, will lead to very high leakage ground current, making it unsafe, therefore not usable for transformerless PV applications.
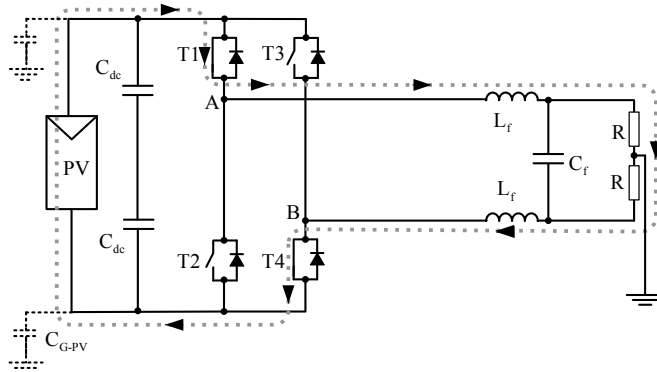

Fig. 5.2. H-Bridge topology with Unipolar PWM, active vector applied to load, using T1-T4 for positive voltage.
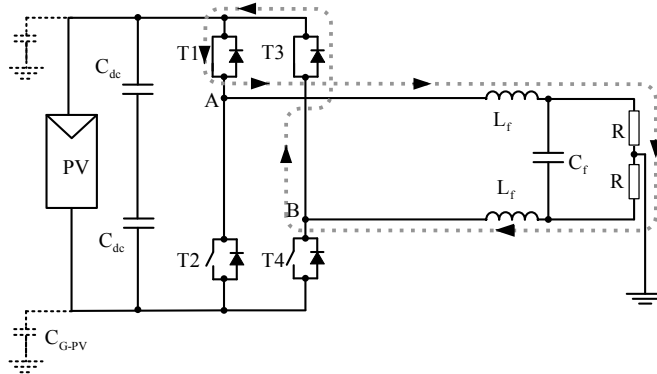
Fig. 5.3. H-Bridge topology with Unipolar PWM, zero voltage applied to load, using T1-T3 for positive voltage
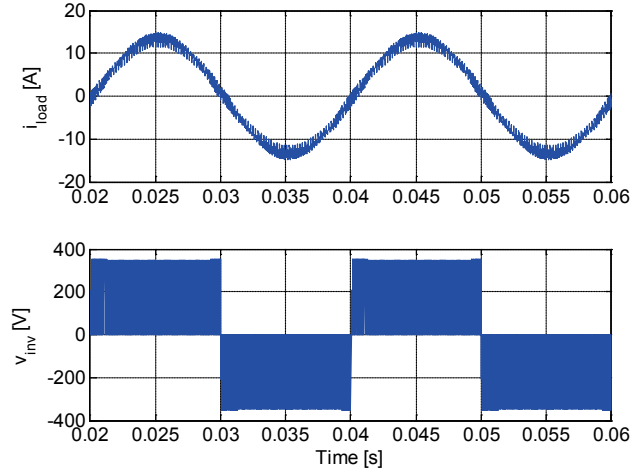
Fig. 5.4. H-Bridge topology with Unipolar PWM, load current and inverter output voltage.
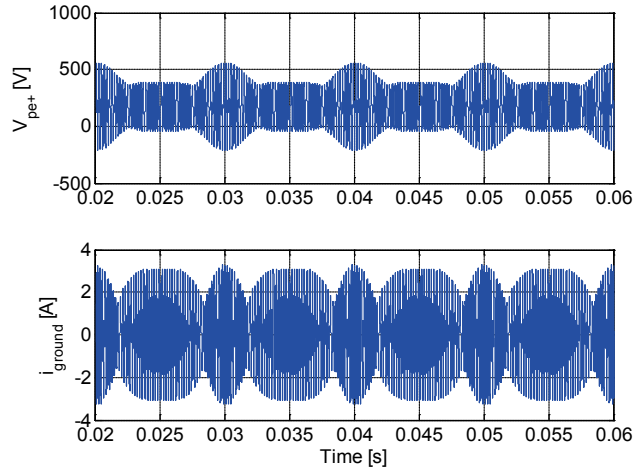
Fig. 5.5. H-Bridge topology with Unipolar PWM, voltage to ground and ground leakage current.

5.2.2 HERIC – Highly Efficient and Reliable Inverter Concept

This topology, shown in Fig. 5.6, combines the advantages of the three-level output voltage of the unipolar modulation with the constant common-mode voltage, as in the case of bipolar modulation. This way the efficiency of the inverter is increased, without compromising the common-mode behavior of the whole system.

The zero voltage vector is realized using a bidirectional switch, shown in the grey background in Fig. 5.6. This bidirectional switch is made up of two IGBTs and two diodes (T5-T6). During the positive half-wave of the load (or grid) voltage, T6 is switched ON and is used during the freewheeling period of T1 and T4. On the other hand, during the negative half-wave T5 is switched ON and is used during the freewheeling period of T2 and T3 [51].
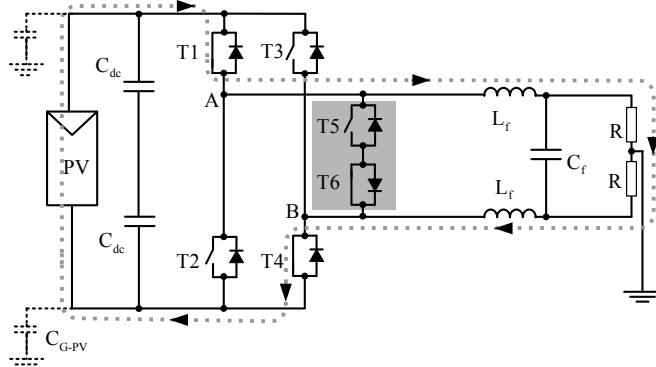
Fig. 5.6. HERIC topology, active vector applied to load,
using T1-T4 during positive half-wave.

This way, using T5 or T6 as detailed in Fig. 5.7, the zero voltage vector is rea-
lized by short-circuiting the output of the inverter, and during this period the PV array
is separated from the grid, because T1-T4 or T2-T3 are turned OFF.
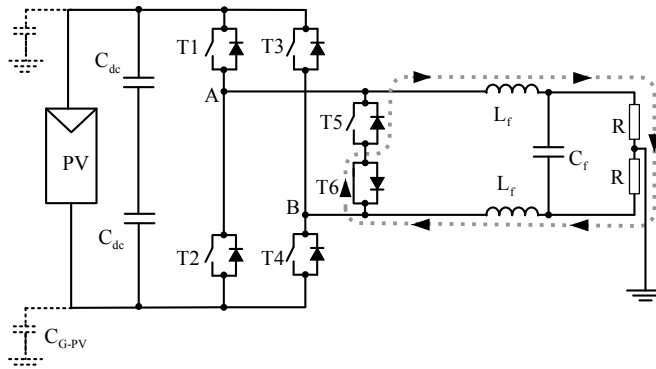
Fig. 5.7. HERIC topology, zero voltage applied to load,
using S6 during positive half-wave.

As shown in Fig. 5.8, the output voltage of the inverter has three levels and the
load current ripple is very small, although in this case the frequency of the current is
equal to the switching frequency.

As seen in Fig. 5.9, the inverter generates no common-mode voltage. Therefore
the leakage current through the parasitic capacitance of the PV array would be very
small.
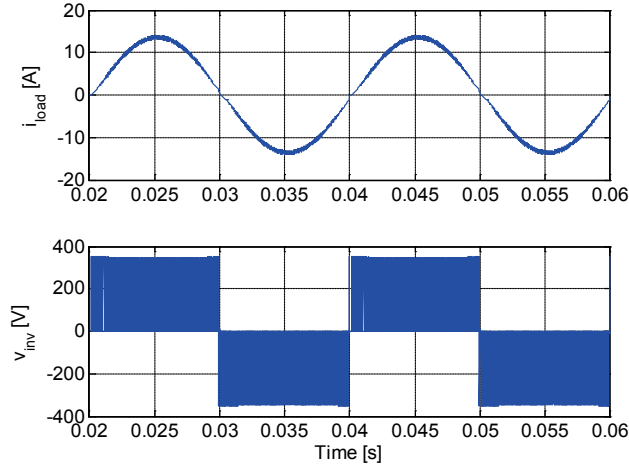
Fig. 5.8. HERIC topology, load current and inverter output voltage.
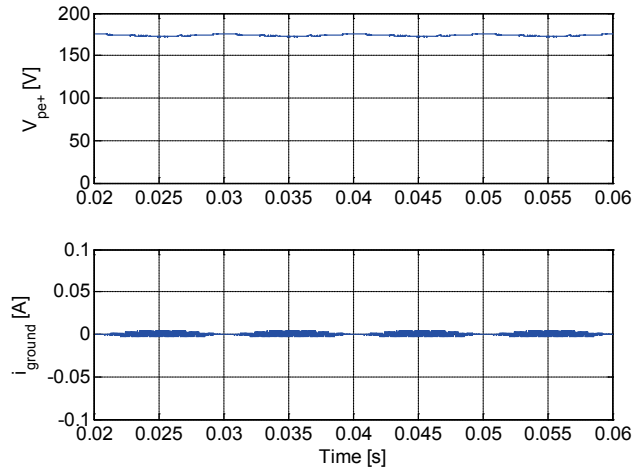
Fig. 5.9. HERIC topology, voltage to ground and ground leakage current.

5.2.3 Proposed topology (HB-ZVR)

Another solution for generating the zero voltage state can be done using a bidirectional switch made of one IGBT and one diode rectifier bridge. The topology is detailed in Fig. 5.10, showing the bidirectional switch, as an auxiliary component with a grey background. This bidirectional switch is clamped to the midpoint of the DC-link capacitors in order to fix the potential of the PV array also during the zero voltage period, when T1-T4 and T2-S3 are open. An extra diode is used to protect the lower DC-link capacitor from short-circuiting.

During the positive half wave, T1-T4 are used to generate the active vector, supplying a positive voltage to the load, as shown in Fig. 5.10.

The zero voltage state is achieved by turning ON T5 when T1-T4 are turned OFF, as shown in Fig. 5.12. The gate signal for T5 will be the complementary gate signal of T1-T4, with a small dead-time to avoid short-circuiting the input capacitor.

Using T5, it is possible for the grid current to flow in both directions, this way the inverter can also feed reactive power to the grid, if necessary.

During the negative half wave of the load voltage, T2-T3 are used to generate the active vector, and T5 is controlled using the complementary signal of T2-T3 and generates the zero voltage state, by short-circuiting the outputs of the inverter and clamping them to the midpoint of the DC-link.

During the dead-time, between the active vector and the zero state, there is a short period while all the switches are turned OFF, when the freewheeling current finds its path through the anti-parallel diodes to the input capacitor. This is shown in Fig. 5.11 and leads to higher losses, compared to the HERIC topology where the freewheeling current finds its path through the bidirectional switch, either through T5 or T6, depending on the sign of the current.
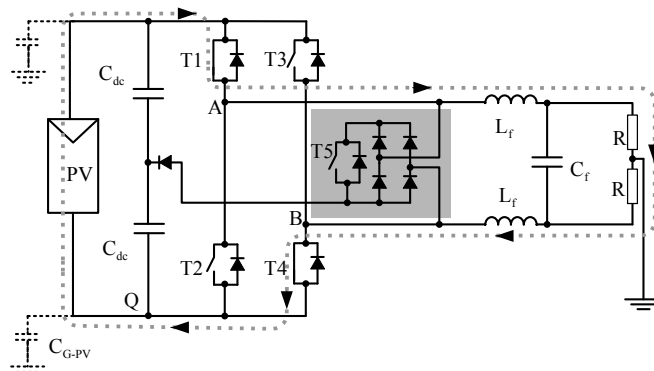
Fig. 5.10. HB-ZVR topology, active vector applied to load,
using T1-T4, during positive half-wave.

Fig. 5.11. HB-ZVR topology, dead-time between turn-OFF of T1-T4
and turn-ON of T5, during positive half-wave.

*Fig. 5.12. HB-ZVR topology, zero voltage applied to load,
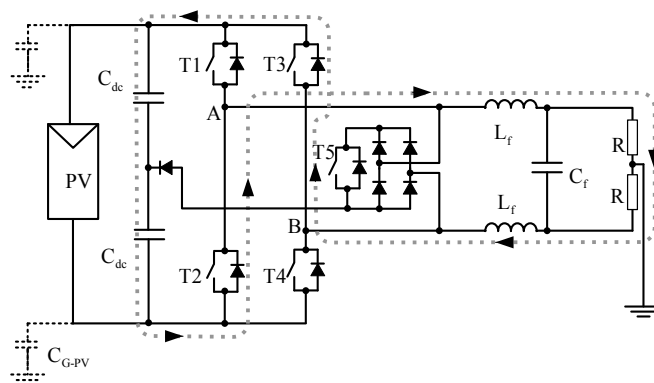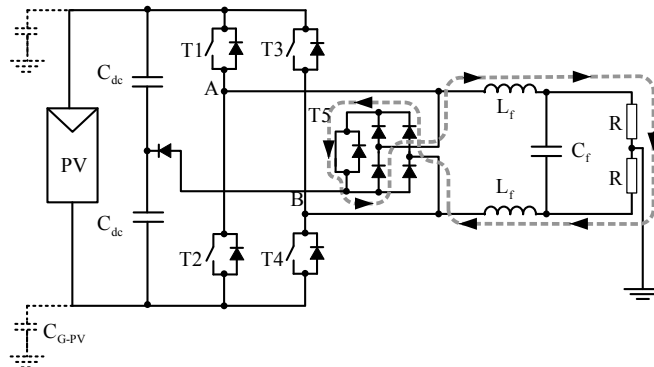using T5, during positive half-wave.*
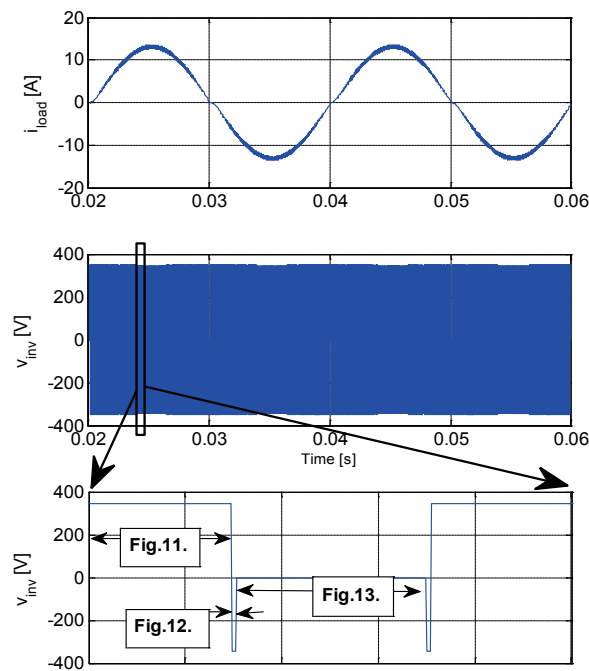
Fig. 5.13. HB-ZVR load current and inverter output voltage.
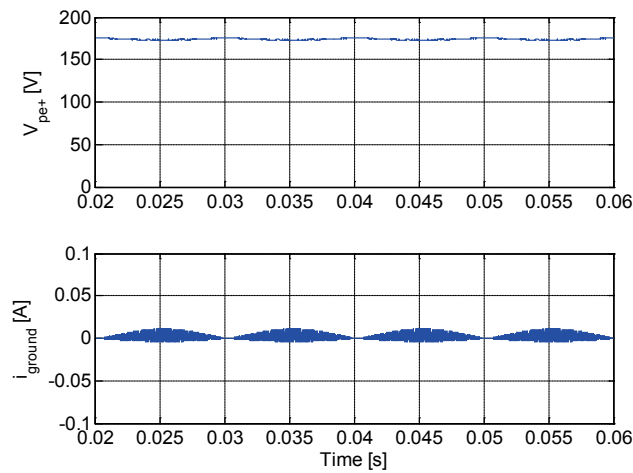
Fig. 5.14: HB-ZVR topology, voltage to ground and ground leakage current.

As shown in Fig. 5.13, the output voltage of the inverter has three levels, taking into account the freewheeling part during dead-time. In this case also, the load current ripple is very small and the frequency is equal to the switching frequency.

To show that this topology does not generate a varying common-mode voltage, V_{cm} has been calculated for the switching states with regard to the positive, zero and negative vectors:

$$V_{cm} = \frac{V_{AQ} + V_{BQ}}{2} \tag{5.1}$$

$$\text{Positive: } V_{AQ} = V_{dc}; \ V_{BQ} = 0 \Rightarrow V_{cm} = \frac{V_{dc}}{2} \tag{5.2}$$

$$\text{Zero: } V_{AQ} = \frac{V_{dc}}{2}; \ V_{BQ} = \frac{V_{dc}}{2} \Rightarrow V_{cm} = \frac{V_{dc}}{2} \tag{5.3}$$

$$\text{Negative: } V_{AQ} = 0; \ V_{BQ} = V_{dc} \Rightarrow V_{cm} = \frac{V_{dc}}{2} \tag{5.4}$$

As detailed by equations (5.1)-(5.4), the common-mode voltage is constant for all switching states of the converter. Therefore the leakage current through the parasitic capacitance of the PV array would be very small, as observed in Fig. 5.14.

5.3 Experimental results

In the experimental results, the setup has the same parameters as was used in the simulations: V_{dc}=350 V, C_{dc}=250 μF, L_f=1.8 mH, C_f=2 μF, f_{sw}=8 kHz (in case of the Unipolar PWM it is only 4 kHz), dead-time=2.5 μs.

To compare the behavior of the different inverters, all three topologies have been tested using the same components. PM75DSA120 Intelligent Power Modules with maximum ratings of 1200 V and 75 A from Mitsubishi as IGBTs and DSEP 30-06BR with maximum ratings of 600 V 30 A as diodes from IXYS have been used in the diode bridge of the proposed topology.

The modular-based setup shown in Fig. 5.15 makes it possible to test the different topologies: H-Bridge with bipolar or unipolar modulation, the HERIC topology and the proposed HB-ZVR, using the same components.

5.3.1 H-Bridge with Unipolar PWM (experiment)

The main advantage of the H-Bridge inverter with unipolar switching is that the output voltage has three-levels and the frequency of the output voltage is the double of

the switching frequency, thereby increasing the efficiency of the inverter and decreasing the size of the output filter. But the major drawback of this topology is the high frequency common-mode voltage, which makes it unsuitable to be used in transformerless PV systems.

As seen in Fig. 5.16, the unipolar PWM strategy used in case of the H-Bridge topology generates a high-frequency common mode voltage, measured between the DC+ terminal of the DC-link and ground, shown on Channel 1 in Fig. 5.16.

As also shown in Fig. 5.16, the FFT, represented by Channel M, details the spectrum of the common-mode voltage. This common-mode voltage has very high amplitudes both at DC and the switching frequency. Also, a low frequency component can be seen on the measured voltage, which is caused by the *100 Hz* single-phase power variation.
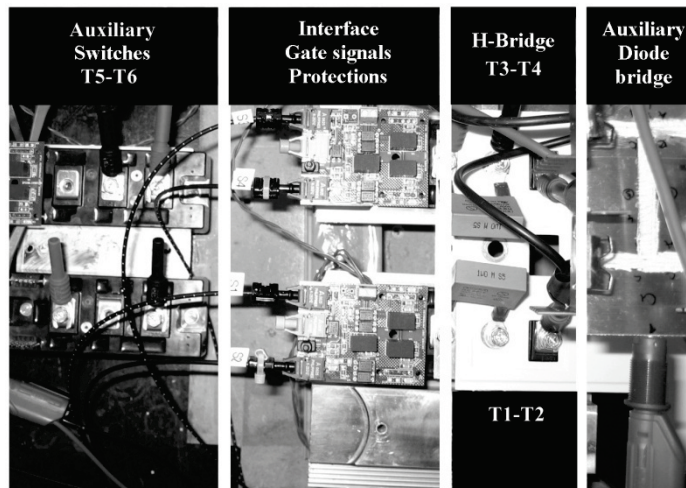
Fig. 5.15. Laboratory setup, showing all the components of the modular solution used for obtaining the experimental results.

Fig. 5.16. Experimental results for H-Bridge topology with unipolar PWM, Channel 1 shows the voltage to ground of the DC+ terminal, Channel 2 shows the ground leakage current and Channel M shows the voltage to ground of the DC+ terminal.

This varying common-mode voltage generates a very high ground leakage current that is only limited by the parasitic capacitance of the PV array. In this case the leakage current reaches to peaks around *6 A* as shown on Channel 2 in Fig. 5.16.

5.3.2 HERIC (experiment)

As presented in the simulation results (subsection 5.2.2), the HERIC topology ge-nerates a constant common-mode voltage by disconnecting the PV from the load (which may also be the grid in a grid connected application) during the state of the zero voltage, when the output of the inverter is short-circuited. This separation ensures that the common-mode voltage acting on the parasitic capacitance of the PV array does not change over time, therefore keeping the leakage current at very low values, well below the standard requirement of *300 mA* given by VDE-0126-1-1, the German standard for grid connected PV systems.

As shown in Fig. 5.17, the voltage measured between the DC+ terminal of the DC-link and ground is constant and has no high frequency content, represented by channel 1 on the scope. An FFT of Channel 1 also shows only a DC component of the measured voltage.

Furthermore, the leakage current, represented on Channel 2 in the scope results in Fig. 5.17, is also very low, with an RMS value around *22 mA*.
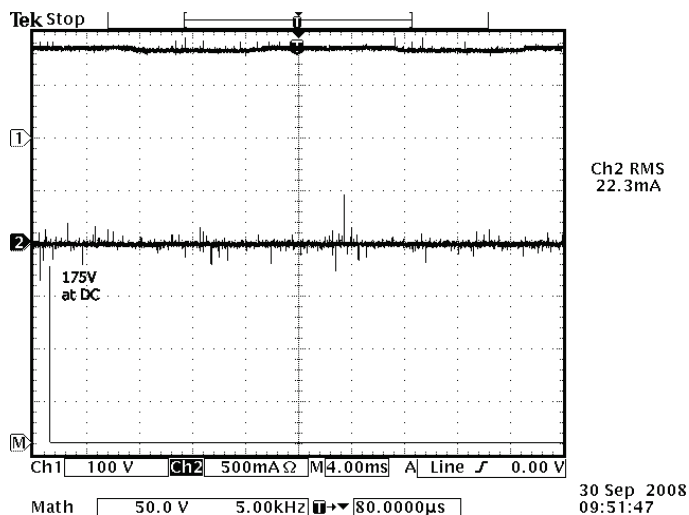
Fig. 5.17. Experimental results for HERIC topology, Channel 1 shows the voltage to ground of the DC+ terminal, Channel 2 shows the ground leakage current and Channel M shows the voltage to ground of the DC+ terminal.

5.3.3 HB-ZVR (experiment)

As mentioned in 5.2.3, the HB-ZVR topology generates the zero voltage state in a similar way to the HERIC topology, but uses another solution for the bidirectional

switch configuration. Of course, the common-mode behavior of the topology is similar to the case of the HERIC topology.

As shown in Fig. 5.18, the voltage measured between the DC+ terminal of the DC-link and ground is constant and has no high frequency content, represented by Channel 1 on the scope picture. An FFT of this voltage also shows only a DC component without any high frequency components.

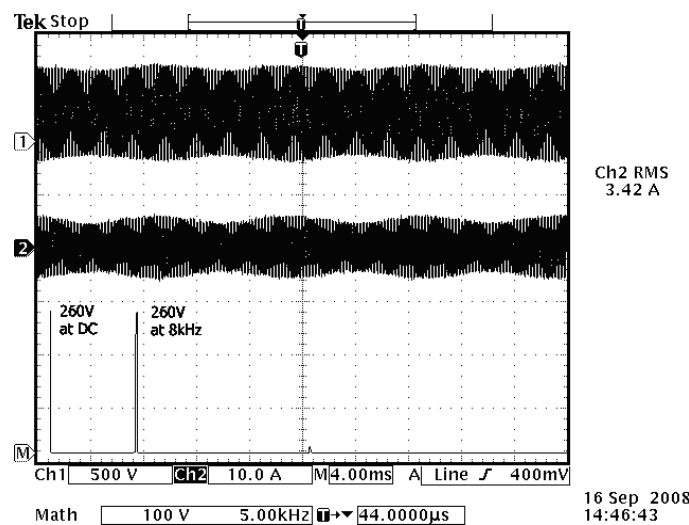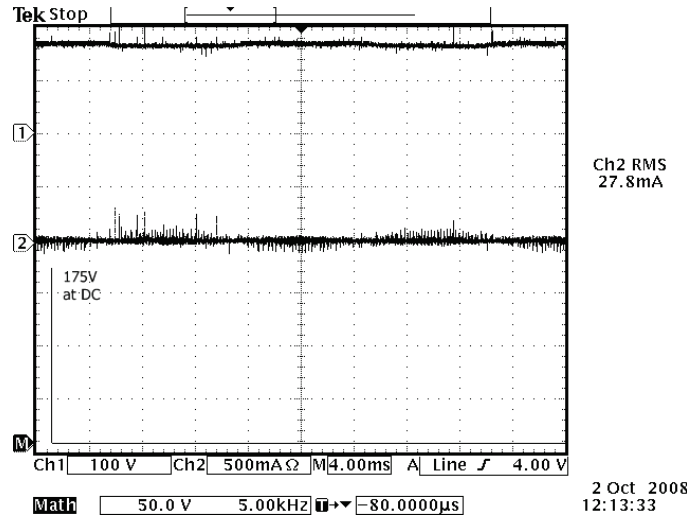*Fig. 5.18. Experimental results for HB-ZVR topology, Channel 1 shows the voltage to ground of the DC+ terminal, Channel 2 shows the ground leakage current and Channel M shows the voltage to ground of the DC+ terminal.*

In this case also, as detailed by Channel 2 in the scope results from Fig. 5.18, the leakage current, has also very low values, with an RMS value around *27mA*.

5.4 Efficiency

In case of a single-phase grid connection, the required minimum DC-link input voltage of the inverter, in the European case, has to be at least *350 V*, otherwise a boost stage is required. The tests have been done with an input voltage of V_{dc}=*350 V*.

The HERIC topology, as also suggested by its name, has very high conversion efficiency throughout the whole working range and has the best efficiency within the compared topologies, as detailed in Table 5-1 and also shown in Fig. 5.19.

The HB-ZVR topology has a slightly lower efficiency, due to the fact that the bidirectional switch is controlled with the switching frequency, while in the case of the HERIC topology, the bidirectional switch is only switched with the mains frequency. With a maximum efficiency of *94.9 %, the HB-ZVR* is a very attractive solution for transformerless PV systems.

The H-Bridge topology with Bipolar PWM (HB-Bip) has the lowest efficiency, due to the high losses as a result of the two level voltage output.

The efficiency of the H-Bridge topology with Unipolar PWM has not been included in the efficiency comparison of the transformerless topologies from Fig. 5.19 and Table 5-1 because of the influence of the galvanic isolation, where extra losses, as high as *2 %*, are possible due to the added transformer.

Nowadays most PV inverters are current controlled, injecting only active power into the utility grid. When there are many inverters injecting active power at the same time, the voltage at Point of Common Coupling (PCC) might rise over the limits stated in the standards and trigger the safety of the inverters, leading to a disconnection or a limit in the power production below the available power. This leads to extra losses because not all the available PV power is fed into the grid. If PV inverters have a P-Q implemented control, the before mentioned drawback could be dealt with by the injection of reactive power, thereby controlling the voltage at PCC. Therefore, the capability of injecting reactive power would be a major advantage of future PV inverters, improving the total production of the PV system.

The advantage of HB-ZVR is that the HERIC topology, with the implemented PWM strategy, is only ideal for PV systems that supply the grid with active power, otherwise said to have the power factor: $\cos\varphi = 1$. This is because the bidirectional switch of the HERIC topology made up of T5 and T6 is not controlled to be turned-ON simultaneously. Therefore current can only flow in a predefined direction, defined by the currently turned-ON switch. In [51] it is mentioned, that for reactive power flow, switches T5 and T6 should be simultaneously controlled, one with the grid frequency, the other one with the switching frequency.

On the other hand, in case of the HB-ZVR, it does not matter what the sign the load current has, it will always find a path through the bidirectional switch, made up of a diode bridge and a switch. This makes it possible to have a reactive power flow that can be used to support the utility grid with additional services any time during the functioning of the inverter.

Table 5-1: Efficiency at different input power with V_{dc}=350 V.

	500W	1000W	1500W	2000W	2500W	2800W
HB-Bip	84,3%	90,2%	92,5%	93,6%	94,3%	94,5%
HERIC	93,4%	94,7%	95,3%	95,6%	95,8%	95,9%
HB-ZVR	90,4%	92,8%	93,8%	94,4%	94,8%	94,9%
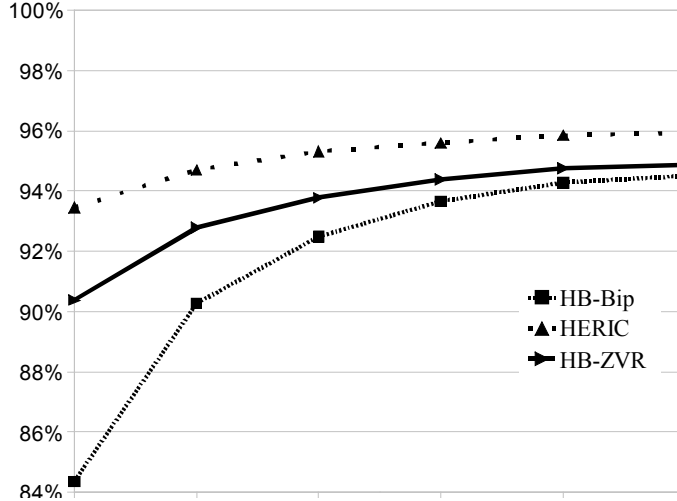
Fig. 5.19. Efficiency curve of the different topologies (V_{dc}=350 V).

A disadvantage of HB-ZVR is the lower conversion efficiency, than that of the HERIC topology, due to the high-frequency switching pattern of the auxiliary switch T5, while in case of the HERIC topology T5 and T6 are switched at the grid frequency.

The efficiency of the tested topologies can be further increased by using 600V IGBTs and, for the HB-ZVR, faster switches with shorter dead-time will also increase the efficiency.

5.5 Summary

This chapter introduced a novel transformerless topology derived from HERIC, but with an alternative solution for the bidirectional switch, used to generate the zero voltage state. The constant common-mode voltage of the HB-ZVR topology and its high efficiency makes it an attractive solution for transformerless PV applications, although the efficiency is lower than the HERIC, but higher than for the HB-Bip.

Chapter 6

Conclusion

This chapter summarizes the work done during the period of the PhD project and finishes with recommendations for future work regarding the areas that can still be improved.

6.1 Summary

The work presented in this thesis deals with analyzing and modeling of transformerless PV inverter systems regarding the leakage current phenomenon that can damage solar panels and pose human safety risks.

The major task of this research was the investigation and verification of transformerless topologies and control strategies that would minimize the leakage current of PV inverter topologies in order to comply with the standard requirements and make them safe for human interaction.

The thesis is divided into two parts: Part I – Report and Part II – Publications. Part I is a summary report of the work done throughout the research and contains 6 chapters.

Chapter 1 begins with an introduction of grid-connected PV systems, giving some details about the background and motivation regarding this PhD project. It continues with the problem formulation, the objectives and the limitations of the work and finishes with a list of the main contributions.

Chapter 2 highlights the advantages of transformerless PV inverters compared to topologies with galvanic isolation. It is shown that transformerless topologies are smaller in size and have higher efficiencies than inverters with high-frequency or low-frequency transformers. Furthermore, a summary of several transformerless PV inverter topologies is presented, detailing many different topology structures that are used by the PV industry or have been proposed as transformerless PV inverters. Finally the

parasitic capacitance of the PV array is discussed and measured in case of several commercial PV panels, emphasizing the safety issues regarding ground leakage currents due to varying voltages imposed over this capacitance.

In Chapter 3, several single-phase and three phase topologies are investigated, focusing on the ground voltage measured at the terminals of the PV array as well as the suitability of each topology in transformerless grid connected PV systems. It is shown that, in case of the single-phase topologies, the H-Bridge with Unipolar PWM is not suitable for transformerless PV systems, due to the way the zero voltage vector is achieved, leading to very high leakage ground currents, limited only by the parasitic capacitance of the PV array. It is still possible to achieve unipolar output voltage, as is the case of the HERIC, H5, NPC and other topologies, and the common-mode voltage is kept constant by either disconnecting the PV array from the grid during the zero voltage vector or by connecting the midpoint of the DC-link to the neutral of the grid. The ground leakage current can be further reduced in certain cases, by choosing a modulation strategy like the staggered PWM, as was the case for the 3FBSC topology. It can therefore be concluded that the common-mode behavior of a PV system is influenced by the chosen topology and modulation strategy.

Chapter 4 offers a comprehensive analysis of the single- and three-phase transformerless converter with respect to the problem of the leakage current that flows through the parasitic capacitance of the PV array. The adopted common-mode model of the system reveals that connecting the supply neutral to the middle of the DC-link capacitors will result in low-ripple voltage at both DC-link terminals of the PV array leading to a very low leakage current level, below the VDE 0126-01-01 standard requirement of *300mA*. However, the presence of inductance in the neutral line can lead to high frequency components in the common-mode voltage, leading to leakage ground currents, higher than the allowed level given in the standard. Therefore, it is crucial that the neutral line has very low inductance in transformerless PV systems where the middle of the DC-link is connected to the grounded neutral of the grid.

In Chapter 5, a new topology called H-Bridge Zero Voltage Rectifier (HB-ZVR) is proposed where the zero voltage is achieved by short-circuiting the grid voltage through the LCL filter, using a diode bridge rectifier and one switch. During the zero voltage period, the mid-point of the DC-link is clamped to the short-circuited grid. A comparison of known transformerless topologies and the HB-ZVR is performed using simulation, focusing on the voltage to earth and ground leakage current. Furthermore experimental results are shown, confirming the simulations. And, finally, the efficiency curve of the compared topologies is detailed. The constant common-mode voltage of the HB-ZVR topology and its high efficiency makes it an attractive solution for transformerless PV applications.

6.2 Main contributions

A short list of contributions is included in the order they appear in the thesis.

- Review and simulation of PV topologies

A comprehensive review is presented modeling several single- and three-phase transformerless topologies, focusing on the leakage ground current. It has been shown that the H-Bridge topology with unipolar PWM, as well as the three-phase full bridge topology, generate very high leakage current and are therefore not suitable as transformerless PV inverters. It is also emphasized that connecting the midpoint of the DC-link to the neutral of the grid will substantially reduce the generated leakage current in the case of the half-bridge or neutral-point clamped topologies, although the chosen grid side filter configuration might negatively influence the common-mode behavior of the topology.

- Interleaved PWM

The capacitor in the inverters' DC-link tends to get reduced, due to cost reduction from the manufacturers side. This means that the ripple in the DC-link will be increased, leading to higher leakage ground currents through the parasitic capacitance of the PV array. This thesis includes a new application of the interleaved PWM for three-phase inverters that has been modeled in simulation. The ripple of the DC-link voltage is reduced, thereby further reducing the leakage current in case of the three-phase full bridge split capacitor topology.

- Modeling of common-mode voltage

The leakage current of a certain topology is greatly influenced by the generated common-mode voltage that will be imposed on the parasitic capacitance of the PV array. To show the influence on the common-mode behavior of the topology in the case of inductor unbalance or inductance in the neutral wire, a model-based method for calculating the total common-mode voltage of transformerless topologies has been developed in this thesis.

- New topology

Nowadays, PV inverters feed only active power to the grid, having a power factor of 1. When there are many inverters injecting active power at the same time, the voltage at Point of Common Coupling might rise over the limits stated in the standards and trigger the safety of the inverters leading to disconnection or limit the power production below the available power. To overcome the before-mentioned disadvantage, a new high efficiency transformerless PV inverter topology called HB-ZVR (with very low leakage ground current) is proposed. The topology uses a bidirectional switch for short-circuiting the output of the converter during the zero voltage period using a switch and a diode bridge, capable of active and reactive power injection.

6.3 Future work

There are several research tasks for future work and some of these are mentioned below:

- During the presented work, simulations included ideal components and the efficiency of the topologies has not been calculated. Nevertheless, by taking into account switching and conduction losses for switching elements (a possibility given by the PLECS toolbox in MATLAB/Simulink®) the efficiency can also be calculated in simulation, also including losses for the passive components.

- DC-current injection is of great interest in transformerless PV inverters. New topologies or control strategies could be investigated, that eliminate or minimize the DC part in the injected AC current.

- In Chapter 5 a novel transformerless topology has been proposed, namely HB-ZVR. Further investigations are possible to improve the efficiency of the proposed topology, by choosing better components: for example 600V SiC switches and SiC diodes.

Appendix A

The measuring performance of two commercially available differential current sensors was tested. A setup was built for this purpose at AAU. This appendix details the test for the LEM CT 0.2-P and TELCON HES25VT current sensors, provided by PowerLynx A/S. A sketch for the proposed test setup can be seen in Fig. A.1, and the equipment used is listed also below:

- Power supply for *20 A* AC current: three-phase grid connection, *32 A* max. current
- R$_1$: variable resistor
- R$_2$: low power resistor, *500 Ω, 1 A*
- DUT (current probe)
- DC supply for *100 mA*: GW Instek GPS 4303
- Multimeter: Fluke 45 used for measuring current on the low power side
- Multimeter: Fluke 179 used for measuring the sensor output voltage

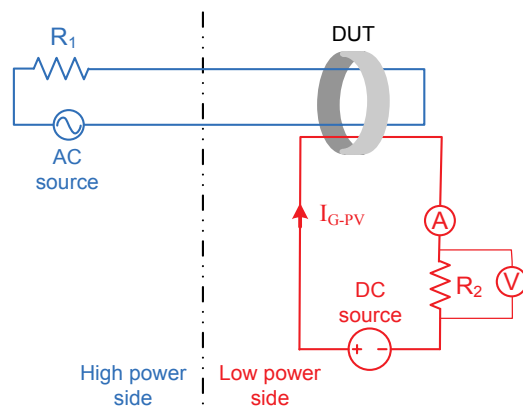*Fig. A.1 Laboratory setup for testing the step response of the sensors*

The grid was used in order to produce an AC current of *20 A* in the high power side, using resistor: *R$_1$=11 Ω*. DUT represents the Device Under Test, which is the current probe that is being tested. The high power wire is twice put through the DUT in order to cancel out its influence. Therefore the DUT only measures the controlled

leakage current produced by the low power side. The low power side is separate from the high power side and is used to produce a DC current up to *100 mA*, which simulates the "leakage current" that has to be precisely measured by the DUT.

A.1 LEM CT-0.2P

According to its datasheet, the sensor was supplied with *±15 V* and since the output is a current source, it was paralleled with a R_L=*10 kΩ* resistor [67]. Therefore the voltage output of the sensor should be *5 V* in case of a *200 mA* current sensed by the LEM CT-0.2-P. Since the measured value of the resistor was *9.96 kΩ*, the output of the sensor should only be *4.95 V* in case of a *200 mA* measured current.

A.1.1 Step response

The test includes the sensor response for *20, 50* and *100mA* step change in the leakage current. The step response was viewed using an oscilloscope. The step response was repeated both with and without current in the high power side. In Fig. A.2 and Fig. A.3 the step response of the transducer for *20 mA, 50 mA,* and *100 mA* current levels can be seen.
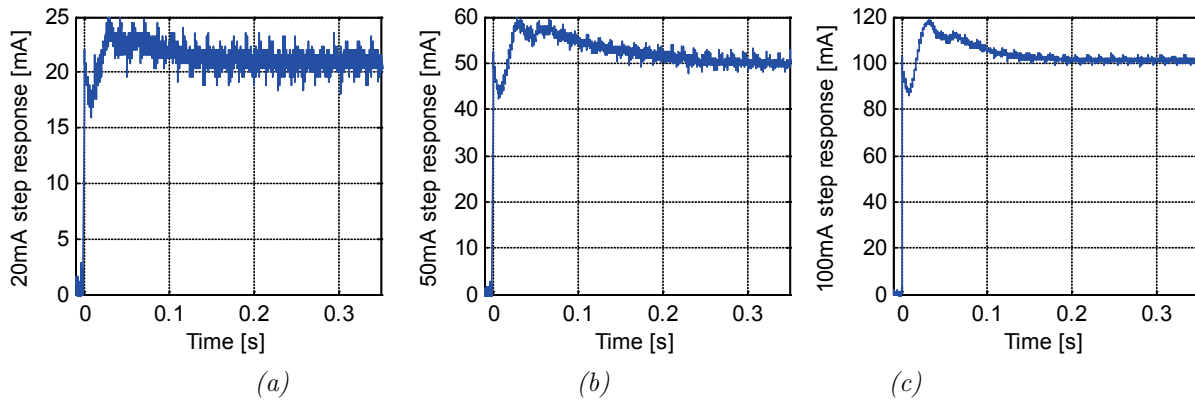

(a)   (b)   (c)

Fig. A.2 LEM CT 0.2-P step response for 20 mA (a), 50 mA (b) and 100 mA (c) leakage current and with no current in high power side

As can be observed in Fig. A.2 and Fig. A.3, the sensor responds immediately, only having an oscillation, within the range of *±20%*. But this overshoot settles in *0.2 s* in case of all readings.
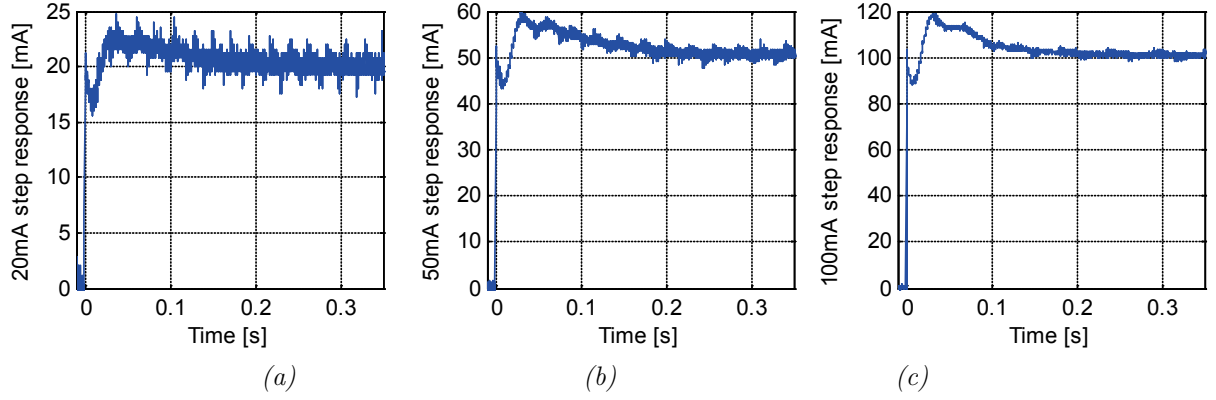
Fig. A.3 LEM CT 0.2-P step response for 20mA (a), 50mA (b) and 100mA (c) leakage current and with 20A current in high power side

In order to compare the behaviour of the sensor with and without current in the high power side, the step response for both readings was compared. The red curve represents the step response with no current in the high power side, while the blue one represents the other case, with *20 A* AC current flowing through the high power side. As can be observed, there is no major difference between the two cases, no matter what the level of the reference current was.

Fig. A.4 Step response comparison for LEM CT 0.2-P

The steady state values of the output of the sensor were also measured and are presented in Table A-1 and Table A-2, where:

- I_{ref} – current reference value
- $I_{Fluke45}$ – Fluke 45 measurement
- V_{out} – sensor output
- I_{meas} – calculated current, based on R_L and V_{out}
- ε – absolute error

The absolute error is calculated based on the sensor output and the Fluke45 current measurement. The Fluke45 has a $\pm 0.05\%$ accuracy for DC values.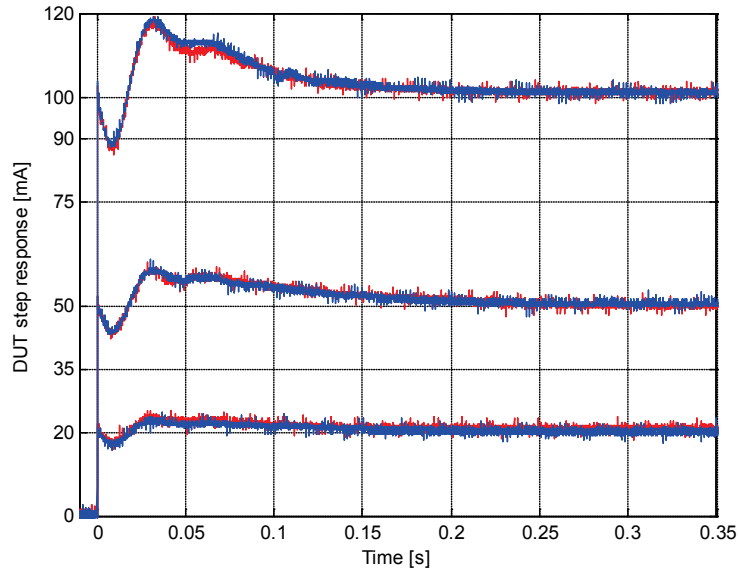 I_{meas} was calculated using the measured resistance value of $R_L=9.96\ k\Omega$. The calculated absolute error is increasing linearly with the current level and reaches a maximum value of *0.38 mA* in case of the *100 mA* current measurement.

Table A-1: Measured steady state data for LEM CT 0.2-P, when there was no current in the high power side

I_{ref} [mA]	$I_{Fluke45}$ [mA]	V_{out} [V]	I_{meas} [mA]	ε [mA]
20	20.11	0.499	20.20	0.09
50	50.11	1.252	50.28	0.17
100	100.14	2.503	100.52	0.38

Table A-2: Measured steady state data for LEM CT 0.2-P, when there were 20 A in the high power side

I_{ref} [mA]	$I_{Fluke45}$ [mA]	V_{out} [V]	I_{meas} [mA]	ε [mA]
20	20.01	0.499	20.04	0.03
50	50.14	1.252	50.28	0.14
100	100.27	2.505	100.60	0.33

A.1.2 Problems

- When the sensor was supplied with ± 15 V (as recommended in the datasheet), there was a voltage present on the output of the sensor which would act as a DC offset in the case of all measurements. This value was around 50 mV. By tuning the input voltage to ± 14.1 V this DC offset was minimized to $1\div 3$ mV.

- Another frequent problem was the appearance of another DC offset on the sensor output. This offset had a value of up to 140 mV, but would disappear after a few resets of the sensor. Reset means a supply disconnect followed by a reconnect (OFF-ON). This phenomenon was observed only in case of resets. If the output of the sensor stabilized around 0, this type of offset would not reap-

pear during the readings. The available LEM CT 0.2-P sensors were tested and the same offset problems appeared in both cases with slightly different values.

A.1.3 "Capacitor discharge" test

The used circuit included a capacitor with a discharge time in the range of *1µs* and a current limitation of *20 A* peak. A sketch for the proposed test setup can be seen in Fig. A.5. As can be seen in Fig. A.6, the capacitor was first charged and then discharged through a resistance. The influence of this high frequency discharge current was investigated.
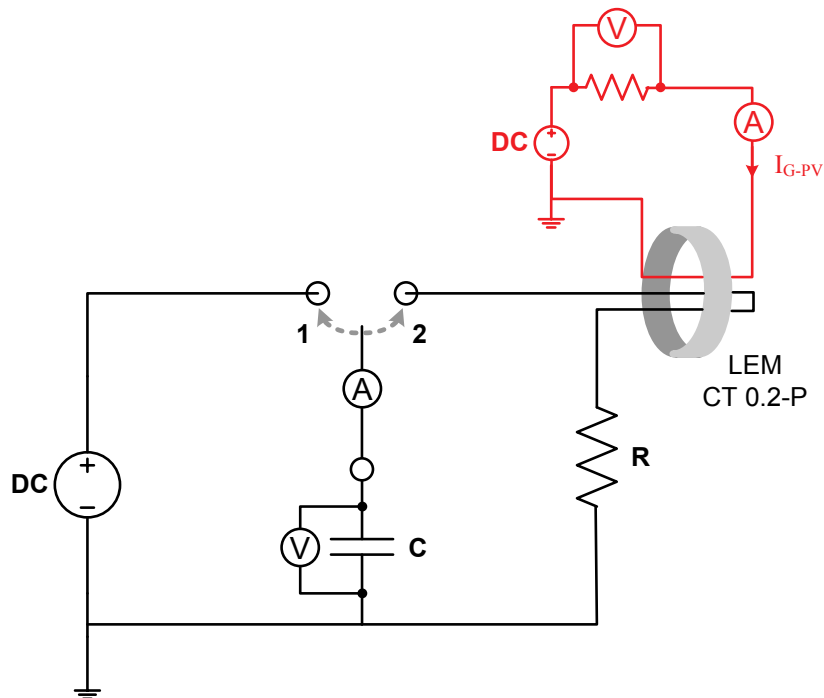
Fig. A.5 Laboratory test-setup for discharge test for the LEM CT 0.2-P

The measurement results show that there are some high frequency oscillations present in the sensor output due to the high discharge current of the capacitor.
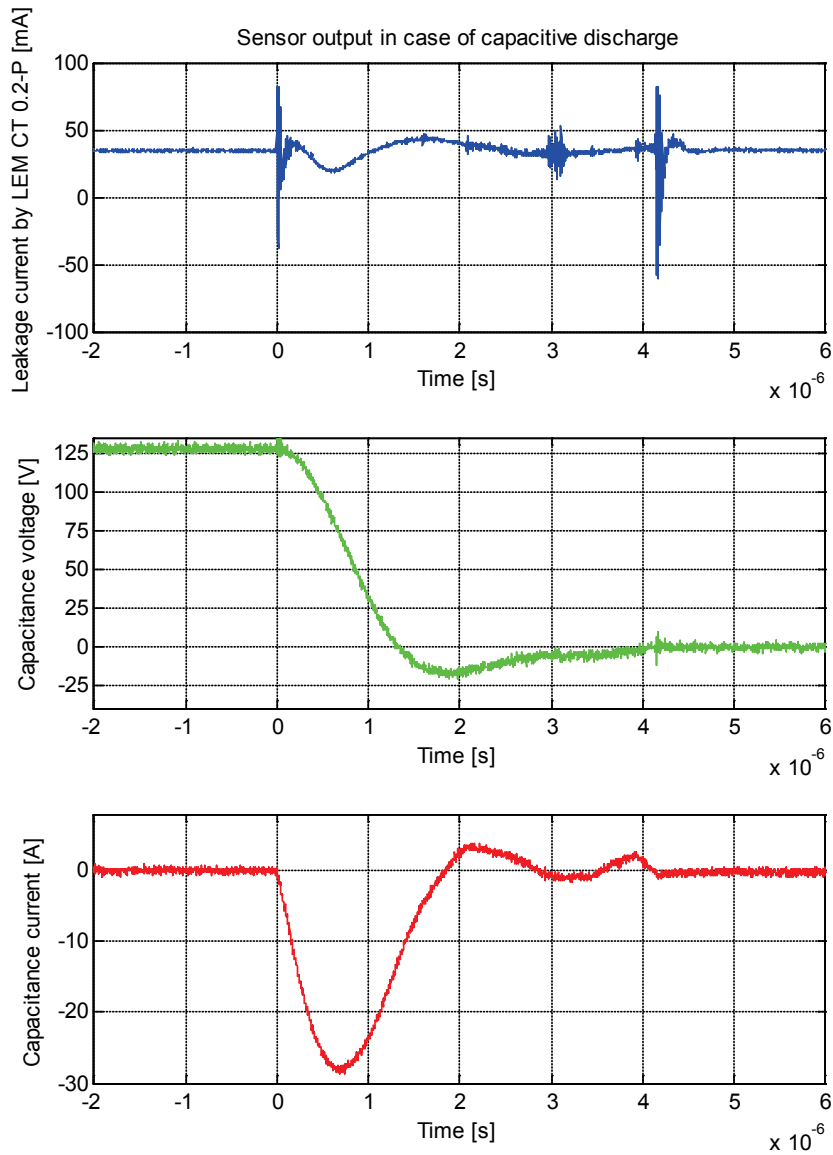
Fig. A.6: Capacitive discharge test

A.2 Telcon HES 25VT sensor test results

Test setup is presented in Fig. A.1. The same test conditions apply, as were also the case for the LEM sensor:

- *20 A* RMS current in high power side (if the case)
- R_2 = variable resistor for *20 mA, 50 mA* and *100 mA* leakage current
- R_{sense} = *26.1 kΩ* (so that at *200 mA* the sensor output should be *5 V*, the same scaling was used for the LEM CT 0.2-P sensor too)

- the zero offset adjustment was done with a variable resistance; when there was no current through the sensor, the output of the sensor was between *10mV - 30 mV* (lower than *1.2 mA* offset)

A.2.1 Step response

The sensor output voltage and the voltage on *R2* were measured and compared. The blue line is the sensor output voltage (Voltages are recalculated to the current reference in mAmps) and the red line is the reference, the voltage applied on *R2*. Three step responses have been measured: for *20 mA, 50 mA* and *100mA*. The rise time of the sensor is very fast, around *2.5 ms*. This can be observed on Fig. A.7.
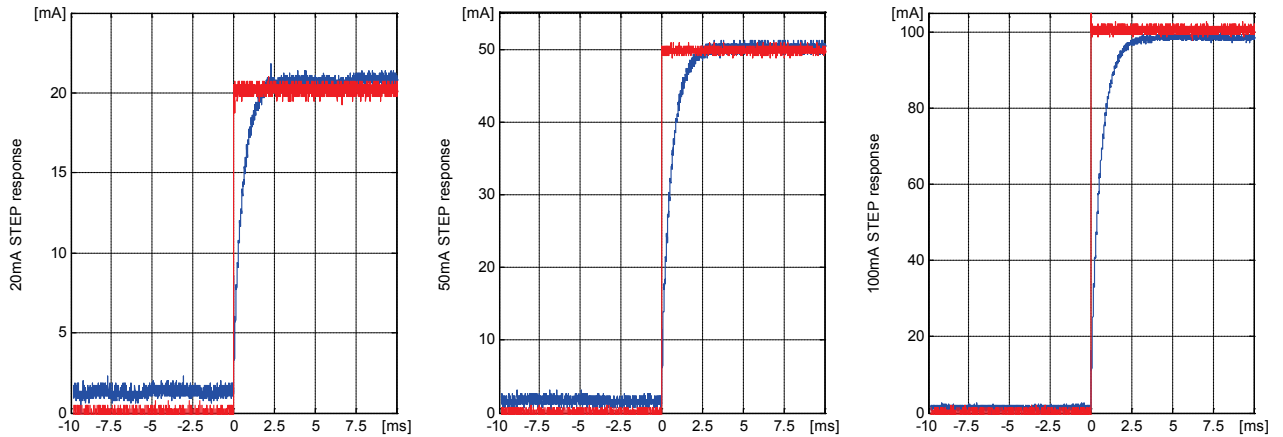
Fig. A.7: Step response for different current levels, when no current in high side

A.2.2 Step response with 20A 50Hz AC current in high power side

When there is power in the high power side, the output of the sensor will contain a *50 Hz* ripple. This *50 Hz* ripple has *10 mA* amplitude and it is added to the measurement so that the output of the sensor is a sinusoidal signal with a DC offset. The blue line is the sensor output voltage (the values in Voltages are recalculated to the current reference in mAmps) and the red line is the reference, the current through *R2* (see Fig. A.8.)
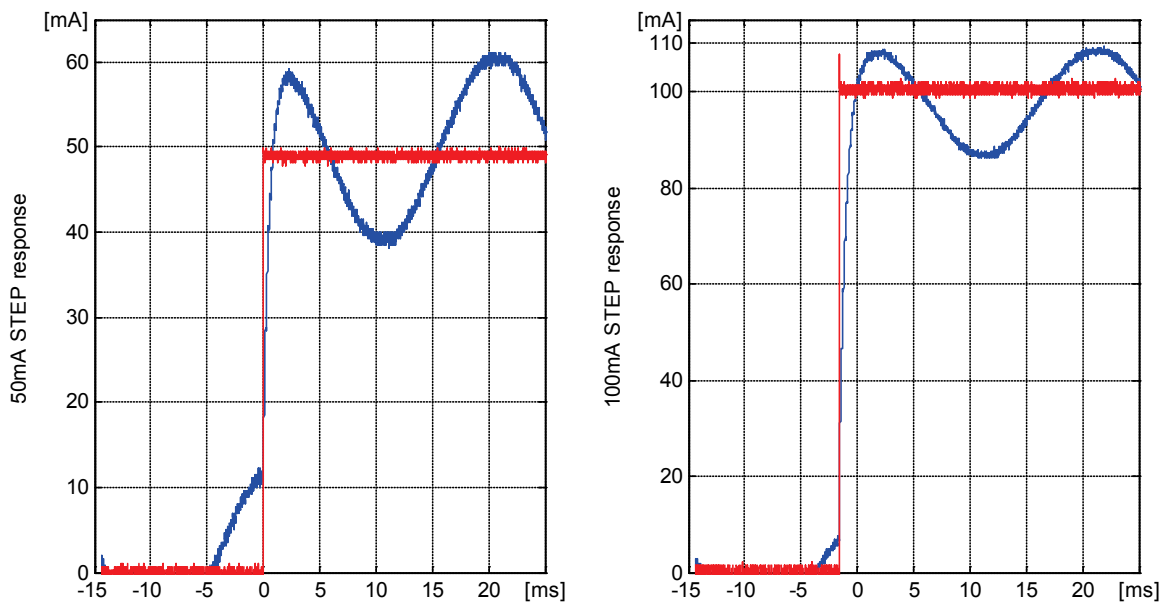
Fig. A.8: Step response for different current levels, when 20A 50Hz AC current in high side

Fig. A.9 presents the sensor output and the reference when there is power in the high power side. On the left graph there is a *23 mA* current in the low power side and on the right graph there is no leakage current present in the low power side. In both cases a *50 Hz* component can be observed, which is due to the presence of the *20 A* current in the high power side. The blue line is the sensor output voltage (Voltages are recalculated to the current reference in mAmps) and the red line is the reference, the current through *R2*.
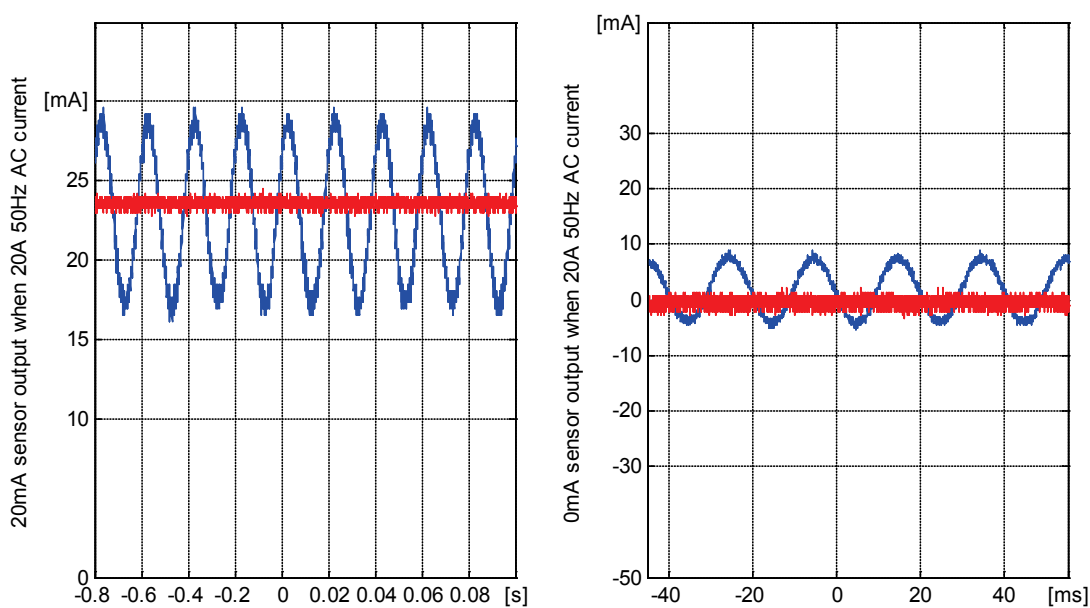

Fig. A.9: Test results for 20 mA and 0 mA(zero) leakage current,

The plastic casing of the sensor was removed for further testing. Fig. A.10 shows the real sensor without the protective plastic casing.

A.2.3 Sensor output DC offset

The offset of the sensor output depends on the Hall element position relative to core air gap. A small displacement of the core results in an offset variation of *±100 mV* with R_{sense}=*26 kΩ*. Touching the core with the wire was enough displacement in order to change the offset.
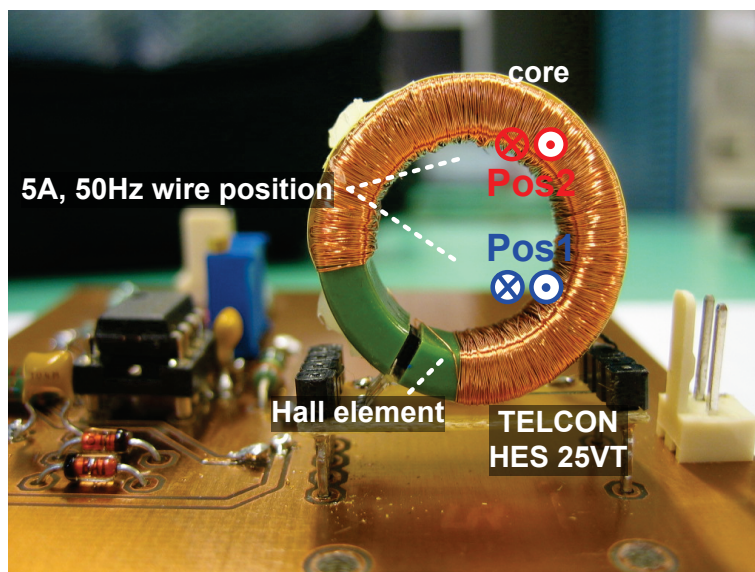
Fig. A.10: Telcon HES 25VT sensor, without the plastic casing

A.2.4 Sensor output influenced by 50Hz current

The 50Hz influence was further tested. Both cases are presented, the wires having been placed in two different positions, shown with labels "Pos1" and "Pos2" in Fig. A.10. The maximum influence was when the high-power wires, having a *5 A* peak current at *50 Hz*, were nearest to the Hall element (marked with Pos 1 in Fig. A.10).

The output of the sensor can be seen in Fig. A.11 in blue line, while the red line shows the sensor output when the high-power wire was furthest from the Hall element (Pos2).
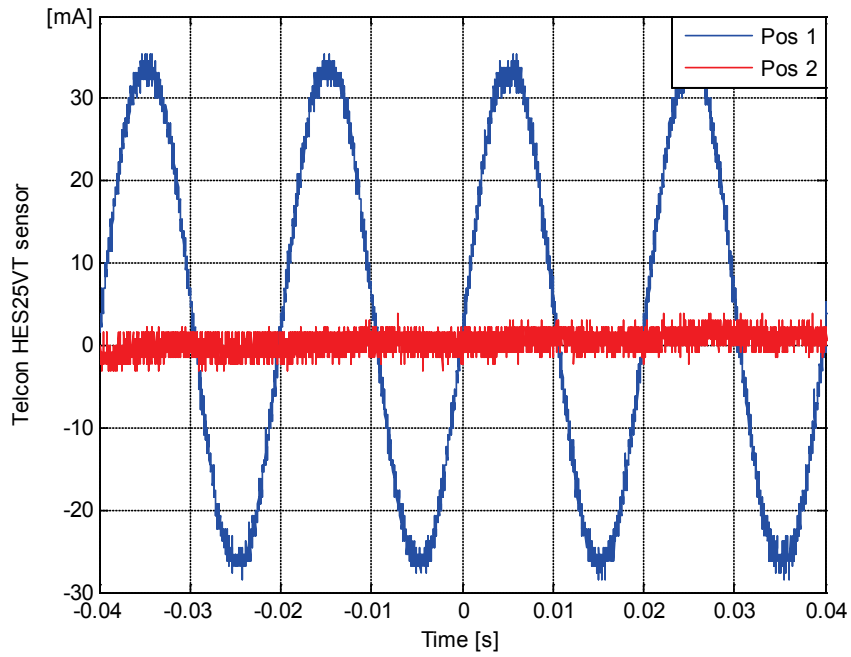
Fig. A.11: Sensor output, when no leakage current, only 5 A, 50 Hz current in high-power wires

Observation:

The position of the wire used to generate the leakage current in the low power side (red wire in Fig. A.1) had no influence on the sensor output.

References

[1] W. Kleinkauf, G. Cramer, and M. Ibrahim; "PV Systems Technology - State of the art developments and trends in remote electrification"; SMA Technologie AG, Dec. 01, 2005.

[2] M. Calais and V. Agelidis; "Multilevel converters for single-phase grid connected photovoltaic systems, an overview"; in *IEEE - International Symposium on Industrial Electronics*, 7-10 Jul. 1998, pp. 224-229

[3] N. Jenkins; "Photovoltaic systems for small-scale remote power supplies"; *Power Engineering Journal*, vol. 9, no. 2, Apr. 1995, pp. 89-96

[4] M. Svrzek and G. Sterzinger; "Solar PV Development: Location of Economic Activity"; Renewable Energy Policy Report 2005.

[5] IEA-International Energy Agency; "Trends in Photovoltaic Applications: Survey report of selected IEA countries between 1992 and 2006"; Report IEA-PVPS T1-16:2007, 2007.

[6] IEA-International Energy Agency; "Trends in Photovoltaic Applications: Survey report of selected IEA countries between 1992 and 2007"; Report IEA-PVPS T1-17:2008, 2008.

[7] EPIA; "Global market outlook for photovoltaics until 2013"; European Photovoltaic Industry Association, 2009.

[8] M.J. de Wild-Scholten, E.A. Alsema, E.W. ter Horst, M. Bächler, and V.M. Fthenakis; "A Cost and Environmental Impact Comparison Of Grid-Connected Rooftop And Ground-Based Pv Systems"; in *21th European Photovoltaic Solar Energy Conference*, 4-8 Sep. 2006, pp. 1-7

[9] M. Abella and F. Chenlo; "Choosing the right inverter for grid-connected PV systems"; *Renewable Energy World*, vol. 7, no. 2, Mar-Apr. 2004, pp. 132-147

[10] S. Kjær, J. Pedersen, and F. Blaabjerg; "A review of single-phase grid connected inverters for photovoltaic modules"; *IEEE Transactions on Industry Applications*, vol. 41, no. 5, Sep. 2005, pp. 1292- 1306

[11] J.M. Carrasco et al.; "Power-Electronic Systems for the Grid Integration of Renewable Energy Sources: A Survey"; *IEEE Transactions on Industrial Electronics*, vol. 53, no. 4, Aug. 2006, pp. 1002-1016

[12] H. Häberlin; "Evolution of inverters for grid connected PV-systems from 1989 to 2000"; in *17th European Photovoltaic Solar Energy Conference*, 22-26 Oct. 2002

[13] M Meinhardt and G. Cramer; "Past, Present and Future of grid connected Photovoltaic- and Hybrid-PowerSystems"; in *IEEE - Power Engineering Society Summer Meeting*, 16-20 Jul. 2000, pp. 1283-1288

[14] M. Calais, J. Myrzik, T. Spooner, and V.G. Agelidis; "Inverters for single-phase grid connected photovoltaic systems-an overview"; in *IEEE 33rd AnnualPower Electronics Specialists Conference*, 23-27 Jun 2002, pp. 1995 - 2000

[15] M. Meinhardt, G. Cramer, B. Burger, and P. Zacharias; "Multi-string-converter with reduced specific costs and enhanced functionality"; *Solar Energy*, vol. 69, no. 1-6, 2000, pp. 217-227

[16] M. Meinhardt and G. Cramer; "Multi-String-Converter: The next step in evolution of String-Converter Technology"; in *Proceeding of European Power Electronics Conference*, 2001

[17] Danish Standard Association; "DS/HD 60364-7-712 Electrical installations of buildings – Part 7-712: Requirements for special installations or locations – Solar photovoltaic (PV) power supply systems"; 2005.

[18] IEEE Std 1547.1-2005. IEEE Standard Conformance Test Procedures for Equipment Interconnecting Distributed Resources with Electric Power Systems.

[19] IEEE 929-2000. Recommended Practice for Utility Interface of Photovoltaic (PV) Systems.

[20] IEC 61727; "Characteristics of the utility interface for photovoltaic (PV) systems"; International Electrotechnical Commission, IEC 61727, 2002.

[21] BS EN 61000-3-2. (2001) Electromagnetic Compatibility - Part 3-2: Limits - Limits for harmonic current emmisions (equipment input current up to and including 16A per phase).

[22] DKE Deutsche Kommission Elektrotechnik Electronik Informationstechnik im DIN un VDE; "Selbsttätige Freischaltstelle zwischen einer netzparallelen Eigenerzeugungsanlage und dem öffentlichen Niederspannungsnetz"; DIN VDE 0126-1-1, 2006.

[23] V. Salas and E. Olias; "Overview of the state of technique for PV inverters used in low voltage grid-connected PV systems: Inverters below 10 kW"; *Renewable and Sustainable Energy Reviews*, 2009, pp. 1-10

[24] S. Rollier, B. Richard, and M. Keller; "Earth leakage control in solar inverters"; *Power System Design Europe*, May 2005

[25] Ministerio de economia; "Real Decreto 1663/2000 Article 12"; 2000.

[26] T. Ishikawa; "Grid Connected Photovoltaic Power Systems: Survey of Inverter and Related Protection Equipments"; Report IEA PVPS T5-05: 2002, 2006.

[27] L. Gertmar, P. Karlsson, and O. Samuelsson; "On DC Injection to AC Grids from Distributed Generation"; in *11th European Conference on Power Electronics and Applications*, 11-14 Sep. 2005, pp. 1-10

[28] B. Burger; "Auslegung und Dimensionierung von Wechselrichtern für netzgekoppelte PV-Anlagen"; in *20. Symposium Photovoltaische Solarenergie, Staffelstein*, 11 Mar. 2005

[29] H. Häberlin, Ch. Liebi, and Ch. Beutler; "Inverters for grid connected PV-Systems: Test results of some new inverters and latest reliability data of the most popular inverters in Switzerland"; in *14th European Photovoltaic Solar Energy Conference*, 30 Jun. - 4 Jul. 1997

[30] H. Häberlin, L. Borgna, M. Kaempfer, and U. Zwahlen; "New tests at grid connected PV inverters: Overview over test results and measured values of total efficiency"; in *21st European Photovoltaic Solar Energy Conference*, 4-8 Sep. 2006

[31] H. Häberlin, M. Kämpfer, and U. Zwahlen; "Neue Tests an Photovoltaic - Wechselrichtern: Gesamtübersicht über Testergebnisse und gemessene totale Wirkungsgrade"; in *21. Symposium Photovoltaische Solarenergie*, 2006

[32] M. Meinhardt; "Improvement of Photovoltaic Inverter Efficiency – Targets, Methods, Limits"; SMA Technologie AG, 2005?

[33] A. Schlumberger; "Market survey on inverters 2007"; *Photon International*, vol. 4, 2007

[34] S. Jain and V. Agarwal; "A Single-Stage Grid Connected Inverter Topology for Solar PV Systems With Maximum Power Point Tracking"; *IEEE Transactions on Power Electronics*, vol. 22, no. 5, Sep. 2007, pp. 1928-1940

[35] J.M.A. Myrzik; "Novel Inverter Topologies for Single-Phase Stand-Alone or Grid Connected Photovoltaic Systems"; in *4th IEEE International Conference on Power Electronics and Drive Systems*, 2001, pp. 103- 108

[36] M. Calais, J. Myrzik, T. Spooner, and V.Agelidis; "Inverters for single-phase grid connected photovoltaic systems – overview and prospects"; in *17th European Photovoltaic Solar Energy Conference*, 22-26 Oct. 2001, pp. 224-229

[37] J. Myrzik and M. Calais; "String and module integrated inverters for single phase grid connected photovoltaic systems – a review"; in *IEEE - Power Tech Conference Proceedings*, 23-26 Jun. 2003

[38] M.F. Rahman and L. Zhong; "A new, transformerless, photovoltaic array to utility grid interconnection"; in *IEEE International Conference on Power Electronics and Drive Systems*, 26-29 May 1997, pp. 139-143

[39] R. Cáceres and I. Barbi; "A Boost DC–AC Converter: Analysis, Design and Experimentation"; *IEEE Transactions on Power Electronics*, vol. 14, no. 1, Jan. 1999, pp. 134-141

[40] N. Vazquez, J. Almazan, J. Alvarez, C. Aguilar, and J. Arau; "Analysis and experimental study of the buck, boost and buck-boost inverters"; in *30th Annual IEEE Power Electronics Specialists Conference*, vol. 2, 1999, pp. 801-806

[41] N. Kasa, H. Ogawa, T. Iida, and H. Iwamoto; "A Transformer-Less Inverter using Buck-Boost Type Chopper Circuit for Photovoltaic Power System"; in *IEEE*

International Conference on Power Electronics and Drive Systems, 27-29 Jul. 1999, pp. 653-658

[42] Y. Xue, L. Chang, and P. Song; "Recent developments in topologies of single-phase buck-boost inverters for small distributed power generators: an overview"; in *IEEE The 4th International Power Electronics and Motion Control Conference*, vol. 3, 14-16 Aug. 2004, pp. 1118-1123

[43] Y. Xue, L. Chang, and S.B. Kjær; "Topologies of Single-Phase Inverters for Small Distributed Power Generators: An Overview"; *IEEE Transactions on Power Electronics*, vol. 19, no. 5, Sep. 2004, pp. 1305- 1314

[44] N. Kasa, T. Iida, and H. Iwamoto; "An inverter using buck-boost type chopper circuits for popularsmall-scale photovoltaic power system"; in *The 25th Annual Conference of Industrial Electronics Society*, 29 Nov. - 3 Dec. 1999, pp. 185-190

[45] Ch.M. Wang; "A Novel Single-Stage Full-Bridge Buck-Boost Inverter"; *IEEE Transactions on Power Electronics*, vol. 19, no. 1, 2004, pp. 150-158

[46] D. Karschny; "Flying inductor topology"; DE 196 42 522 C1, Apr. 23, 1998.

[47] D. Schekulin; "Transformatorlose Wechselrichter Schaltungsanordnung"; DE 197 31 218 C1, Mar 18, 1999.

[48] M. Meinhardt and P. Mutschler; "Inverters without transformer in photovoltaic applications"; in *European Conference on Power Electronics and Applications*, 1995, pp. 86-91

[49] H. Hinz and P. Mutschler; "Voltage source inverters for grid connected photovoltaic systems"; in *2nd World Conference and Exhibition on Photovoltaic Solar Energy Conversion*, Jul. 1998, pp. 2045-2048

[50] H. Hinz and P. Mutschler; "Single phase voltage source inverters without transformer in photovoltaic applications"; in *The 7th International Power Electronics & Motion Control Conference*, Sep 1996, pp. 3/161-3/165

[51] H. Schmidt and Ch. Siedle and J. Ketterer; "EP 1 369 985 A2";, Dec. 10, 2003.

[52] M. Victor, F. Greizer, and S. Bremicker and U. Hubler; "EP 1 626 494 A2";, 2005.

[53] R. Gonzales, J. Lopez, P. Sanchis, and L. Marroyo; "Transformerless Inverter for Single.Phase Photovoltaic Systems";, vol. 22, no. 2, Mar. 2007, pp. 693-697

[54] S. Saha and V.P. Sundarsingh; "Novel grid-connected photovoltaic inverter"; *IEE Proceedings of Generation, Transmission and Distribution*, vol. 143, no. 2, Mar. 1996, pp. 219-224

[55] S. Funabiki, T. Tanaka, and T. Nishi; "A new buck-boost-operation-based sinusoidal inverter circuit"; in *IEEE - Power Electronics Specialists Conference*, vol. 4, 23-27 Jun. 2002, pp. 1624-1629

[56] M. Kusakawa, H. Nagayoshi, K. Kamisako, and K. Kurokawa; "Further improvment of a transformerless voltage-boosting inverter for AC modules"; in *Solar Energy Material Solar Cells*, vol. 67, Mar. 2001, p. 379–387

[57] H.S. Choi, Y.J. Cho, J.D. Kim, and B.H. Cho; "Grid-Connected Photovoltaic Inverter with Zero-Current-Switching"; in *International Conference on Power Electronics*, Oct. 2001, pp. 251-255

[58] M. Calais, V.G. Agelidis, L.J. Borle, and M.S. Dymond; "A transformerless five level cascaded inverter based single phase photovoltaic system"; in *IEEE 31st Annual Power Electronics Specialists Conference*, vol. 3, 18-23 Jun. 2000, pp. 1173-1178

[59] J.A. Gow and C.D. Manning; "Photovoltaic converter system suitable for use in small scale stand-alone or grid connected applications"; *IEE Proceedings of Electric Power Applications*, vol. 147, no. 6, Nov. 2000, pp. 535-543

[60] H. Schmidt, B. Burger, and Chr. Siedle; "Gefährdungspotenzial transformatorloser Wechselrichter – Fakten und Gerüchte"; in *18. Symposium Photovoltaische Sonnenenergie*, 2003, pp. 89-98

[61] C. Bendel, P. Funtan, J Kirchhof, and D. Nestle; "Wechselrichterwechselwirkungen - Testergebnisse aus dem Forschungsprojekt SIDENA"; in *19. Symposium Photovoltaische Solarenergie*, 2004

[62] P. Zacharias, M. Köhl, K. Vanoli, and A. Herrfeld; "Qualifizierung und Qualitätssicherung zur Lebensdauer-Optimierung und Ertragskontrolle: Rückwirkungen auf Technologieentwicklung und Montage"; 2007.

[63] N. Henze and T. Degner; "Radio Interference of Photovoltaic Power Systems"; in *16th International Wroclaw Symposium and Exhibition on EMC*, 25-28 Jun. 2002, pp. 1-6

[64] O. Lopez, R. Teodorescu, and J. Doval-Gandoy; "Multilevel transformerless topologies for Single-Phase Grid-Connected Converters"; in *IEEE 32nd Annual Conference on Industrial Electronics*, 2006, pp. 5191-5196

[65] C. Bendel, P. Funtan, J. Kirchhof, and G. Klein; "Sicherheitsaspekte bei Einsatz und Prüfung von transformatorlosen Wechselrichtern – Ergebnisse aus dem Projekt SIDENA"; in *21. Symposium Photovoltaische Solarenergie*, 7-10 Mar. 2006

[66] Eisner Safety Consultants; "Leakage Current (Part 1)"; May 2002.

[67] LEM; "Current transducers CT 0.1. 0.4-P; datasheet; 080909/14";

[68] TELCON; "Hall Effect Current Transformers HES25VT, HES50VT HES100VT, HES25HR, HES50HR and HES100HR; datasheet";

[69] S.V. Araujo, A. Engler, B. Sahan, and F. Antunes; "LCL filter design for grid-connected NPC inverters in offshore wind turbines"; in *IEEE - 7th International Conference on Power Electronics*, 22-26 Oct. 2007, pp. 1133-1138

[70] N. Mohan and T.M. Undeland and W.P. Robbins; *Power Electronics: Converters, Applications, and Design.*: Wiley, 2002.

[71] H. Schmidt, B. Burger, and K. Kiefer; "Wechselwirkungen zwischen Solarmodulen und Wechselrichtern"; Fraunhofer-Institut für Solare Energiesysteme ISE,.

[72] D. Schekulin, P. Küber, and O. Schanz; "Modular Transformerless Inverters for Grid Connection of Large PV Generators"; in *EuroSun '96*, 1996, pp. 868-871

[73] B. Burger, B. Goeldi, H. Laukamp, and H. Schmidt; "Higher system efficiency in three phase plants through system voltages above 1000V"; in *23rd European Photovoltaic Solar Energy Conference*, 2008, pp. 2755-2757

[74] A. Nabae, I. Takahashi, and H. Akagi; "A New Neutral-Point-Clamped PWM Inverter"; *IEEE Transactions on Industry Applications*, vol. IA-17, no. 5, 1981, pp. 518-523

[75] B. Sahan, A.N. Vergara, N. Henze, A. Engler, and P. Zacharias; "A Single-Stage PV Module Integrated Converter Based on a Low-Power Current Source Inverter"; *IEEE Transactions on Industrial Electronics*, vol. 55, no. 7, Jul. 2008, pp. 2602-2609

[76] L.H. Kim et al.; "Analysis of a new PWM method for conducted EMI reduction in a field oriented controlled induction motor"; in *Applied Power Electronics Conference and Exposition*, 2006, p. 7

[77] Danfoss Solar A/S; "TripleLynx Inveerter datasheet"; 2009.

[78] R. Bruendlinger, C. Mayr, J. Kirchof, M. Moschakis, S. Nguefeu B. Bletterie; "Identification of general safety problems, definition of test procedures and design-measures for protection"; Österreichisches Forschungs- u. Prüfzentrum Arsenal GmbH, 2006.

[79] R. Gonzales, E. Gubia, J. Lopez, and L. Marroyo; "Transformerless Single-Phase Multilevel-Based Photovoltaic Inverter"; *IEEE Transactions on Industrial Electronics*, vol. 55, no. 7, Jul. 2008, pp. 2694-2702

[80] E. Gubia and A. Ursua, J. Lopez and L. Marroyo P. Sanchis; "Ground Currents in Single-phase Transformerless Photovoltaic Systems"; *Progress in Photovoltaics: research and Application*, 2007, pp. 629-650

[81] M. Calais, V. Agelidis, and M. Meinhardt; "Multilevel Converters for Single-Phase Grid Connected Photovoltaic Systems: an overview"; *Solar Energy*, vol. 66, no. 5, 1999, pp. 325-335